THE INTERSECTION OF CELL ENVELOPE MAINTENANCE AND METABOLIC VERSATILITY IN *STAPHYLOCOCCUS AUREUS*

By

Troy Burtchett

A DISSERTATION

Submitted to
Michigan State University
in partial fulfillment of the requirements
for the degree of

Microbiology and Molecular Genetics – Doctor of Philosophy

2025

ABSTRACT

Adapting to changes in environmental conditions is an essential process that ensures maximal fitness of an organism is maintained. For bacterial pathogens residing in the host, these changes include alterations in oxygen availability, nutrient abundance, and the presence of antimicrobials. Failure to meet these challenges limits the pathogenic potential of the bacterium, therefore, a better understanding of how bacterial pathogens respond to environmental changes will aid the development of treatment strategies to combat microbial infections. *Staphylococcus aureus* is an opportunistic pathogen that employs a diverse set of metabolic pathways to adapt to new host environments and stressors, which is driven by a branched aerobic respiratory chain and the ability to transition into a fermentative state of growth known as the small colony variant (SCV). The branched respiratory chain is powered by two terminal oxidases, CydAB and QoxABCD, and loss of either terminal oxidase leads to tissue specific colonization defects. Infections caused by SCVs are often resistant to antibiotic treatment, frequently leading to prolonged infections with worse clinical outcomes for the patient. In line with the goal of identifying novel therapeutic targets, this dissertation explores the pathways supporting the metabolic versatility of *S. aureus* including synthesis of lipoteichoic acid (LTA) and the isoprenoid biosynthetic pathway.

LTA is a cell surface polymer that has been predicted to maintain surface ion homeostasis. Previous reports demonstrated that limiting the metabolic potential of *S. aureus* cells in which LTA synthesis is disrupted reduces viability. Accordingly, we sought to determine the mechanism driving this phenotype. The membrane embedded anchor on which LTA is synthesized is generated by YpfP, and inactivation of this enzyme results in LTA that is elongated and less abundant. Membrane potential of the *ypfP* mutant was maintained during aerobic growth, however, induction of SCV growth resulted in a loss of membrane potential and reduced viability. Suppressor mutants

in the *ypfP* mutant background that displayed increased SCV viability were isolated and characterized. The suppressor mutants exhibited LTA that was more similar to the WT and anaerobic membrane potential was partially restored, demonstrating that LTA supports SCV viability via maintenance of ion homeostasis.

Further investigation of pathways supporting metabolic versatility identified the isoprenoid biosynthetic pathway as essential for cellular respiration. Isoprenoids are molecules containing 5-carbon repeating units and are synthesized by prenyl diphosphate synthases (PDS). Farnesyl diphosphate (FPP) serves as a substrate for three downstream cellular processes: pigment production, cell envelope maintenance, and synthesis of respiratory cofactors. The only known PDS to synthesize FPP is IspA, however, *ispA* mutants still produce FPP, suggesting another FPP-producing PDS is present. Investigation of this pathway identified a high level of redundancy in which other PDSs not previously known to produce FPP are able to contribute to FPP dependent pathways. Studying the effects of isoprenoid synthesis disruption on respiration revealed a preference of the CydAB terminal oxidase for chain length of menaquinone, demonstrating the impact of isoprenoid synthesis on metabolic versatility.

Lastly, a chemical library screen was performed to identify inhibitors of the fatty acid kinase (FAK) system. The FAK system is used to acquire exogenous fatty acids and limits the efficacy of antimicrobials that target endogenous fatty acid synthesis. Disruption of these pathways limits the production of the fatty acids necessary for cell membrane synthesis and thus inhibits growth of the cell. A putative FAK system inhibitor was identified and demonstrated to work synergistically with triclosan, a known inhibitor of endogenous fatty acid synthesis. This work demonstrates the feasibility of a dual therapy strategy for inhibition of cell membrane synthesis and lays the groundwork for expanding the toolkit available for treatment of *S. aureus* infections.

This thesis is dedicated to my grandfather, James Burtchett.
I know you would have been proud of me.

ACKNOWLEDGEMENTS

First and foremost, I want to thank my mother and father for instilling in me the importance of education and how it can be used to achieve a better life. This would not be possible without your continued support, and for that I am deeply grateful.

Also, to my sisters, Hayley, Stephanie, and Kelly. Thank you for being the best big sisters anyone could ask for.

I would like to thank my thesis advisor, Dr. Neal Hammer. You created an environment that fostered creativity and the comfortability to take risks. Because of your guidance, I am a far better scientist now than I was when I entered the lab. Thank you to my thesis committee, Drs. Sean Crosson, Shannon Manning, and Kristin Parent. You all took the time out of your busy schedules to meet, discuss my data, and provide constructive feedback about my work. Your guidance has helped prepare me for the next step of my career, and I am grateful for your invaluable support.

I would also like to thank the members of the Hammer lab, both past and present. Dr. Joshua Lensmire, you were always willing to show me how to perform a technique I was unfamiliar with or help interpret the meaning of confusing data. Your help enabled me to have such a great start in the lab. Dr. Rajab Curtis, you helped me remember there is life outside the lab. Thank you for the times you "kidnapped" me, those are memories I will cherish for the rest of my life. Dr. Paige Kies, you set the perfect example of what a scientist should strive to be. Your unwavering integrity and dedication to science was inspiring. Joelis Lama-Díaz, thank you for not allowing me to be an introvert. You pulled me out of my shell, which helped me make friends and have a better experience during the stressful time that is grad school. I will forever value our friendship. Dr. Cristina Kreamer-Zimpel, you are always willing to have discussions with me, both scientific and non-scientific, even though you most certainly have more important things to do. You continually

go above and beyond what is expected of a post-doc, and that has had a lasting impact not only on myself and my work, but other members of the lab as well. To the newest members of the lab, Jessica Lysne and Fatma Afify, you both made immediate impacts upon joining and contribute to the open and collaborative atmosphere. Thank you for carrying on the great culture we have created in the lab. Jess, I will miss hearing your laugh from three buildings away.

To the undergraduate students I have had the privilege of mentoring: Nick Carlier, Helen Spence, and Jessica Bailey. Working with you has been an absolute pleasure and enriching experience. Nick, I wish you the best of luck in PA school, I know you are going to do great. Helen, you are quickly becoming a skilled researcher and there is not a doubt in my mind that you will find success in the next step of your career. Jessica, it has been the most unique experience of my life to watch you grow as a scientist. The proudest moment I have had as a mentor was the first time you interpreted the data from an experiment yourself and explained to me what the next step should be.

I would also like to express my gratitude to the MGI department. This has been such a welcoming environment. Roseann Bills and Amber Bedore, without your help I would have been lost with the paperwork and technical aspects that come along with getting a PhD. To my fellow colleagues on the 5th floor of BPS, the collaborative environment here has helped me countless times either by the sharing of reagents, helping me understand a method I was unfamiliar with, or just having a friendly conversation. There was never a time when I felt I could not stop by another lab for help, and that was invaluable for designing better experiments and completing projects.

I have had the pleasure of collaborating with many scientists during my PhD. Dr. Shingo Fujisaki, Tomotaka Jitsukawa, Miu Yasui, and Momoko Kaneko all contributed their time and effort to generating the mass-spec data used in Chapter 3. Dr. Eric Hegg allowed me to use the HPLC in his lab and Dr. Elise Rivett showed me how to quantify extracted hemes: data that was

used in Chapter 3. I would like to thank Dr. Erika Lisabeth for performing the high throughput drug screening described in Chapter 4, and her constant enthusiasm for discussing and helping interpret the screening results.

Ben, Ryan, Caceti, Danny, Evan, Tristan, Emma, and Natalie: the people I collectively call my “swim friends”. Once upon a time during undergrad I joined the swim club and met the most amazing and caring people. From the D&D sessions and anime nights to the vacation/group-get-togethers, you all have provided a much needed reprieve from the unyielding pressure of grad school. Your friendships have shaped my life for the better.

And last, but certainly not least, I want to thank my bees. Beekeeping has been such a fulfilling experience, and I am thankful I could continue this hobby during my PhD. It allowed me to express my creativity in a way that no other activity could offer. Taking care of them has been a therapeutic experience and significant source of stress relief. I am truly fortunate to have had the opportunity to work with these magnificent creatures.

TABLE OF CONTENTS

Chapter 1: The metabolic versatility of *Staphylococcus aureus*.

Abstract

Bacterial pathogens modify their metabolic pathways in response to alterations in environmental conditions. Changes in nutrient availability, terminal electron acceptor abundance and external stressors such as antibiotics and the host immune system all influence the energy generating pathways a bacterium can utilize. Overcoming these challenges to sustain energy production is known as metabolic versatility, which is largely centered around maintaining redox balance, proton motive force, and generation of ATP. The human pathogen *Staphylococcus aureus* is capable of utilizing distinct metabolic modalities to proliferate in the host including: a branched aerobic respiratory chain and fermentation, which function to balance redox potential and generate energy in the hostile host environment. Further, cell surface structures called teichoic acids are hypothesized to play an instrumental role in facilitating metabolic versatility via maintenance of proton motive force. A thorough understanding of the mechanisms that support metabolic versatility is essential to understanding *S. aureus* pathogenesis and will lead to novel therapeutic strategies.

Introduction

Staphylococcus aureus is a Gram-positive opportunistic pathogen and the leading cause of skin and soft tissue infections in the United States (1). To establish infection and circumvent the immune system, *S. aureus* generates a vast array of virulence factors (2). However, an underappreciated aspect of *S. aureus* pathogenesis is the way it employs metabolic versatility during infection. Metabolic versatility refers to the ability of a bacterium to modulate its energy generating pathways to meet the fluctuating demands of its environment. These fluctuations include variations in oxygen concentration, nutrient availability and the presence of antimicrobials. *S. aureus* must overcome these challenges by maintaining energy production, for which three pathways are present: glycolysis, aerobic respiration and anaerobic respiration (3–5). A requirement for energy production

is the maintenance of redox balance via the recycling of electron carriers. *S. aureus* achieves this through specialized pathways that adapt to new host environments, thus ensuring continued metabolic activity (4, 6, 7).

Several studies have demonstrated that limiting *S. aureus* metabolic versatility reduces virulence and is therefore a promising strategy for treating or preventing infection (4, 7–9). To this end, it is necessary to identify pathogen-specific pathways that support the transition between different metabolic states. Notably, the *S. aureus* cell envelope possesses features distinct from the host which are predicted to support metabolic versatility (10, 11). Namely, wall teichoic acid (WTA) and lipoteichoic acid (LTA) have been hypothesized to play a role in maintaining the proton motive force (PMF) (12). The PMF is comprised of two components: membrane potential ($\Delta\Psi$), which is the summation of all ions contributing to the electrical charge across the cell membrane, and the proton gradient (ΔpH) (13). The PMF is essential for viability and serves as an energy source for cellular processes, such as ATP production (14). Here, the energy generating pathways and redox balancing mechanisms of *S. aureus* will be described along with their known roles in supporting infection. Additionally, the role of cell envelope structures in supporting metabolic versatility will be discussed.

S. aureus balances redox potential via respiration and fermentation

Cellular respiration relies upon electrons provided from glycolysis and the tricarboxylic acid (TCA) cycle (15). Glycolysis enzymatically oxidizes glucose by transferring electrons to NAD^+, yielding NADH, ATP and pyruvate as the end products (15, 16). The pyruvate from glycolysis feeds into the TCA cycle where it is further oxidized, generating additional NADH and another electron carrier $FADH_2$, as outlined in figure 1-1 (15). In *S. aureus*, electrons from NADH and $FADH_2$ are transferred to the electron carrier menaquinone (MK), regenerating NAD^+ and FAD^+,

respectively, thus balancing the redox potential of the cell (5). MK subsequently transfers the electron to a terminal reductase. During aerobic respiration S. aureus utilizes two terminal oxidases, CydAB or QoxABCD, to reduce oxygen to water (4). *S. aureus* is also capable of anaerobic respiration, whereby the alternative terminal electron acceptor nitrate (NO_3) is reduced to nitrite (NO_2) through the activity of the nitrate reductase NarGHJI. NO_2 is further reduced by the nitrite reductase NirBD, generating ammonia (NH_3) (3). A consequence of aerobic respiration and anaerobic respiration is the generation of a proton gradient across the cell membrane, which is essential for coordinating cell division machinery and providing the energy needed for nutrient transport (17–19). Additionally, ATP synthase is powered via the PMF by harvesting energy generated by protons traveling down the concentration gradient, and in doing so catalyzes the production of ATP (15, 20).

In the absence of external terminal electron acceptors respiration is impeded, leaving glycolysis as the only ATP generating pathway. Furthermore, in environmental conditions that promote respiration arrested growth the redox balancing property of respiration is eliminated. This is due to the loss of activity of the membrane embedded type II NADH dehydrogenase (NDH-2), which transfers electrons from either NADH or $FADH_2$ to MK (21) (Fig. 1-1). Consequently, an alternative pathway must be used to regenerate the NAD^+ needed to sustain glycolysis. To achieve this, pyruvate serves as the terminal electron acceptor, causing *S. aureus* to primarily generate lactic acid (Fig. 1-1) (15). In addition to lactic acid fermentation, *S. aureus* is capable of fermenting pyruvate to 2,3-butanediol, acetate or ethanol (22).

S. aureus employs three seemingly redundant lactate dehydrogenases to carry out lactate fermentation: Ldh1, Ldh2 and Ddh (23). Each of these enzymes use NADH as an electron donor to reduce pyruvate to lactate. In 2,3-butanediol fermentation α-acetolactate synthase (ALS) and α-

acetolactate decarboxylase (ALDC) are used to regenerate NAD^+ while producing 2,3-butanediol (24). Acetate and ethanol fermentation begin with the same step, utilizing either pyruvate dehydrogenase (PDH) or pyruvate formate lyase (PFL) to produce acetyl-CoA. Once generated, acetyl-CoA can feed into the acetate fermentation pathway using phosphotransacetylase (PTA) and acetate kinase (AckA) to produce acetate (25). Notably, this pathway does not regenerate NAD^+, however a single ATP is produced, contributing to the energy yield of the cell (24, 25). Conversely, acetyl-CoA can feed into the ethanol fermentation pathway, where a two-step process carried out by alcohol dehydrogenase (ADH) regenerates 2 NAD^+ in the production of ethanol, giving this pathway the greatest redox balancing power compared to the others (24–26).

Unlike respiration, the process of fermentation does not generate PMF. Instead, ATP from glycolysis is used by ATP synthase to run in reverse and pump protons to the outside of the cell (27). Due to the limited oxidation of glucose and the need to spend ATP to generate PMF, the use of fermentation to balance the redox potential of the cell overall yields less energy than aerobic respiration or anaerobic respiration.

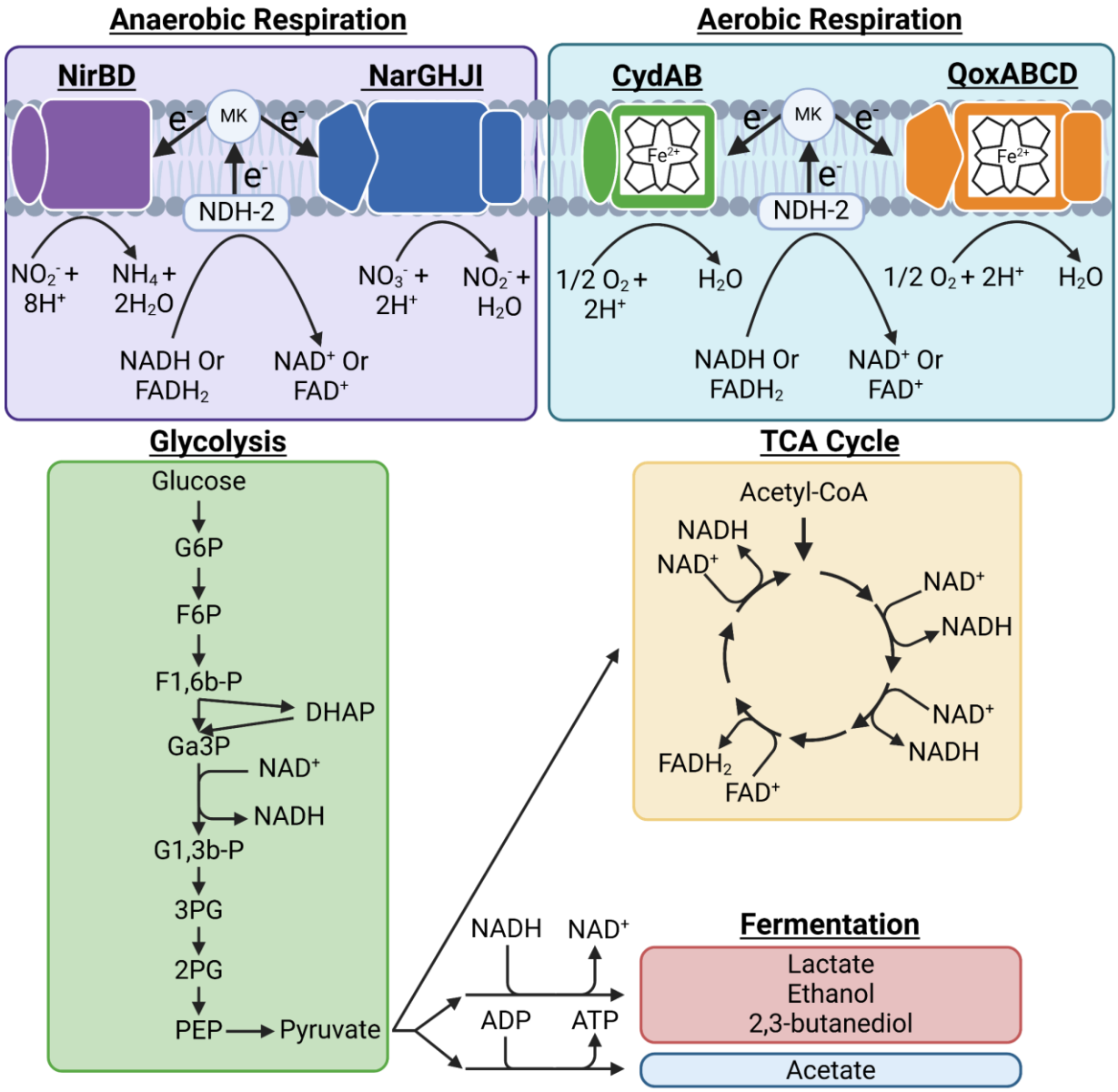

Figure 1-1. Respiration and Fermentation balance the redox potential of the cell by regenerating NAD+ and FAD+.

Glycolysis (green) and the tricarboxylic acid (TCA) cycle (yellow) generate NADH during oxidation of glucose and acetyl-CoA, respectively. Respiration and fermentation balance the redox potential of the cell by regenerating the NAD^+ needed for glycolysis and the TCA cycle. Anaerobic respiration (purple) and aerobic respiration (light blue) regenerate NAD^+ and FAD^+ via reduction of an external terminal electron acceptor. Fermentation consists of a redox balancing pathway (red), which utilizes pyruvate as an internal terminal electron acceptor, and an ATP generating pathway (blue). NDH-2 refers to the type II NADH dehydrogenase that transfers electrons from either NADH or $FADH_2$ to menaquinone (MK) Figure made in Biorender.

Adaptation of respiratory pathways facilitates *S. aureus* infection

The branched aerobic respiratory chain of *S. aureus* consists of a *bd* type terminal oxidase (CydAB) and an aa_3 type terminal oxidase (QoxABCD), both of which require heme for their activity (4, 28). Each of these terminal oxidases are capable of performing aerobic respiration in the absence of the other (4). However, there are characteristics unique to each terminal oxidase, which together promote maximal fitness in the host. First, the efficiency with which carbon sources are utilized is influenced by terminal oxidase activity. QoxABCD was shown to be essential for utilization of amino acids as a carbon source, as a *qoxA* mutant failed to proliferate when provided amino acids as the sole source of carbon (28). Second, CydAB and QoxABCD differ in the heme species they require for their activity. CydAB remains active with heme *b* as the sole heme species available, while QoxABCD requires isoprenoid modified hemes, heme *o* or heme *a*, for its activity (28). Third, the *bd* family of terminal oxidases have high affinity for oxygen and are capable of carrying out aerobic respiration at reduced oxygen levels (29, 30). This is notable, as *S. aureus* is known to colonize hypoxic environments in the human host, such as the lungs of cystic fibrosis patients (31, 32). Furthermore, infections caused by *S. aureus* often manifest as abscesses in which the infection is present in a confined area, causing localized inflammation and the buildup of a puss-filled tissue pocket (33). This environment is usually low in oxygen, a condition that reduces neutrophil mediated killing of *S. aureus* (31, 32, 34). Therefore, the utilization of a high affinity terminal oxidase may enable a low level of aerobic respiration in oxygen limiting environments, and thus greater energy yield, while promoting *S. aureus* survival in the presence of neutrophils.

The unique qualities of the terminal oxidases support colonization of different niches within the host. A *cydB* mutant was shown to exhibit reduced colonization of the heart, while a *qoxA* mutant had reduced colonization of the liver in a mouse model of systemic infection (4). Further,

the terminal oxidases may coordinate to promote survival during intracellular growth. Though not often thought of as an intracellular pathogen, *S. aureus* can invade host cells through a fibronectin bridging mechanism (35, 36). Consequently, *S. aureus* has been observed replicating inside epithelial and immune cells (37–40). Proteomic analysis revealed greater abundance of CydAB during intracellular *S. aureus* proliferation compared to staphylococci cultured extracellularly (41). At the same time, lower levels of QoxABCD were detected in internalized cells (41). These findings provide evidence that *S. aureus* engages its metabolic versatility by altering the aerobic respiratory pathway to adapt to new environmental conditions, highlighting the importance of specialized components in aerobic respiration.

In the absence of oxygen and in the presence of an alternative electron acceptor such as NO_3, *S. aureus* switches from aerobic respiration to anaerobic respiration (42). *S. aureus* encodes nitrate reductase, NarGHJI, that reduces NO_3 to NO_2, which can be further reduced by nitrite reductase, NirBD, to yield NH_3 (22). NO_3 is present in human skin and blood at concentrations of 80 μM and 25 nmol/g, respectively (43, 44), though whether these concentrations are sufficient to sustain a meaningful level of anaerobic respiration is not known. In the context of *S. aureus* pathogenesis, anaerobic respiration has been understudied, with most research focusing on the impact of aerobic respiration and fermentation during infection. However, a recent study has shown that a *narG* mutant has reduced virulence in a mouse model of skin infection (45), but it remains unclear whether this effect is due to loss of anaerobic respiration or a loss of virulence factor production in the nitrate reductase mutant. Similarly, a *Mycobacterium bovis* nitrate reductase mutant was also shown to be less virulent in a mouse skin infection model (46), indicating that anaerobic respiration may support bacterial infection of epidermal tissue.

S. aureus fermentation pathways adapt to the environment to maintain redox potential

Similar to the branched respiratory chain, *S. aureus* possesses a branched fermentative pathway that it can modulate in response to changing environmental conditions. When provided glucose as the sole carbon source, it was found that proteins involved in all four fermentative pathways increased in abundance upon shifting to anaerobic growth conditions, with lactate fermentation and ethanol fermentation having the greatest increase (22, 25). However, when pyruvate was provided, *S. aureus* primarily relied on the acetate and lactate fermentative pathways (25), likely to generate ATP through acetate fermentation while simultaneously maintaining redox balance via lactate fermentation.

While *S. aureus* can adapt its fermentative pathways in response to carbon source availability, it can also modulate fermentation in response to the host immune system. Nitric oxide (NO•) is an antimicrobial produced by phagocytes during the innate immune response that arrests bacterial growth via inhibition of both respiration and fermentation (7, 47). However, *S. aureus* harbors fermentative pathways that are resistant to NO•. All three lactate dehydrogenases (Ldh1, Ldh2 and Ddh) are resistant to NO•, however, Ldh1 is the only lactate dehydrogenase that increases transcription in response to nitrosative stress (7). Furthermore, mutants lacking either Ldh1 or Ldh2 were still capable of growing in the presence of NO•, and growth was only inhibited when both Ldh1 and Ldh2 were simultaneously inactivated (23). This finding demonstrates that Ddh is not capable of balancing cellular redox potential as the sole lactate dehydrogenase during nitrosative stress, and that a coordinated effort of Ddh and at least one other lactate dehydrogenase may be necessary. Additionally, *S. aureus* performs 2,3-butanediol fermentation in response to NO•. Metabolomic analysis found that, in addition to lactate, 2,3-butanediol increased in abundance in cells experiencing nitrosative stress, which was corroborated by the finding that the ALDC enzyme

responsible for 2,3-butanediol production also increased in expression (6). Given that a *ldh*1 *ldh*2 double mutant failed to proliferate in the presence of NO•, 2,3-butanediol fermentation alone is likely not sufficient to sustain redox balance. Instead, *S. aureus* relies primarily on lactate fermentation or a combination of lactate and 2,3,butanediol fermentation to maintain viability during NO• exposure.

Gram-positive cell envelope structures and maintenance of proton motive force

S. aureus possesses a diverse physiological toolkit to ensure redox balance of the cell is preserved under different environmental conditions. While these adaptive metabolic pathways are often thought of as a way to maintain ATP production, less attention is given to the maintenance of PMF. The *S. aureus* cell envelope consists of three primary structures: the cell membrane, peptidoglycan, and teichoic acids (48). Together, these structures are hypothesized to maintain PMF either directly or by supporting other structures. Given that PMF is essential for cell viability, disrupting its maintenance is a promising treatment strategy (49). In fact, cationic antimicrobial peptides (CAMPs), which are produced by the host specifically to limit bacterial proliferation, exert their activity by disrupting the cell's ability to maintain PMF, by forming pores in the cell membrane (49).

The cell membrane is a lipid bi-layer composed of phospholipids which organize to form a semi-permeable barrier in which the hydrophilic phosphate heads face the aqueous environment while the fatty acid tails are oriented inward to form a hydrophobic layer. The semi-permeable nature of the cell membrane is essential for the physiology of the cell. Small molecules like oxygen, carbon dioxide and water can passively cross the cell membrane, while charged ions such as protons are non-permeable (50). This allows the cell to generate PMF without the transported protons simply diffusing back across the cell membrane, which enables the use ΔpH as an energy source.

Anchored in the cell membrane is the cell surface polymer LTA, which is made up of repeating units of negatively charged glycerol phosphate (GroP) (10). Two UDP-glucose are added to a membrane-embedded diacylglycerol (DAG) by the glycosyltransferase YpfP to generate the diglucosyl-diacylglycerol (Glc_2-DAG) anchor (51). Glc_2-DAG is flipped to the exterior leaflet of the membrane by the flippase LtaA, where units of GroP are donated from phosphatidylglycerol and added to the anchor by the lipoteichoic acid synthase LtaS (52–54). The length of LTA can vary, with the majority of polymers between 20 and 30 GroP units, however LTA with as few as 4 GroP units has been observed (55, 56).

Though it has not been characterized, *S. aureus* likely modulates LTA chain length. A *ypfP* mutant does not produce the Glc_2-DAG anchor and an *ltaA* mutant is unable to flip Glc_2-DAG to the outer leaflet of the membrane (53). Consequently, in these mutant backgrounds LtaS synthesizes LTA directly on DAG (53, 57). As a result, *ypfP* and *ltaA* mutants produce elongated LTA that is less abundant compared to the WT (58, 59), suggesting a theoretical length determining mechanism may involve the interaction of LtaS with Glc_2-DAG or with YpfP and LtaA.

Surrounding the cell membrane is the peptidoglycan layer, which is comprised of the amino acid linked glycan units n-acetylglucosamine (NAG) and n-acetyl muramic acid (NAM) (48). This layer provides rigidity and influences cell shape. Additionally, it serves as a scaffold on which many subcellular components are bound, including wall teichoic acid (WTA) (11). Similar to LTA, WTA is an external polymer that extends outward from the cell. However, there are three primary characteristics of WTA that make it unique from LTA: 1) WTA is synthesized in the cytoplasm before being transported to the outside of the cell. 2) WTA is comprised of repeating units of Ribitol phosphate (RboP) rather than GroP. 3) WTA is covalently anchored to the peptidoglycan (11).

Synthesis of WTA begins with the addition of GlcNAc to the lipid carrier undecaprenyl

phosphate (Und-P) catalyzed by TarO (60). Subsequently, N-acetylmannosamine (ManNAc) is added to the GlcNAc through a β-1,4 linkage via the activity of TarA to make the GlcNAc-ManNAc anchor on which the rest of the polymer is synthesized (61). Next, two units of GroP are added to the anchor in a stepwise fashion by TarB and TarF, which serves as a linker moiety (11). Between 40 and 60 units of RboP are added to the linker moiety by TarL, which makes up the largest portion of the WTA polymer (62). Similar to the GroP of LTA, RboP is negatively charged and gives the polymer an overall electronegative nature (11). The last biosynthetic step that occurs is the glycosylation of the individual RboP units by either an α- or β-linked GlcNAc carried out by TarM or TarS, respectively (11).

Fully matured WTA is flipped to the outside of the cell by TarGH where it is covalently bound to the NAM unit of the peptidoglycan (11, 63). Studies in *Bacillus subtilis* have determined that the *tagTUV* genes are needed for attachment of WTA to peptidoglycan, which are homologous to the *tarTUV* genes in *S. aureus* (64). However, the mechanism by which this occurs is not known and whether there is specificity for attachment to newly synthesized peptidoglycan or old peptidoglycan has yet to be definitively determined (64).

Gram-positive bacteria are presented with a unique challenge when it comes to maintaining PMF. Unlike their Gram-negative counter parts, Gram-positives do not possess an outer membrane. The outer membrane is permeable to ions only through porins (65) and regulates the exchange of ions through these proteins (66). Thus, Gram-negative bacteria retain charged particles such as protons near the surface of the cell, thereby promoting generation of the PMF. The teichoic acids of Gram-positive bacteria have long been hypothesized to perform a similar role. In 1961, Archibald et al. hypothesized that the negative charge of teichoic acids regulates the passage of cations either to or from the surface of the cell (67). Nine years later, Heptinstall et al. demonstrated that teichoic

acids are capable of binding metal ions such as Mg^{2+}, providing some of the earliest evidence to support an ion-binding role of these cell surface polymers (68). Furthermore, it was shown that protons compete with metal ions for binding sites at the cell surface, indicating that teichoic acids may play a role in proton binding and retention (69), which was corroborated by a study that found WTA is capable of binding protons (70). Together, these studies suggest that teichoic acids contribute to PMF maintenance, and data presented in Chapter 2 supports this hypothesis by demonstrating a role for LTA in promoting $\Delta\Psi$ during fermentative growth.

The ability of Gram-positive bacteria to maintain ion homeostasis of the cell surface environment is essential for viability in the same way that maintaining the periplasm is essential for Gram-negatives. In fact, the space between the outer leaflet of the cell membrane and the outer edge of the cell wall of Gram-positives has been likened to a pseudo periplasm due to the maintained milieu of this area being unique from the surrounding environment (12, 71, 72). This is impressive, as the Gram-positive cell envelope is considered to be exposed to external conditions, and the mechanisms employed to maintain homeostasis must resist rapid environmental changes without the protection afforded by an outer membrane. One way *S. aureus* adapts its cell surface to a changing environment is by neutralizing the negative charge of teichoic acids with D-alanine and reducing the electronegative nature of the lipid bi-layer by the addition of lysine to phosphatidylglycerol (10, 73). The addition of a positively charged D-alanine to the individual GroP units of LTA or RboP units of WTA is carried out by the DltD protein at the cell surface (10). Incorporation of D-alanine residues reduces the overall negative charge of teichoic acid polymers, and thus the cell surface (74, 75). *S. aureus* has been shown to modulate the D-alanylation status of teichoic acids in response to increasing salt concentrations (76), changes in pH (77) and changes in temperature (78), indicating that altering cell surface charge via teichoic acids is important for

adaptation to new environments. Furthermore, the reduced negative charge of the cell surface facilitates resistance towards antimicrobial CAMPs (79). Whether or not D-alanylation of teichoic acids impacts their ability to maintain PMF has not been investigated. However, it is clear that teichoic acids are multifunctional cell surface polymers that influence many physiological aspects of *S. aureus*.

Small colony variants are respiration arrested cells that are adapted to life in the host

Even though it is beneficial for *S. aureus* to utilize diverse energy generating pathways, clinical isolates often harbor mutations in the respiratory pathway that limit the cell to fermentation (80). This seems paradoxical at first, as the ability to switch between metabolic pathways has been established to support *S. aureus* infection. However, it is likely that *S. aureus* only modulates its energy generating pathways when encountering new host environments, and once it has established an infection the need to switch between energy generating pathways may be diminished. This is supported by the fact that the site of infection is usually low in oxygen, favoring fermentative growth (31). Consistent with this idea is that respiration deficient mutants are isolated from diverse tissue types such as the lungs (81), bones (82), skin (83) and heart (84). These respiration arrested isolates are called small colony variants (SCVs) and are categorized by the substrate for which they are auxotrophic. Auxotrophy for hemin and menadione correlates to mutations in heme synthesis and menaquinone synthesis, respectively, which render the cell unable to produce the necessary cofactors to perform respiration (81, 85). Interestingly, a third type of SCV commonly isolated from clinical samples displays auxotrophy for the nucleoside thymidine due to mutation of the *thyA* gene (81, 85). It is thought that *thyA* SCVs acquire thymidine from the surrounding tissue of the host (85), however the molecular underpinnings for why thymidine depletion induces the SCV phenotype is not readily apparent. One study found that *thyA* mutants have reduced expression of

citB, a gene involved in the TCA cycle, theoretically leading to reduced production of NADH and $FADH_2$ to power respiration (86). However, *citB* mutants grow similar to the WT, therefore, it remains uncertain why *thyA* mutants grow as SCVs (87).

Despite the fact that SCVs generate less ATP as a consequence of fermentation, the cell gains physiological traits that are beneficial to survival in the host such as increased resistance to antibiotics and innate immune defenses. SCVs exhibit enhanced resistance to aminoglycoside antibiotics such as gentamicin, which requires a robust membrane potential to cross the cell membrane. SCVs have a reduced membrane potential, thereby reducing gentamicin penetration into the cell, leading to significantly increased MICs compared to respiring *S. aureus* (9, 88, 89). Furthermore, increased resistance has been observed for antimicrobials that do not require membrane potential to enter the cell. Macrolide antibiotics such as erythromycin and clindamycin, which inhibit protein synthesis, were shown to be less effective against some SCVs (89, 90). At the same time, SCVs have demonstrated increased resistance to antibiotics that exert their antimicrobial activity from outside the cell, such as oxacillin, vancomycin, and daptomycin (89–91). The broad range of antibiotic resistance makes treatment of SCV infections difficult, leading to worse clinical outcomes for the patient (92). The SCV antibiotic resistance phenotype is thought to be due to their reduced membrane potential and slow growing nature. However, slow growth is likely only part of the resistance mechanism, with increased biofilm production of SCVs likely also playing a role (80, 85, 93).

The beneficial characteristics of growing as an SCV extend beyond increased antibiotic resistance. In fact, *S. aureus* SCVs were described as early as 1906 (94), well before the widespread implementation of antibiotics in the 1940s (95), indicating that transitioning into the SCV metabolic state provides advantageous features that support survival in the host. One of these features is

increased immune evasion. SCVs invade host cells at a higher rate compared to the WT, which provides protection from the adaptive immune system (96). Furthermore, SCVs have been found to elicit a dampened innate immune response during intracellular growth, likely due to reduced toxin production which would otherwise activate toll like receptors and lead to inflammation (97). Additionally, reduced trained immunity is observed in infections caused by SCVs (98). Trained immunity refers to the "priming" of innate immune cells such as macrophages and is an important factor in preventing secondary infections after initial colonization by a pathogen (99). The accumulation of fumarate is an important aspect in activating the trained immune response (99, 100). However, SCVs produce higher levels of fumarate hydratase which degrades fumarate, presumably lowering the local concentration of this metabolite (98). This is thought to contribute to the persistent and recurrent infections that are characteristic of SCVs (98). Lastly, SCVs also exhibit increased resistance to CAMPs produced by the host. CAMPs are highly potent antimicrobials that can have IC_{50} concentrations in the micromolar range with some in the nanomolar range (101–104). One aspect contributing to their potency is their positive charge, which is thought to increase their interaction with the negatively charged surface of bacterial cells (73, 105). Importantly, some CAMPs can cross the host cell membrane and exert an antimicrobial effect on intracellular bacteria, which conventional antibiotics struggle to do (101). These characteristics make CAMPs highly effective at limiting bacterial infections, including those caused by respring *S. aureus* (106–108). However, SCVs are less susceptible to these CAMPS (108). Similar to the resistance mechanism of SCVs for aminoglycosides, it is thought that reduced membrane potential plays a role in modulating the electrostatic interaction of CAMPs with the surface of the cell, thus increasing resistance (109). However, direct evidence supporting this hypothesis has yet to be reported.

Isoprenoid synthesis contributes to metabolic versatility in *S. aureus*

Isoprenoids are molecules comprised of 5-carbon (C_5) repeating units that can be elongated, condensed, or covalently bound to other metabolites to generate the largest class of secondary metabolites known (110). In *S. aureus*, isoprenoid synthesis contributes to the production of five metabolites: the carotenoid pigment staphyloxanthin, the glycan carrier lipid II, and the respiratory cofactors heme *o*, heme *a*, and MK (Fig. 1-2) (28, 111–114). Isoprenoid synthesis begins with the condensation of the universal isoprenoid precursors isopentenyl diphosphate (IPP) and dimethylallyl diphosphate (DMAPP) carried out by the prenyl diphosphate synthase (PDS) IspA (115, 116). This condensation reaction generates a C_{10} isoprenoid, which is further elongated by IspA via the addition of another IPP to generate the C_{15} isoprenoid farnesyl diphosphate (FPP). FPP serves as a substrate for all isoprenoid containing metabolites produced by *S. aureus* (Fig. 1-3). For the production of respiratory cofactors, FPP can either be used directly for generation of heme *o* and heme *a* (collectively called prenylated hemes) or elongated for use in MK synthesis.

Prenylated heme synthesis is initiated by CtaB, which adds FPP to heme *b* to produce heme *o*. Further modification of heme *o* is carried out by CtaA via the addition of a carbonyl group to generate heme *a* (117). These prenylated hemes serve as cofactors for the QoxABCD terminal oxidase, and mutants deficient for prenylated heme production are restricted to CydAB for respiration (28). This is consequential, as restriction to either terminal oxidase influences carbon source utilization (28). Moreover, mutants utilizing only CydAB for respiration display colonization defects in the liver of systemically infected mice (4), further demonstrating the importance of prenylated heme-dependent respiration in supporting maximal fitness in the host.

The production of MK also supports *S. aureus* pathogenesis. Mutants of the MK synthesis pathway display the SCV phenotype and exhibit virulence defects in a mouse model (9). However,

unlike prenylated hemes which are generated by the direct addition of FPP, MKs incorporate longer isoprenoids, thus elongation of FPP is required. A previous study in *B. subtilis* demonstrated that HepT produces the isoprenoids that are the same length as those attached to MK (118). This led to the hypothesis that HepT is involved in MK synthesis, which is confirmed in Chapter 3. It has been established that *S. aureus* produces three MK species which differ only in the length of the isoprenoid moiety. These MK species are denoted as MK-7, MK-8, and MK-9, where the number refers to the C_{35}, C_{40}, and C_{45} incorporated isoprenoids, respectively (113, 114). It is important to note, however, that the Smith strain of *S. aureus*, harbors a point mutation in *hepT* which leads to the production of MK-10 (113). It is likely that production of MK-10 is rare in *S. aureus*, as strain Smith is the only *S. aureus* reported to produce this MK species. Furthermore, data outlined in Chapter 3 demonstrate that *S. aureus* also produces MK-5 and MK-6, and that production of these shorter chain MKs is dependent on HepT. The significance of producing MKs that vary in isoprenoid tail length is not known. However, data presented in Chapter 3 suggest that terminal oxidases exhibit preferences for isoprenoid tail length of MKs. Therefore, the composition of the MK pool may function to regulate terminal oxidase activity, thus influencing the metabolic potential of the cell. It has been established that the most abundant MK produced in *S. aureus* is MK-8, followed by MK-7 and MK-9 (113, 114). However, a regulatory mechanism for MK pool composition has not been reported. Therefore, it is unclear if the cell can alter production to favor MKs of specific tail lengths in response to environmental changes. Investigation of this aspect could reveal a previously unknown mechanism of respiratory regulation in *S. aureus*.

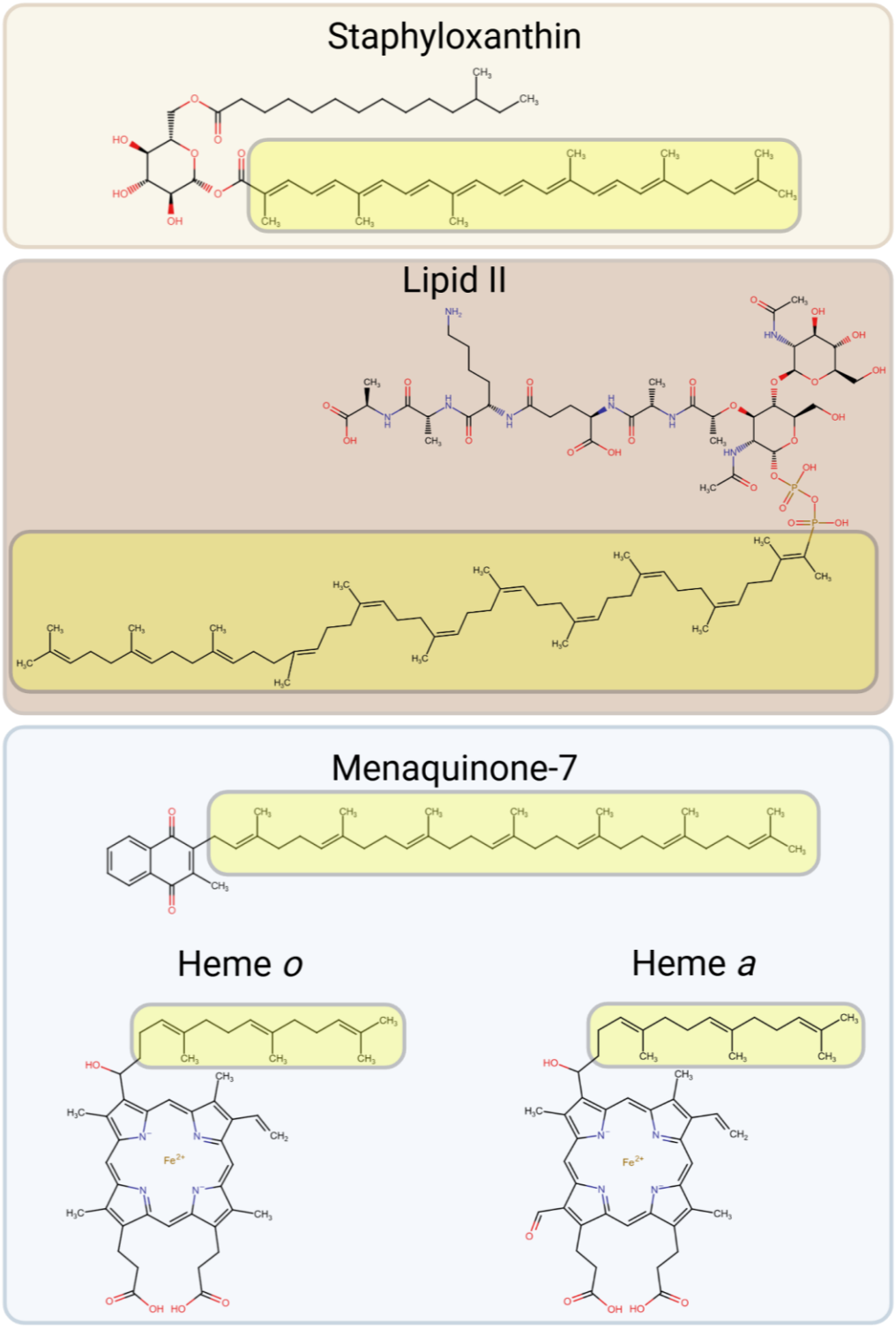

Figure 1-2. Isoprenoid containing metabolites of *Staphylococcus aureus*.
The molecular structures of isoprenoid containing metabolites synthesized by *S. aureus*. The isoprenoid moiety of each metabolite is highlighted in yellow. Background colors represent the following classifications: carotenoid pigment (light brown), Cell wall maintenance (brown), respiratory cofactors (light blue). Figure made in Biorender.

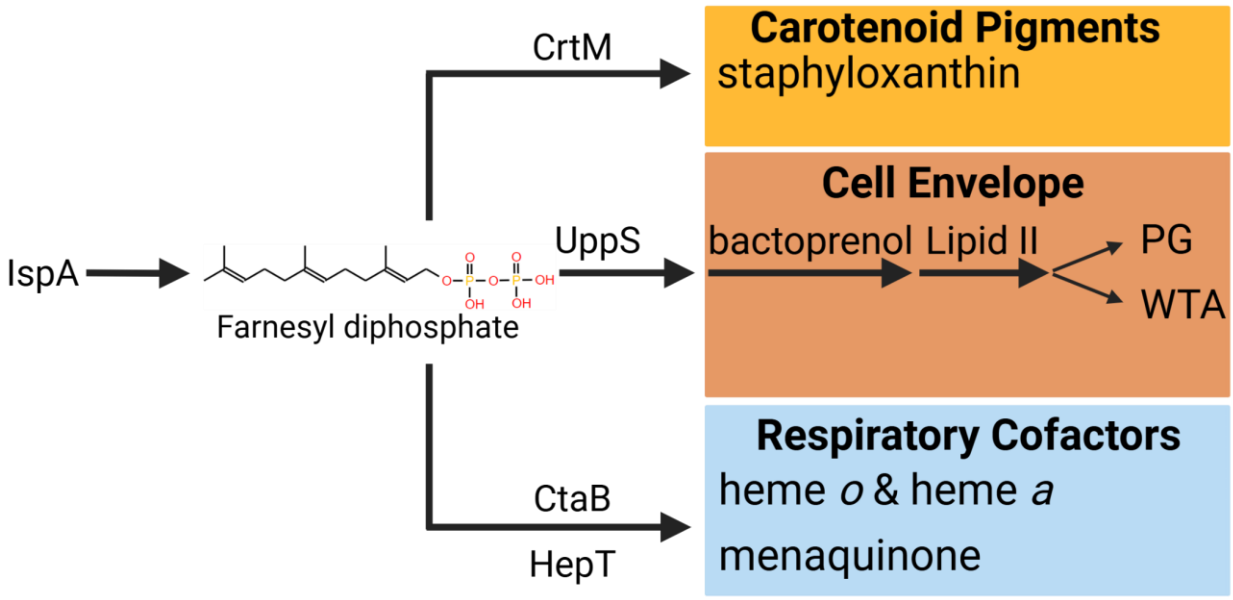

Figure 1-3. The current model by which isoprenoids are synthesized in *Staphylococcus aureus*.
A simplified model of isoprenoid biosynthesis depicting the three cellular processes supported by isoprenoid production. Farnesyl diphosphate is produced by IspA, which serves as a substrate for CrtM in carotenoid pigment production, UppS in lipid II synthesis, and CtaB or HepT in the production of respiratory cofactors. Figure made in Biorender.

Concluding remarks

In this chapter, we examined how *S. aureus* generates energy and employs specialized strategies to maintain redox balance in the presence of a hostile host immune system. *S. aureus* metabolic versatility enables adaptation to new host environments and allows the pathogen to overcome challenges that include changes in nutrient availability, the presence of antimicrobials that promote respiration arrest, and the availability of terminal electron acceptors. Cell surface structures such as WTA and LTA have long been hypothesized to facilitate metabolic versatility through the maintenance of PMF. Data presented in Chapter 2 support this hypothesis and provides the first evidence that LTA plays a role in supporting ion homeostasis by promoting PMF. In environments that impair aerobic respiration, *S. aureus* adopts a respiration arrested metabolic state, which serves as a specialized adaptation towards persistence in the host. The identification of

pathways that enable *S. aureus* to transition between different metabolic states is a critical factor in the capacity of the organism to cause disease. Therefore, these mechanisms represent targets for therapeutic intervention. In this dissertation, pathways that support the metabolic versatility of *S. aureus* will be explored and evaluated for their potential as drug targets. Additionally, a high throughput chemical screen to identify small molecules that target cell membrane synthesis is described.

Chapter 2: Crucial Role for Lipoteichoic Acid in the Metabolic Versatility and Antibiotic Resistance of *Staphylococcus aureus*.

Work presented in this chapter has been published as Burtchett T, Shook J, Hesse L, Delekta P, Brzozowski R, Nouri A, Calas A, Spanoudis C, Eswara P, Hammer N. 2023. Crucial Role for Lipoteichoic Acid Assembly in the Metabolic Versatitliy and Antibiotic Resistance of *Staphylococcus aureus*. Infect Immun 91:e005500-22.

Abstract

Staphylococcus aureus is a public health threat due to the prevalence of antibiotic resistance and the capacity of this organism to infect numerous organs in vertebrates. To generate energy needed to proliferate within tissues, *S. aureus* transitions between aerobic respiration and fermentation. Fermentation results in a distinct colony morphology called the small-colony variant (SCV) due to decreased membrane potential and ATP production. These traits promote increased resistance to aminoglycoside antibiotics. Consequently, SCVs are associated with persistent infections. We hypothesize that dedicated physiological pathways support fermentative growth of *S. aureus* that represent potential targets for treatment of resistant infections. Lipoteichoic acid (LTA) is an essential component of the Gram-positive cell envelope that functions to maintain ion homeostasis, resist osmotic stress, and regulate autolytic activity. Previous studies revealed that perturbation of LTA reduces viability of metabolically restricted *S. aureus*, but the mechanism by which LTA supports *S. aureus* metabolic versatility is unknown. Though LTA is essential, the enzyme that synthesizes the modified lipid anchor, YpfP, is dispensable. However, *ypfP* mutants produce altered LTA, leading to elongation of the polymer and decreased cell association. We demonstrate that viability of *ypfP* mutants is significantly reduced upon environmental and genetic induction of fermentation. This anaerobic viability defect correlates with decreased membrane potential and is restored upon cation supplementation. Additionally, *ypfP* suppressor mutants exhibiting restored anaerobic viability harbor compensatory mutations in the LTA biosynthetic pathway that restore membrane potential. Overall, these results demonstrate that LTA maintains membrane potential during fermentative proliferation and promotes *S. aureus* metabolic versatility.

Introduction

Staphylococcus aureus poses a considerable threat to public health due to its capacity to

rapidly develop resistance to antibiotics and infect numerous organs in vertebrates. The latter is underscored by the fact that *S. aureus* is the leading cause of skin and soft tissue infection, endocarditis, and osteomyelitis (119–121). Additionally, *S. aureus* is also prevalent in the lungs of people afflicted with cystic fibrosis (CF) (122, 123). CF patients are often colonized with *Pseudomonas aeruginosa* and receive multiple rounds of aminoglycoside antibiotics to treat bacterial infection (124). In response to both of these environmental challenges, *S. aureus* develops inactivating mutations in pathways that support aerobic respiration, such as heme synthesis (4, 125, 126). Consequently, heme auxotrophs can be isolated from CF patients (81). In addition to enhanced resistance to aminoglycosides, genetic inactivation of heme synthesis results in a distinct colony morphology referred to as the small-colony variant (SCV). SCVs rely exclusively on fermentation to proliferate, as aerobic respiration is inhibited in these cells. Impaired respiration leads to reduced proton motive force (PMF), which explains enhanced SCV aminoglycoside resistance, as import of the antibiotic is dependent upon the PMF (127). PMF comprises the proton gradient (ΔpH) and membrane potential ($\Delta\Psi$). We provide evidence that ion homeostasis mediated by the essential cell envelope polymer lipoteichoic acid (LTA) is a key factor in maintaining the membrane potential in *S. aureus* cells in which respiration is arrested.

The staphylococcal cell envelope contains two teichoic acid polymers, LTA and wall teichoic acid (WTA), which together make up a "continuum of anionic charge" (12, 128, 129). *S. aureus* synthesizes type 1 LTA, consisting of a glycolipid anchor, diglucosyl-diacylglycerol (Glc_2-DAG), to which a chain of 1,3-linked glycerolphosphates (GroP) is attached (130, 131). Synthesis of the Glc_2-DAG glycolipid anchor is catalyzed by the enzyme YpfP, which uses UDP-glucose as a substrate to covalently link two glucose moieties to diacylglycerol present on the inner leaflet of the plasma membrane (51, 53, 57). Glc_2-DAG is flipped to the exterior leaflet of the plasma

membrane by LtaA, which is cotranscribed with *ypfpP*. LtaS transfers GroP moieties from phosphatidylglycerol to Glc_2-DAG, creating mature LTA (54). Despite the fact that LTA is indispensable, LtaS is the only essential enzyme in the pathway, indicating that this protein is a potential target for therapeutic intervention (132). Conversely, *ltaA* and *ypfP* mutants are viable, but both mutant strains produce altered LTA. In some strain backgrounds inactivation of *ypfP* reduces cell-associated LTA nearly 90% (57).

A molecular explanation for the essentiality of LTA has been elusive, as LTA is involved in numerous physiological processes, such as ion homeostasis and regulation of autolysin (51, 57, 68). Neutralizing the negative charge of LTA GroP via addition of D-alanine allows *S. aureus* to resist cationic antimicrobial peptides (79). Cells that conditionally lack LTA display extreme morphological defects (54). Previous reports showed that perturbing the metabolic potential of some *S. aureus* strains in which LTA or WTA production is impeded reduces viability, and it has been postulated that LTA-mediated ion homeostasis contributes to the PMF, but direct evidence has not been presented (51, 70, 133). We build on these studies to show that inactivation of *ypfP* impairs proliferation of cells in which respiration is arrested. The *ypfP* mutant with arrested respiration exhibits reduced membrane potential and reduced viability. The anaerobic proliferation defects are suppressed upon supplementation with the alternative electron acceptor KNO_3 or cations. Additionally, *ypfP* suppressor mutants have restored respiration-arrested viability and membrane potential. Together, these results support the conclusion that the LTA glycolipid anchor facilitates maintenance of the membrane potential under respiration-arresting, fermentative growth conditions.

Results

Respiration arrest impairs proliferation of *S. aureus ypfP* mutants

S. aureus arrests respiration upon exposure to aminoglycoside antibiotics, resulting in the development of resistant colonies (125, 134, 135). To assess LTA contributions to aminoglycoside resistance, we challenged *S. aureus* with 5 µg/mL of the clinically relevant aminoglycosides gentamicin and tobramycin. Compared to the number of aminoglycoside-resistant colonies generated in the corresponding wild-type (WT) strains, the *ypfP* mutant produced considerably fewer resistant colonies (~63% and ~76% decreased for gentamicin and tobramycin, respectively) (Fig. 2-1A). To further investigate the aminoglycoside sensitivity, we monitored the morphology of WT and *ypfP* mutant cells in response to gentamicin via florescence microscopy (Fig. 2-2). The untreated WT and *ypfP* mutant appear similar, as indicated by membrane staining (FM4-64, red). While gentamicin treatment caused abnormal membrane clumping in the WT (46%; $n = 100$), it was more pronounced in *ypfP* mutant cells (57%; $n = 100$). Increased membrane clumping, possibly due to improper membrane invagination or loss of membrane integrity, is an indicatin that cells are *en route* to lysis (136) and provides a visual depiction of the increased gentamicin susceptibility of *ypfP* mutant cells (Fig. 2-2).

Lungs of CF patients are often colonized with *S. aureus* and the Gram-negative opportunistic pathogen *Pseudomonas aeruginosa*. Studies have shown that *P. aeruginosa* induces respiration arrest and development of SCVs in *S. aureus* via production of 2-heptyl-4-hydroxyguinolone *N*-oxide (HQNO) and pyocyanin (137–141). As coculture with *P. aeruginosa* induces *S. aureus* respiration arrest and the *ypfP* mutant demonstrates impaired capacity to resist aminoglycosides, we reasoned that the *ypfP* mutant would be more susceptible to *P. aeruginosa*, HQNO, and/or pyocyanin. To test this, a lawn of WT *S. aureus* or the *ypfP* mutant was plated onto

tryptic soy agar (TSA) and *P. aeruginosa* PAO1 was spotted on top (137). The zone of inhibition induced by *P. aeruginosa* was quantified. Compared to WT zones of inhibition (~13 mm), the *ypfP* mutant demonstrates a larger area of inhibited growth (~17 mm) (Fig. 2-1B). We hypothesized that the increased sensitivity of the *ypfP* mutant is due to the respiration-inhibiting effects of HQNO or pyocyanin and used Kirby-Bauer disk diffusion assay with HQNO or pyocyanin to test this. Compared to WT cells, the *yfpP* mutant demonstrated enhanced susceptibility to HQNO but not pyocyanin (Fig. 2-1C and data not shown). In total, these findings demonstrate that genetic inactivation of *ypfP* sensitizes *S. aureus* to respiration arrest induced by *P. aeruginosa* coculture and exposure to aminoglycosides.

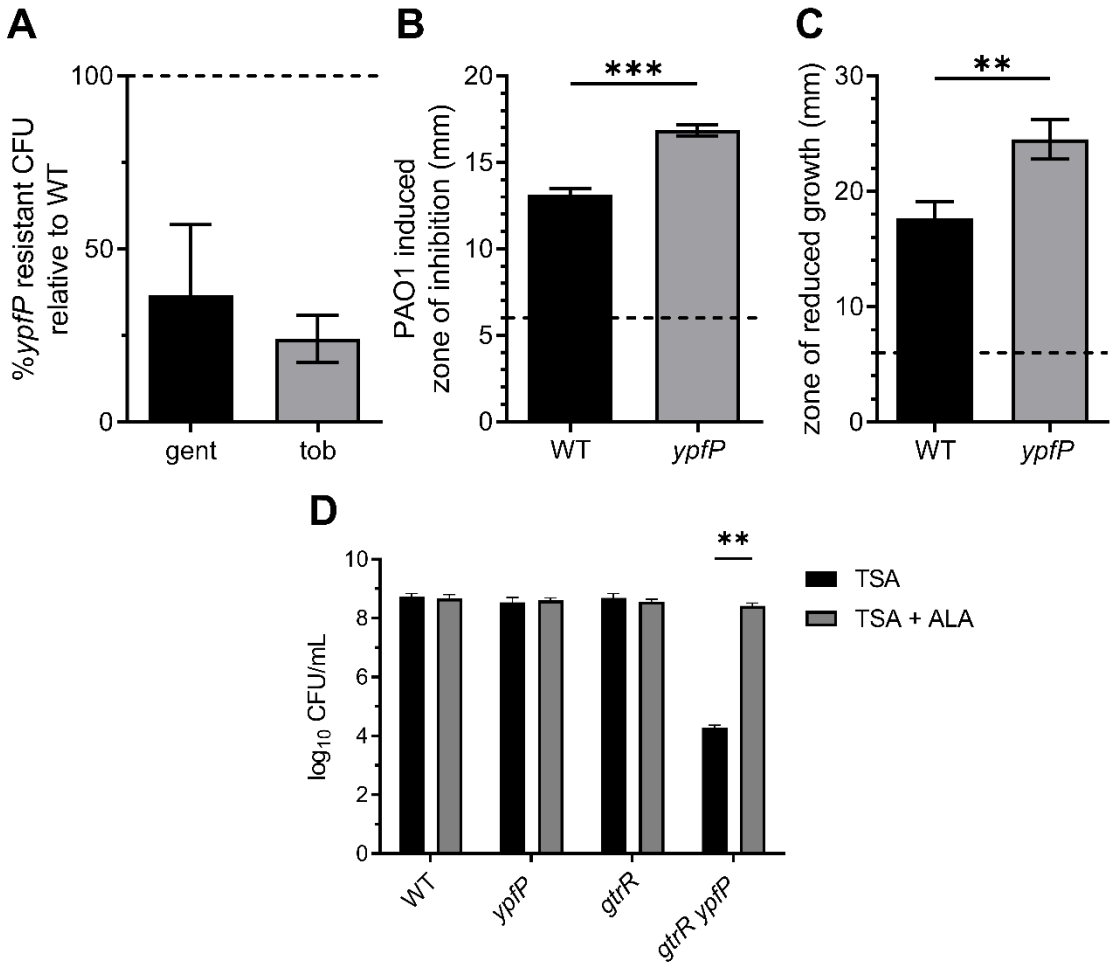

Figure 2-1. Respiration-arresting conditions impair S. aureus ypfP proliferation.
(A) CFU of WT or *ypfP* mutant cells grown on TSA supplemented with 5 μg mL^{-1} of gentamicin (gent) or tobramycin (tob) were enumerated after 24 h at 37°C. Values are percentages of the WT value, where the number of CFU of the *ypfP* mutant was divided by the number of CFU of the WT and the WT value was set to 100% (dotted line). Data are means from at least five independent experiments. Error bars represent one standard deviation from the mean. (B) Zones of inhibited growth generated by colonies of *P. aeruginosa* spotted on top of *S. aureus* WT or *ypfP* mutant lawns were measured after 24 h at 37°C. Data are means from three independent experiments performed in triplicate. Statistical significance was determined by an unpaired two-tailed *t* test for unequal variance. $P < 0.0001$. Error bars represent one standard deviation from the mean. (C) The zone of reduced growth generated by HQNO on lawns of WT or *ypfP* mutant cells was measured after 24 h at 37°C. Data are means from three independent experiments performed in triplicate. Error bars represent one standard deviation from the mean. Statistical significance was determined by an unpaired two-tailed *t* test for unequal variance. $P < 0.01$. (D) CFU of WT and *ypfP*, *gtrR* or *gtrR ypfP* mutant strains were quantified after 24 h (for respiring colonies) or 48 h (for respiration arrest colonies) of growth on TSA or TSA supplemented with ALA at 37°C. Error bars represent one standard deviation for three independent experiments. Statistical significance was determined by two-way analysis of variance (ANOVA) with a Šidák method for multiple comparisons. **, $P < 0.01$.

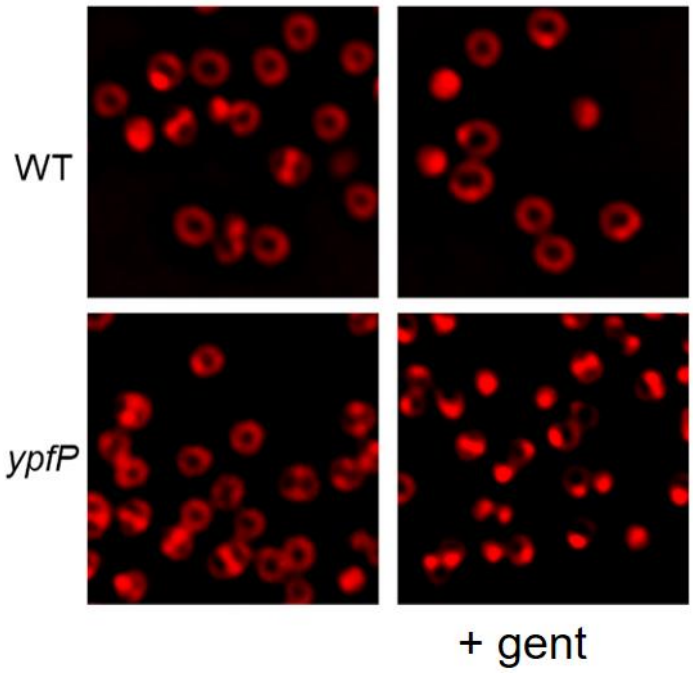

Figure 2-2. Exposure to gentamicin causes increased morphological defects and membrane clumping in the ypfP mutant.
Fluorescence micrographs of FM4-64 (red) stained WT and *ypfP* mutant cells following treatment without (left panels) or with 2 µg mL^{-1} gentamicin (right panels). Scale bar, 1 µm.

A limitation of using small molecules or competition with other organisms to induce respiration arrest is the potential for off-target effects. To further resolve the role of the LTA glycolipid anchor in *S. aureus* metabolic versatility, we genetically inactivated *ypfP* in a heme synthesis SCV mutant, a Δ*gtrR* (formerly *hemA*) mutant, which has been previously used as a model SCV in *S. aureus* (4). Heme synthesis and respiration is restored in the Δ*gtrR* mutant upon supplementation with the heme precursor δ-aminolevulinic acid (ALA) (4). This allows the Δ*gtrR* cells to perform continuous aerobic respiration as the strain undergoes additional genetic manipulation. Subsequent phenotypic analysis of the resulting double mutant under respiration-arresting conditions is achieved by simply culturing the cells in medium devoid of ALA. Plating the Δ*gtrR ypfP* double mutant on solid medium lacking ALA results in an approximately 4-log

decrease in CFU compared to WT or Δ*gtrR ypfP* mutant cells plated on medium supplemented with ALA (Fig. 2-1D). In total, these results imply that inactivation of *ypfP*, which lacks the LTA glycolipid anchor and reduces cell-associated LTA, impairs proliferation of *S. aureus* during respiration arrest (51, 53, 57).

Anaerobiosis reduces *ypfP* mutant viability

We reasoned that the viability defect of the Δ*gtrR ypfP* mutant could be attributed exclusively to respiration arrest or to a combination of respiration arrest and increased oxidation. To distinguish between these possibilities, we enumerated CFU generated by the *ypfP* mutant cultured under aerobic and anaerobic conditions. The *ypfP* mutant cells cultured anaerobically demonstrated a 4-log reduction in viability (Fig 2-3A); a similar decrease was observed when respiration was arrested in a Δ*gtrR ypfP* double mutant (Fig. 2-1D). Supplementation of the anaerobic cultures with the alternative electron acceptor KNO_3 rescues *ypfP* mutant viability, supporting the conclusion that reduced viability results from decreased respiration (Fig. 2-3A) The *ypfP* mutant cells also exhibit a significant lag phase compared to the WT when cultured in anaerobic conditions, although the mutant cells ultimately achieved a WT-like terminal optical density at 600 nm (OD_{600}) (Fig. 2-3B). A growth defect was not observed when *ypfP* cells were cultured aerobically (Fig. 2-4). Together, these results show that *ypfP* is needed for maximal anaerobic proliferation.

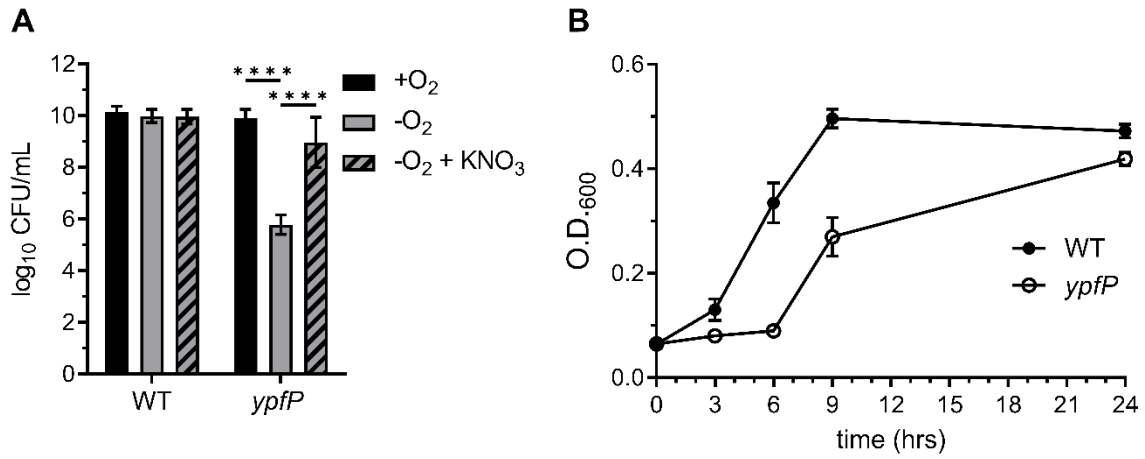

Figure 2-3. ypfP mutant cells demonstrate reduced anaerobic proliferation.
(A) CFU of WT or *ypfP* mutant bacteria generated after incubation under aerobic ($+O_2$) or anaerobic ($-O_2$) conditions were enumerated after 24 h at 37°C. Potassium nitrate (KNO_3; 100 mM) was used to induced anaerobic respiration. Data are means from three independent experiments performed in triplicate. Error bars represent one standard deviation from the mean. Statistical significance was determined by a two-way ANOVA with Tukey's multiple-comparison test. ****, $P < 0.0001$. (B) The WT and the *ypfP* mutant were subcultured 1:100 from an overnight culture and grown anaerobically at 37°C. Growth was measured at the indicated time points by monitoring OD_{600}. The experiment was performed in triplicate. Error bars represent standard deviations from the mean.

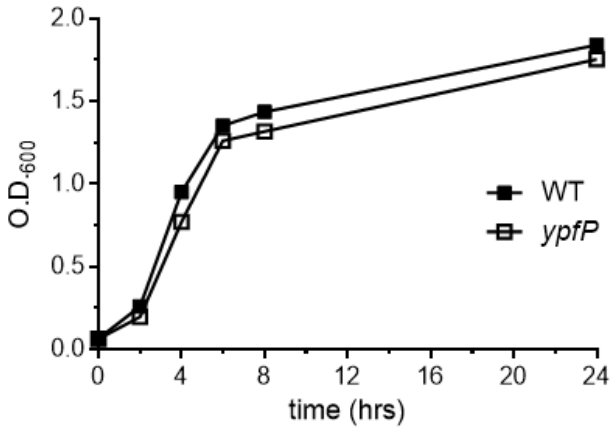

Figure 2-4. S. aureus ypfP mutant cells demonstrate wild type-like aerobic growth kinetics. WT and *ypfP* were sub-cultured 1:100 from an overnight culture and grown anaerobically at 37° C. Growth was measured at indicated time points by monitoring optical density at 600 nm (OD_{600}). The experiment was performed in triplicate. Error bars represent one standard deviation from the mean.

The anaerobic viability defect is specific to inactivation of *ypfP*

The *ypfP* mutant demonstrates reduced growth under multiple respiration-arresting conditions and an ovet viability defect when cultured anaerobically. YpfP produces Glc_2-DAG that is flipped to the outer leaflet of the cytoplasmic membrane by LtaA (Fig. 2-5A) (10). *ypfP* is cotranscribed with *ltaA*, and the transposon insertion used to inactivate *ypfP* is located upstream of *ltaA* (Fig. 2-5B). Therefore, the phenotypes we observed could be due to polar effects on *ltaA* and not specific to inactivation of *ypfP* (53). To test this, complementation plasmids using the pOS P_{lgt} vector carrying *ypfP*, *ltaA*, or *ypfP ltaA* were transformed into the *ypfP* mutant to determine the contribution of each gene to decreased anaerobic viability (142). *ypfP* mutant cells harboring a WT copy of *ypfP* rescued viability whereas *ypfP* mutant cells containing an empty vector displayed reduced anaerobic viability. Complementation of the *ypfP* mutant with *ltaA* resulted in a futher reduction in anaerobic viability compared to the empty vector control (Fig. 2-5C). These results demonstrate that the viability defect is due to *ypfP* inactivation. Consistent with this, the

ltaA mutant generated WT CFU when cultured anaerobically (data not shown).

ypfP mutant lack Glc_2-DAG, and consequently, LTA is anchored to DAG (53, 57). Similarly, LTA is also predominantly anchored to DAG in *ltaA* mutants despite Glc_2-DAG production in this mutant background (53). Although GroP is anchored to the same molecule in both mutants, cell-associated LTA profiles produced by these mutants are distinct (53, 57). Our results show that genetic inactivation of *ypfP*, but not *ltaA*, reduces anaerobic viability. Therefore, we reasoned that the LTA profile produced by the *ypfP* mutant in respiration-arresting environments may be altered further. To test this, we surveyed LTA produced in each mutant strain under aerobic an anaerobic conditions via immunoblotting. In addition to the previously reported distorted LTA profiles produced by aerobically cultured *ypfP* and *ltaA*mutant cells (Fig. 2-5D), anaerobically cultured *ypfP* mutant demonstrate further alterations to LTA underscored by loss of a high-moleular-weight (HMW) species and gain of low-molecular-weight species (Fig. 2-5D) (53). Notably, anaerobiosis does not affect LTA production in the *ltaA* mutant, implicating altered LTA production as a contributing factor to reduced proliferation of the *ypfP* mutant during respiration arrest.

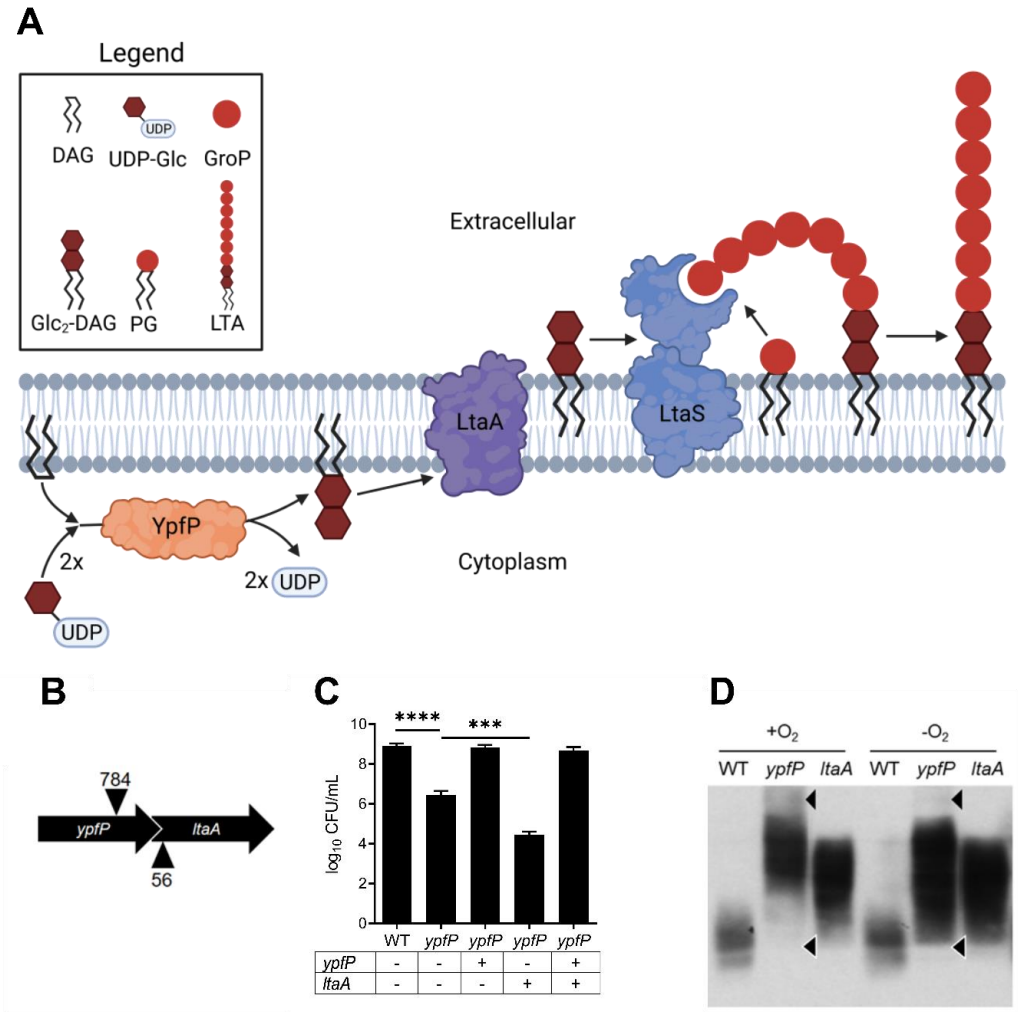

Figure 2-5. ypfP, not ltaA is responsible for alterations in viability and LTA production under anaerobic conditions.

(A) The LTA-biosynthetic pathway in *S. aureus*. YpfP uses DAG and two UDP glucose (UDP-Glc) molecules to generate the lipid anchor Glc_2DAG. Glc_2-DAG is then flipped to the outer leaflet of the membrane by LtaA, and glycerol phosphate (GroP) taken from phosphatidylglycerol (PG) is added directly to the anchor by LtaS. Illustration created using Biorender. (B) Illustration of the *ypfP ltaA* operon demonstrating the 41-bp *ypfP-ltaA* overlap. Locations of transposon insertions are indicated with arrowheads. (C) WT and *ypfP* mutant NWMN cells harboring the *S. aureus* expression vector pOS containing the indicated genes were spot plated on TSA and incubated in an anaerobic chamber for 24 h of growth at 37°C prior to CFU enumeration. Data are means from three independent experiments performed in triplicate. Error bars represent one standard deviation from the mean. Significance was determined via two-tailed *t* test. ****, $P < 0.0001$; ***, $P < 0.001$. (D) Representative immunoblot using a monoclonal anti-LTA antibody and a secondary antibody conjugated with horseradish peroxidase shows the altered LTA profiles of NWMN *ypfP* and *ltaA* mutants cultured under aerobic ($+O_2$) and anaerobic ($-O_2$) conditions compared to the WT. Differences in the LTA profile are indicated with arrowheads.

Supplementation of the growth medium with cations rescues the anaerobic viability defect of the *ypfP* mutant

Generation of the PM is essential. PMF is a summation of the differences between intracellular and extracellular pH (ΔpH) and charge (ΔΨ) (143). *S. aureus* in which respiration is arrested demonstrates reduced membrane potential, and LTA has been proposed to maintain ion homeostasis (12, 68, 133). In keeping with these facts, we hypothesized that loss of ion homeostasis in anaerobically cultured *ypfP* mutant cells leads to further perturbation of the membrane potential, resulting in reduced proliferation during respiration arrest. To quantify the membrane potential of *ypfP* mutant cells, we used the fluorescent dye $DiOC_2$ (diethyloxacarbocyanine iodide) (4, 144). Aerobically cultured WT and *ypfP* mutant cells generated similar membrane potentials, however, upon induction of anaerobiosis, the membrane potential generated by the *ypfP* mutant was significantly decreased (Fig. 2-6A). To discern between membrane potential and ΔpH, we used small-molecule inhibitors that specifically target each component of the PMF. First, we cultured the *ypfP* mutant in the presence of the proton ionophore nigericin or carbonyl cyanide 3-chlorophenyl hydrazine (CCCP) (145). However, no difference was observed in the *ypfP* mutant response to these ionophores under aerobic and anaerobic growth conditions (data not shown). Conversely, anaerobically cultured *ypfP* mutants are significantly more resistant to valinomycin, a potassium-specific ionophore that disrupts the membrane potential, than anaerobically grown WT cells (Fig. 2-6B) (146). We hypothesize that enhanced valinomycin resistance is consistent with a diminished membrane potential, as cells generating a depleted membrane potential would display great resistance to membrane potential-targeting ionophores, In keeping with this, we reasoned that increasing the abundance of extracellular charge by supplementing anaerobically cultured *yfpP* cells with cations would

overcome proliferation defects associated with respiration arrest and fermentative growth. To test this, we added KCl, NaCl, or H^+ ions to anaerobically cultured *ypfP* mutants. Supplementation with 0.5 M KCl or 1 M NaCl rescued the anaerobic *ypfP* mutant viability (Fig. 2-6C). Similarly, decreasing the pH of the medium to 6.0 also rescued the viability defect of the *ypfP* mutant (Fig. 4D).

Another function attributed to LTA is maintenance of osmotic homeostasis, and addition of salts also increases osmolarity of the medium. To discern between ion homeostasis and osmotic stress, we exposed anaerobically cultured *ypfP* mutants to the osmoprotectant glycine betaine (GB). However, addition of 1 mM or 0.5 M GB did not increase anaerobic viability (Fig. 2-6C and data not shown), indicating that perturbation of ion homeostasis is the major driver of the phenotype.

The *ypfP* mutant displayed an extended lag phase in anaerobic liquid culture but ultimately reached WT-like levels of growth (Fig. 2-3B). We hypothesized that the ability of the *ypfP* mutant to eventually reach an endpoint OD_{600} similar to that of the WT is due to acidification of the medium. To test this, the pH and OD_{600} of anaerobic WT and *ypfP* mutant cultures were monitored over time (Fig. 2-6E). Proliferation of the WT coincided with a drop in pH to ~4.9. Proliferation of the *ypfP* mutant was delayed but also coincided with a drop in pH to levels similar to those of the WT. In total, these data demonstrate that the defects in proliferation during respiration arrested associated with *ypfP* mutations are due to impaired ion homeostasis resulting in a reduced capacity to maintain the membrane potential.

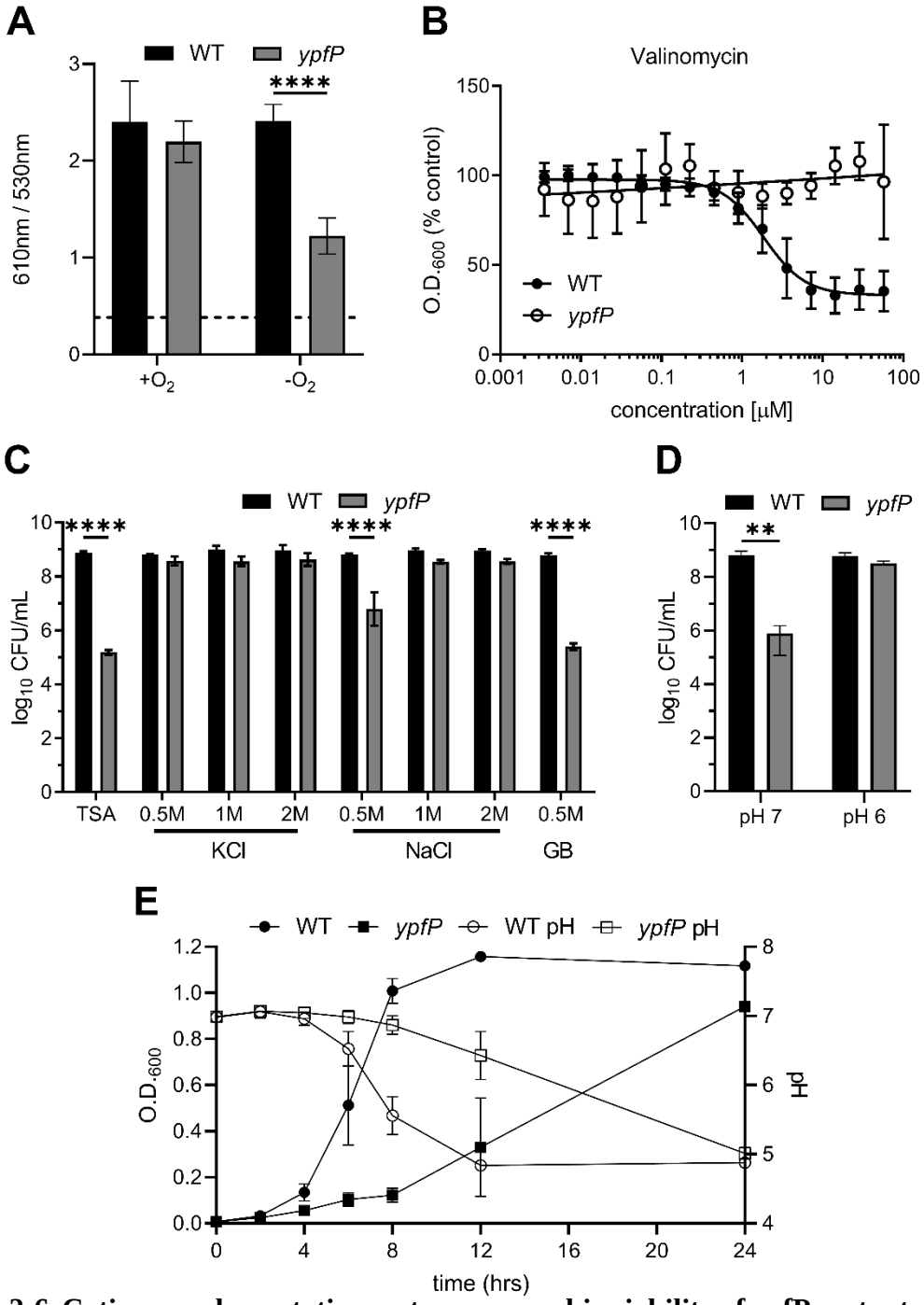

Figure 2-6. Cation supplementation restores anaerobic viability of ypfP mutants undergoing respiration arrest.

(A) Membrane potential of the WT and *ypfP* mutant. The *y* axis shows the quotient of the 610 nm and 530 nm emission spectra. Data are means from three independently performed experiments performed in technical triplicate. Error bars represent one standard deviation from the mean. Significance was determined using two-way ANOVA. ****, $P < 0.0001$. (B) The antimicrobial activity of the potassium-specific ionophore valinomycin was determined for WT and *ypfP* mutant cells.

Figure 2-6 (cont'd)
The WT and the *ypfP* mutant were normalized to an OD_{600} of 0.5 and were allowed to grow in liquid medium in the presence of various concentrations of valinomycin anaerobically for 16 h. Cells were suspended by pipetting, and the OD_{600} was measured. Results are percent OD_{600} compared to that of the untreated control. The mean for five independent experiments performed in triplicate is shown. The regression line was mapped using GraphPad Prism. Error bars represent one standard deviation from the mean. (C) Anaerobic viability of the WT and the *ypfP* mutant on medium supplemented with various concentrations of KCl, NaCl, or the osmoprotectant GB. CFU were enumerated after 24 h of growth at 37°C. Data are means from three independent experiments performed in triplicate. Error bars represent one standard deviation from the mean. (D) Anaerobic viability of the WT or the *ypfP* mutant on medium buffered to a pH of 7 or 6. CFU were enumerated after 48 h of growth at 37°C. Data are means from three independent experiments performed in triplicate. Error bars represent one standard deviation from the mean. (E) The WT and the *ypfP* mutant were subcultured 1:100 in TSB, and the OD_{600} and pH were measured at the indicated time points. The data are averages from three independent experiments. Error bars represent one standard deviation from the mean. (B and C) Significance was determined using one-way ANOVA with multiple comparisons. ****, $P < 0.0001$; **, $P < 0.005$.

Mutations in the LTA synthesis pathway restore anaerobic viability in the *ypfP* mutant

To determine a potential mechanism for the anaerobic viability defect, the *ypfP* mutant was passaged anaerobically until a suppressor mutant that exhibited WT-like viability was isolated (Fig. 2-7). Passaging was repeated for four independently passaged lineages. Whole genome sequencing revealed that the prophage-associated gene NWMN_1774 and genes in the LTA biosynthetic pathway, *ltaS* and *ltaA*, were commonly mutated in the suppressor strains (Table A-1). Suppressor lineage 1 passage 4 (S1P4) contained a mutation in *ltaS* (G39C). S2P3 and S3P3 harbored identical mutations in *ltaA* (K13N, N14R, F15L and I16V). S4P3 also harbored a heavily mutated *ltaA* which shared many of the same mutations as S2P3 and S3P3 (K13N, N14R, and F15L) though two of them were unique (I16A and L17E). To determine the effect of these mutations, suppressor lineages were cultured aerobically to late exponential phase and their LTA was assessed via immunoblotting. Compared to the parental *ypfP* mutant, the suppressor mutants displayed lower-molecular-weight LTA, though it was still larger than that in the WT (Fig. 2-8A).

Abundance of LTA in S1P4 was similar to that in the parental *ypfP* mutant (Fig. 2-8A, light band), while S2P3, S3P3, and S4P3 all exhibited WT-like LTA abundance (dark bands).

Due to the decreased membrane potential observed in anaerobically cultured *ypfP* cells and the fact that the suppressors produce altered LTA, we next determined whether the suppressor strains also restore anaerobic membrane potential. Notably, the four passaged lineages all exhibited anaerobic membrane potentials similar to that of the WT (Fig. 2-8B). The restored membrane potential of the passaged *ypfP* mutants suggests that producing WT-like LTA maintains membrane potential. The ability fo the suppressor mutants to resist aminoglycosides was determined. *S. aureus* resists aminoglycosides by entering a fermentative state; therefore, we hypothesized that a *ypfP* suppressor mutant with anaerobic viability equal to that of the WT would have an improved ability to gain resistance to gentamicin. A partially restored ability to gain resistance to gentamicin was observed for S2P3, S3P3 and S4P3, but not S1P4 (Fig. 2-8C).

To determine whether mutations observed in *ltaS* and *ltaA* are responsible for the increased anaerobic viability of the suppressor lineages, the mutated alleles of these genes were cloned into pOS P_{lgt} and used to compement the parental *yfpP* mutant (Fig. 2-8D). Overexpression of WT *ltaS* and *ltaA* in the parental *ypfP* mutant caused further decrease in anaerobic viability compared to the empty vector. The mutated *ltaS* from S1P4 incrased the anaerobic viability of the parental *ypfP* mutant to WT-like levels. S2P3 and S3P3 shared identical *ltaA* mutantsions. Despite three independent suppressor lineages harboring *ltaA* mutantions, there are only two unique mutated *ltaA* alleles, both of which partially restored the anaerobic viability of the parental *ypfP* mutant (Fig. 2-8D). Importantly, expression of WT alleles of *ltaS* or *ltaA* in the parental *ypfP* mutant background did not increase anaerobic viability, indicating that the increase in viability observed is not due to overexpression of the cloned genes but rather the specific mutations within the genes.

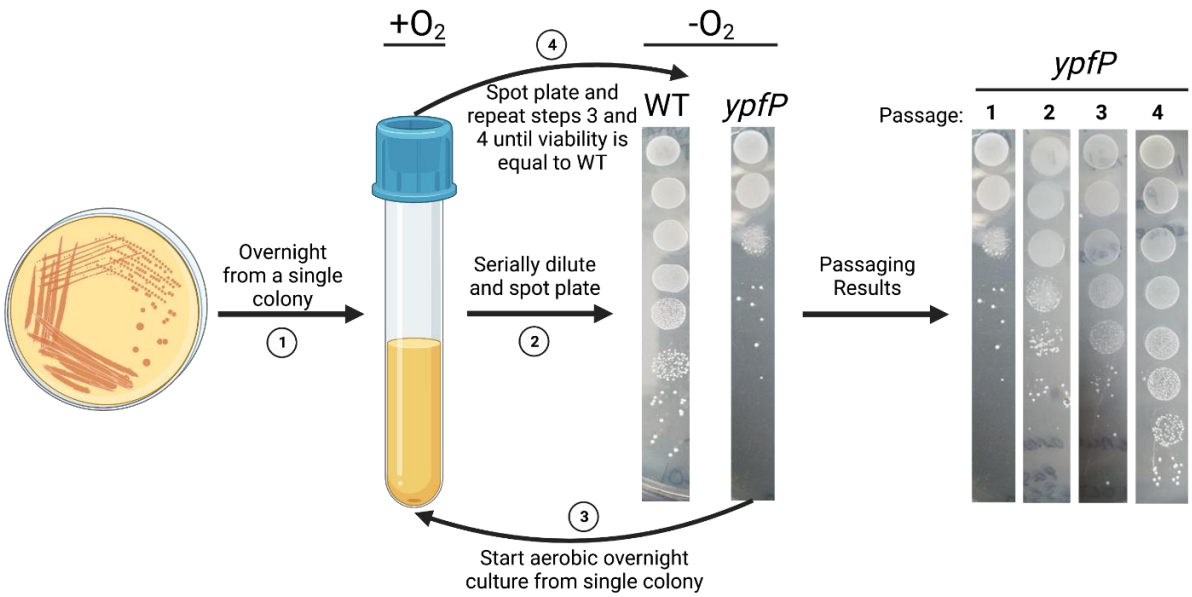

Figure 2-7. An illustration of the method used to isolate ypfP suppressor mutants. For more detailed information see methods. 1) An overnight culture was started from an individual colony. 2) The overnight culture was serially diluted, spot platted, and incubated in anaerobic conditions. 3) An individual colony from the *ypfP* spot plate was used to start an aerobic overnight culture. At this point, one pass has been completed. 4) The passaged *ypfP* mutant was serially diluted and spot plated again and repeated until viability was equal to the WT. Image created using Biorender.

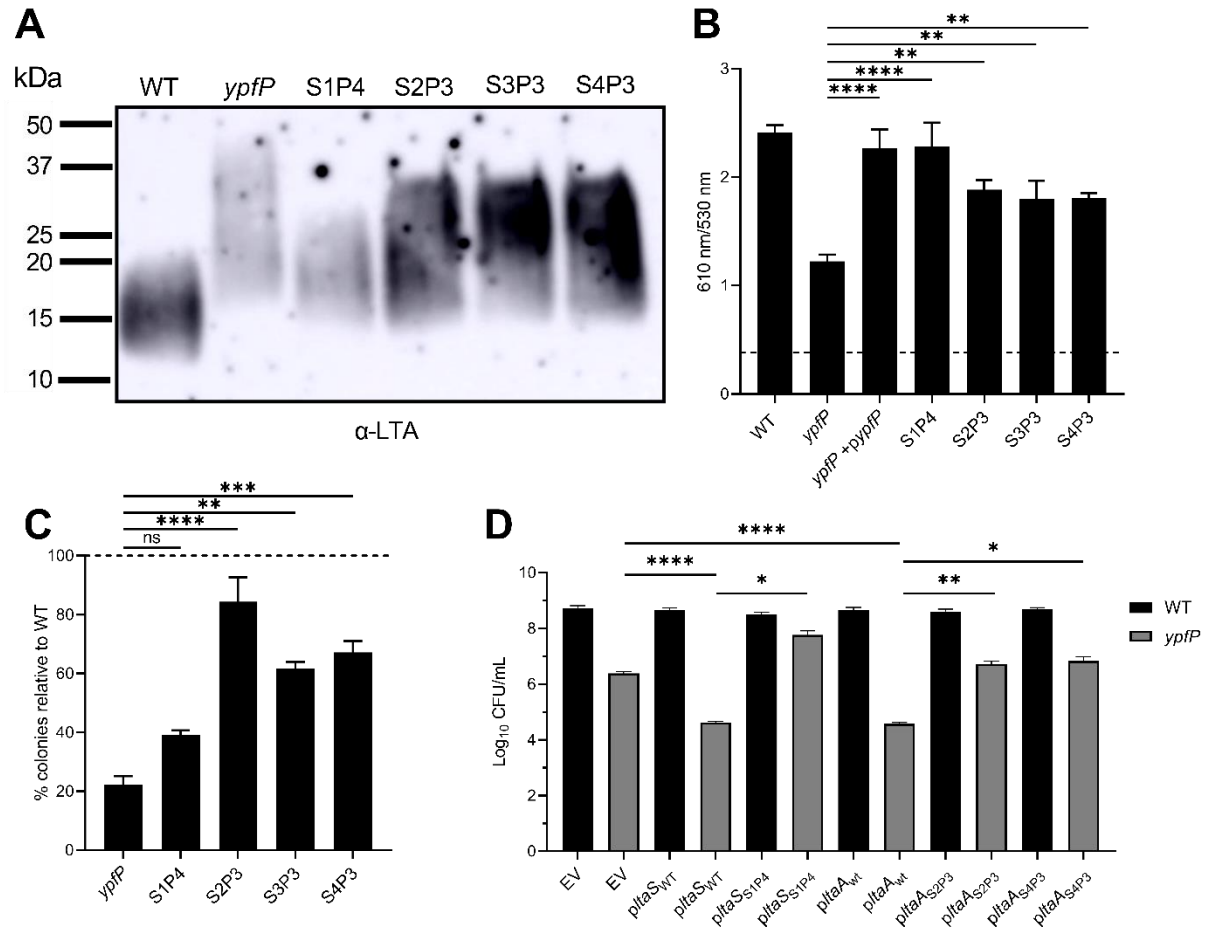

Figure 2-8. Passaged ypfP mutants harbor suppressor mutations that lead to phenotypic differences in membrane potential, gentamicin resistance and LTA.

(A) Immunoblot of LTA isolated from cells grown aerobically to late exponential phase. Passaged *ypfP* mutants are named to reflect the lineage number and the passage at which they reached viability equal to that of the WT. For example, S1P4 represents passaged lineage 1, which reached WT-like viability after four passes under anaerobic conditions. (B) Anaerobic membrane potential was measured using the fluorescent dye $DiOC_2$. Data are means from three independent experiments performed in technical triplicate. Error bars represent one standard deviation from the mean. Significance was determined using one-way ANOVA with multiple comparisons. ****, $P < 0.0001$; **, $P < 0.01$. (C) Percent gentamicin-resistant colonies relative to the WT (dotted line). Data represent 3 independent experiments. Error bars represent one standard deviation from the mean. Significance was determined using one-way ANOVA with multiple comparisons. ****, $P < 0.0001$; ***, $P < 0.001$; **, $P < 0.001$. (D) Strains were serially diluted, spot plated onto TSA, and incubated anaerobically and CFU were enumerated for the WT and the parental *ypfP* mutant complemented with empty pOS (EV), WT *ltaS* or *ltaA* ($ltaS_{WT}$ and $ltaA_{WT}$), mutated *ltaS* from S1P4 ($ltaS_{S1P4}$), or mutated *ltaA* from S2P3 or S4P3 ($ltaA_{S2P3}$ and $ltaA_{S4P3}$). Data are means from 3 independent experiments. Error bars represent one standard deviation from the mean. Significance was determined using a two-tailed *t* test. ****, $P < 0.0001$; **, $P < 0.01$; *, $P < 0.05$.

Discussion

Multiple respiration-arresting conditions impeded proliferation of the *S. aureus ypfP* mutant, including exposure to the clinically relevant aminoglycoside antibiotics gentamicin and tobramycin, treatment with HQNO, and coculture with *Pseudomonas aeruginosa*. We posit that the reduced viability primarily stems from distorted LTA produced by the *ypfP* mutant, based on the observations that (i) alteration of the LTA produced by the *ypfP* mutant is exacerbated when the strain is cultured anaerobically (ii) the anaerobic membrane potential generated in the *ypfP* mutant is significantly reduced, and (iii) the anaerobic viability defect is suppressed by supplementation with cations. The fact that LTA maintains ion homeostasis via binding of external cations to the negatively charged polyglycerol phosphates supports this model (12). If altered production of LTA causes decreased proliferation during respiration arrest, one would predict that inactivation of other LTA synthesis genes, such as *ltaA*, would elicit similar phenotypes. In fact, we observed that anaerobic viability of *ltaA* mutants was similar to that of the WT, indicating that defective proliferation during respiration arrest is specific to mutation of *ypfP* (Fig. 2-5C). On the surface, this result appears to conflict with a model implying a primary role for LTA, but there are significant differences between genetic inactivation of *ltaA* and *ypfP*. The first is that *ltaA* mutants retain production of Glc_2-DAG, which accumulates in the membrane (53). This finding supports the notion that Glc_2-DAG is protective in the *ltaA* mutant. However, another considerable difference between the mutants is the LTA they produce (Fig. 2-5D) (53). Ntoably, we demonstrate that whereas anaerobic growth further alters LTA produced by the *ypfP* mutant, it is relatively unperturbed in *ltaA* mutants (Fig. 2-5D). Additionally, our findings are similar to phenotypes observed when LTA production is completely ablated via *ltaS* mutation. *ltaS* mutant cells display severe viability defects that are suppressed by supplementation with high salt (54, 147, 148). The

finding that anaerobic proliferation defects observed in *ypfP* mutants phenocopy *ltaS* inactivation, albeit to a lesser degree, lends additional support to the inference that disrupting LTA production is the primary driver of the respiration arrest-related growth defect. Therefore, defining the molecular nature of LTA produced in anaerobically cultured *ypfP* mutant cells will likely provide additional mechanistic details of ion homeostasis in *S. aureus*. For example, LTA GroP can be modified via addition of D-alanine residues to neutralize the negative charge and increase resistance to antimicrobial peptides (79). How this modification impacts ion homeostasis and membrane potential is uncertain but is an important consideration. Kiriukhin et al. found that LTA isolated from a *ypfP* mutant contained increased D-alanine compared to WT (51), while Fedtke et al. observed no difference in the D-alanylation status of LTA in *ypfP* mutant and WT cells (57). This conflicting evidence makes it unclear whether *ypfP* mutant LTA is differentially D-alanylated; however, further investigation is warranted for a more complete understanding of the role LTA and its modifications play in maintaining membrane potential. An alternative explanation for the observed phenotypes is that an unknown YpfP function also contributes. In keeping with this supposition, the YpfP homolog in *Bacillus subtilis*, UgtP, regulates cell division by inhibiting assembly of the FtsZ ring (149); however, a bacterial two-hybrid experiment failed to show an interaction between *S. aureus* YpfP and FtsZ proteins (150).

The essentiality of LTA has been established (132). It is interesting, then, that disruption of LTA would have such an impact on viability in cells with respiration arrest but have no discernible effect on respiratory growth. Our data suggest that LTA functions to maintain membrane potential; however, only the anaerobically cultured *ypfP* mutant displayed reduced membrane potential (Fig. 2-6A). A possible explanation is that during aerobic growth, the electron transport chain is functional and generates a proton gradient at the surface of the cell at a rate that is sufficiently high

to maintain membrane potential despite the loss of cations to the surrounding medium. Conversely, cells in which respiration is arrested hydrolyze ATP in order to generate a proton gradient. Therefore, it is possible that anaerobically cultured cells spend considerable energy generating a proton gradient that is subsequently lost to the surrounding medium, ultimately depleting the ATP of the cell as it attempts to maintain the proton gradient. Such a dynamic is beyond the scope of this work, but warrants further investigation.

Consistent with a modl of LTA supporting anaerobic proliferation, all characterized *ypfP* suppressor lineages were shown to have lower-molecular-wight LTA than the parental *ypfP* mutant (Fig. 2-8A). Similar results were observed by Hesser et al., who found that *ltaS* mutantions in a *ypfP* mutant background resulted in LTA more similar in length to that of the WT (59). While one of our suppressor lineages (S1P4) harbored a mutation I *ltaS*, three others (S2P3), S3P3, and S4P3) all had mutations in *ltaA*, which has not been previously reported to suppress the *ypfP* mutant phenotype. The lower-molecular-weight LTA likely restored the ability of the ell to maintain membrane potential (Fig. 2-8B), highlighting the importance of LTA length in this phenotype. However, when challenged with gentamicin, S1P4, which exhibited decreased LTA abundance, did not regain the capacity to resist the aminoglycoside. In addition to entering a fermentative state to gain gentamicin resistance, it may be possible that the relative abundance of LTA also plays an important role. In keeping with this, S2P3, S3P3 and S4P3 were able to generate gentamicin resistance, and all exhibited relatively greater LTA abundance than the parental *ypfP* mutant (Fig. 2-8A, dark bands). Conversely, S1P4 displayed LTA abundance more similar to that of the parental *ypfP* mutant (Fig. 2-8A, light bands). LTA has been implicated in facilitating resistance to cationic antimicrobial peptides, likely by regulating the cell surface charge via D-alanylation (79, 151), which has been known to affect the binding of aminoglycosides to teichoic acids (152).

Furthermore, abundance of LTA has been shown to promote antibiotic resistance, as *S. aureus* cells with reduced cell-associated LTA were shown to be more sensitive to oxacillin (153). Therefore, it is likely that both the length and abundance of LTA are important factors that coordinate the necessary machanisms needed for gentamicin resistance.

Our results show that the LTA glycolipid anchor is required for maximal metabolic versatility of *S. aureus*. Cells deficient for its production demonstrate severe proliferation defects during respiration arrest, likely due to a loss of membrane potential. We show that cells with LTA more similar to the WT in abundance and size are able to restore fermentative viability and more readily resist aminoglycoside treatment. Therefore, LTA continues to be a promising target for the treatment of recalcitrant *S. aureus* infections, and its disruption could enable the use of antibiotics that were previously ineffective.

Materials and Methods

Bacterial strains and growth conditions used in this study

Bacterial strains used in this study are described in Table A-2. All strains are derivaties of *S. aureus* isolate Newman (NWMN) (154). *S. aureus* was routinely cultured in tryptic soy broth (TSB) or TSA. The *ypfP* and *ltaA* transposon insertion mutants were obtained from the Nebraska Transposon Mutant Library and transduced into the respective backgrounds via phage φ85 transduction protocol as previously described (155). Antibiotic selection of erythromycin cassette-containing resistant recipient cells was achieved with 10 μg/mL erythromycin. Transposon mutants were verified by PCR using primers described in Table A-3. δ-Aminolevulinic acid (ALA) was supplemented at 75 μg/mL. The Δ*gtrR* mutants were checked for hemolytic activity on blood agar (Thermo Fisher Scientific). Mutants that retained hemolytic activity were tested for second-site mutations in the *sae* locus via Sanger sequencing of the *saeS* gene. Tobramycin was used at 5

μg/mL, and gentamicin was used at 5 μg/mL or 2 μg/mL, as indicated. Sodium chloride or potassium chloride was added to TSA at the indicated concentrations and mixed prior to sterilization. The pOS-*ypfP* plasmid was created using primers listed in Table A-3, the restriction enzymes XhoI and BamHI, and traditional ligation cloning methods. Plasmids pOS-*ltaA*, pOS-*ypfPltaA*, pOS-*ltaS*, and pOS-$ltaS_{S1P4}$ were created using the Gibson Assembly cloning kit (New England Biolabs). Plasmids pOS-$ltaA_{S2P3}$ and pOS-$ltaA_{S4P3}$ containing the mutated *ltaA* genes seen in S2P3 and S4P3 were generated via divergent PCR using pOS-$ltaA_{WT}$ as a template with the primers indicated in Table A-3. Linear PCR products were then recircularized before transformation. After construction, all plasmids were transformed into *Escherichia coli* DH5α. Selection of plasmid-containing clones was achieved using 100 μg/mL ampicillin and validated via sequencing performed at the Michigan State University Research Technology and Support Facility using primers pOS seq F and pOS seq R (Table A-3) or Plasmidsaurus. Plasmids were then electroporated into *S. aureus* strain RN4220 as an intermediate host before transformation into *S. aureus* strain NWMN. Selection of plasmid-containing clones in *S. aureus* and maintenance of plasmid-containing strains was achieved using 10 μg mL^{-1} chloramphenicol, unless otherwise specified. Overnight cultures were normalized to an OD_{600} of 1.0 and then diluted 1:100 into TSB for growth curve analysis. Flasks were incubated at 37°C shaking at 225 rpm for aerobic growth kinetics, and polystyrene tubes were incubated without shaking at 37°C in a Coy anaerobic chamber. Three aliquots of 200 μL were pipetted into a 96-well plate, and the OD_{600} was measured at 2-h intervals for aerobic cultures or 3-h intervals for anaerobic cultures.

Determination of percent aminoglycoside resistance

Overnight cultures of WT and *ypfP* mutant cells were normalized to an OD_{600} of 0.1 in phosphate-buffered saline (PBS), and 100 μL was plated onto TSA containing 5 μg/mL gentamicin

or tobramycin. Plates were incubated at 37°C and colonies were enumerated after 24 h. Percent relative resistance was determined by dividing the number of colonies of the mutant strain by the number of colonies of the WT. Values were then plotted, and the WT value was set to 100%.

P. aeruginosa coculture and HQNO Kirby-Bauer assays

Overnight cultures of WT or *ypfP* mutant cells were plated onto 20-mL TSA plates using sterile cotton swabs. Following plating, 2 μL of an overnight culture of *P. aeruginosa* PAO1 was spotted in the middle of the plate. Similarly, 20-mL TSA plates containing the WT or the *ypfP* mutant were prepared, and a sterile Whatman disk containing 10 μL of 1 mg/mL HQNO or pyocyanin (Cayman Chemical) was placed in the center of the plate. Plates were incubated at 37°C overnight. The zone of inhibition and the diameter of the *P. aeruginosa* colony were measured using an electronic caliper (Pittsburgh 6-in. composite digital caliper).

Aerobic and anaerobic CFU enumeration

Overnight cultures were normalized to an OD_{600} of 1.0 in PBS. The normalized culture was serially diluted in PBS in a 96-well plate. Ten microliters of each dilution was spotted onto TSA. Plates were incubated at 37°C aerobically or in an anaerobic chamber (Coy). Colonies were enumerated after 24 h (aerobic) or 48 h (anaerobic), and the number of CFU per milliliter was calculated. Each experiment was performed in biological triplicate, with three technical replicates per biological replicate. The three log values were then plotted using GraphPad Prism.

LTA Western blot analysis

For aerobic versus anaerobic analysis of LTA, overnight cultures were normalized to the OD_{600} of WT cells, subcultured 1:1,000 in TSB, and grown with shaking at 225 rpm at 37°C for 15 h aerobically or anaerobically. After 15 h of growth, the cultures were normalized to the WT OD_{600} in 1-mL aliquots in 2-mL screw-cap tubes containing 0.5 mL 0.1-mm zircon beads. The cells

were subjected to bead beating for 45 s on a Mini-Beadbeater 16 (BioSpec). The tubes were then centrifuged at 300 × *g* for 1 min, and the supernatant was decanted into a fresh sterile 1.5-mL Eppendorf tube. The supernatant was centrifuged at 13,300 × *g* for 15 min to sediment membranes and LTA. The pellet was resuspended in 80 μL of PBS. Twenty microliters of 5× SDS sample buffer was added to the resuspended pellet. Twenty microliters of the mixture was loaded into a 15% poly-bis-acrylamide gel. Samples were run for 10 min at 50 V and then ~2 h at 100 V or until the dye front reached the bottom of the gel. Samples were transferred to polyvinylidene fluoride (PVDF) at 4°C at 100 V for 1 h. The PVDF membrane was blocked using PBST (1× PBS plus 0.05% [vol/vol] Tween 20 plus 5% milk) blocking buffer for 1 h, washed twice in fresh blocking buffer for 10 min each time, and exposed to blocking buffer supplemented with a 1:1,000 dilution of primary anti-LTA (polyglycerol-specific) mouse antibody (Hycult Biotechnology). After 1 h, the membrane was washed twice in blocking buffer and exposed to blocking buffer containing 1:5,000 horseradish peroxidase-conjugated secondary anti-mouse immunoglobulin goat antibody (Millipore) for an additional hour. Enhanced chemiluminescence (ECL) western blotting substrate (Promega) and film were used to detect immunoreactive LTA.

For the analysis of LTA from *ypfP* suppressor lineages, overnight cultures were started from a single colony and grown in TSB overnight at 37°C. Cultures were back diluted 1:100 in fresh TSB and grown aerobically to an OD_{600} equal to 0.7. A 1-mL aliquot was pelleted and resuspended in 45 μL TSM (50 mM Tris, 500 mM sucrose, 10 mM $MgCl_2$; pH 7.5). The cell wall was digested by adding 5 μL of 2 mg/mL lysostaphin and incubating at 37°C for 30 min. After incubation, 50 μL of 2× SDS-PAGE loading buffer was added, and the sample was incubated at 95°C for 30 min. The sample was then centrifuged at 13,000 × *g* for 2 min and the supernatant was collected. A 1-μL volume of proteinase K (Thermo Fisher Scientific) was added to the sample and incubated at 50°C

for 2 h. For each sample, 20 μL was loaded into a 4-to-20% poly-bis-acrylamide gel (Bio-Rad). Samples were run for 30 min at 90 V and then 45 min at 150 V. The gel was then transferred and stained as described above.

Measurement of membrane potential

The electrochemical potential of the cells was determined using the fluorescent dye $DiOC_2$ (Millipore-Sigma). Cultures were grown to exponential phase aerobically (OD_{600} equal to 0.6) or anaerobically (OD_{600} equal to 0.3). All aerobic cultures reached exponential phase after approximately 3.5 h of growth. Anaerobic cultures reached exponential phase at approximately 5 h (WT), 8 h (S1P4, S2P3, S3P3, and S4P3), and 14 h (*ypfP* mutant). Culture volumes of 4 mL were pelleted and resuspended in an equal volume of PBS. Three 1-mL aliquots of the resuspension were made. One aliquot received no treatment, one received 10 μL of 500 μM CCCP as a negative control and 10 μL of 3 mM $DiOC_2$, and the last aliquot received 10 μL of $DiOC_2$. The tubes were incubated in the dark for 25 min at room temperature. After incubation, three 200-μL samples from each tube were pipetted into three wells of a black-walled 96-well plate. Fluorescence emission was measured at 530 nm and 610 nm from an excitation at 488 nm using a Synergy H1 plate reader (Biotek). Autofluorescence values from the untreated samples were subtracted from both the CCCP-treated and non-CCCP-treated samples prior to calculation of the ratio. The data represents the 610-nm fluorescence divided by the 530-nm fluorescence.

Optical density and pH measurements of anaerobic liquid cultures

Overnight 5-mL cultures of the WT and *ypfP* mutant were started from single colonies and grown at 37°C with shaking. Cells were pelleted, washed in PBS, and normalized to an OD_{600} of 1.0. Cultures (100 mL) were inoculated to a starting OD_{600} of 0.01 and grown anaerobically at 37°C in a Coy anaerobic chamber. Ten-milliliter volumes of the WT and *ypfP* cultures were collected at

0-, 2-, 4-, 6-, 8-, 12- and 24-h time points. A 1-mL volume of each time point sample was used to measure OD_{600} with a Genesys 140 Visible spectrophotometer (Thermo Fisher Scientific). The remaining 9 mL of sample was pelleted, and the supernatant was filtered. The pH of the sterile supernatant was measured using a FiveEasy Plus FEP20 pH meter (Mettler Toledo).

Antimicrobial activity assays of PMF-targeting inhibitors

CCCP, valinomycin, and nigericin were solubilized in dimethyl sulfoxide (DMSO). The compounds were serially diluted 2-fold in 96-well plates prior to inoculation. The plates were incubated at 37°C for 16 h, the wells were then resuspended via pipetting, and the OD was measured at 600 nm. The values for the untreated control wells were averaged, and this value was used to represent 100% growth. The values for the rest of the wells were averaged and compared to that 100% value. Experiments were performed in at least biological triplicate with three technical replicates per biological replicate unless otherwise indicated. The results for technical replicates were averaged for each biological replicate, and the values for biological replicates were graphed using GraphPad Prism. The regression line for nonlinear fit was used to determine the best fit line.

Fluorescence microscopy

S. aureus cultures were grown overnight at 37°C in TSB and subsequently diluted 1:10 in fresh medium. Cultures were then grown to mid-log phase (OD_{600} equal to 0.5) at 37°C and treated with 2 μg/mL gentamicin, where indicated, for a period of 2 h. Following the growth period, 1-mL aliquots of the cultures were washed in 1× PBS, and then cell pellets were resuspended in 100 μL of 1× PBS. Cells were stained with 1 μg/mL FM4-64 in order to visualize the cell membrane. Five microliters of sample was transferred to a glass-bottom culture dish (MatTek) and then covered with a 1% agarose pad. All imaging was conducted at room temperature using a DeltaVision Core microscope system (Applied Precision/GE Healthcare) equipped with an environmental chamber.

All images were captured using a Photometrics Coolsnap HQ2 camera, and data were deconvolved using SoftWorx software supplied by the microscope manufacturer.

Isolation of *ypfP* suppressor mutants and SNP analysis

From individual colonies, overnight cultures of WT and the *ypfP* mutant were incubated at 37°C with shaking. Cultures were normalized to an OD_{600} of 1.0 in TSB. Normalized growth was serially diluted in PBS in a 96-well plate, and 10 µL of each dilution was spotted on two TSA plates, one of which was incubated aerobically (as a control) at 37°C and the other anaerobically at 37°C. Large, individual *ypfP* mutant colonies were selected from the anerobic plate and cultured aerobically in 5 mL TSB at 37°C with shaking. The overnight culture was then serially diluted again and spot plated as described above, along with a newly cultured WT as a reference for viability. This process was repeated until a *ypfP* suppressor mutant was obtained that had viability equal to that of the WT and is visually summarized in Fig. 2-7.

Genomic DNA was isolated from 5-mL overnight cultures started from individual colonies grown aerobically at 37°C with shaking. The culture was pelleted and resuspended in 485 µL TSM. A volume of 15 µL 2 mg/mL lysostaphin was added to the resuspension and incubated at 37°C for 30 min. The samples were then pelleted, and the Wizard genomic DNA purification kit (Promega) was used to isolate the genomic DNA. Whole-genome sequencing was performed via Illumina sequencing at the Microbial Genome Sequencing Center. Sequence read processing, alignment, and single nucleotide polymorphism (SNP) analysis were performed using Geneious Prime version 2022.0.2. The genomic sequence of *S. aureus* strain Newman (GenBank accession number AP009351.1) was used as a reference genome for all genomic analysis.

Acknowledgments

The following were provided by the Network on Antimicrobial Resistance

in *Staphylococcus aureus* (NARSA) for distribution by BEI Resources, NIAID, NIH: *Staphylococcus aureus* subsp. *aureus* strain JE2 transposon mutant NE1663 (NR-48205, SAUSA300_0918, *ypfP*) and NE462 (NR-47005, SAUSA300_0917, *ltaA*). We thank Olaf Schneewind at the University of Chicago for supplying the pOS complementation plasmid, Chris Waters at Michigan State University for the *P. aeruginosa* PAO1 strain, and members of the Hammer and Eswara laboratories for critical evaluation of the manuscript.

This work was funded by the American Heart Foundation 16SDG30170026 (N.D.H.), start-up funds provided by Michigan State University (N.D.H.), and the National Institutes of Health R35 GM133617 (P.J.E.) and R21 AI144504 (N.D.H.).

Chapter 3: A redundant isoprenoid biosynthetic pathway supports *Staphylococcus aureus* metabolic versatility.

Abstract

Isoprenoids are ubiquitous molecules that serve as fundamental building blocks for life. In bacteria, isoprenoids are precursors for carotenoid pigments, respiratory cofactors, and essential sugar carrier lipids such as lipid II. Isoprenoid synthesis initiates via condensation of the five-carbon (C_5) precursors, isopentenyl diphosphate (IPP) and dimethylallyl diphosphate (DMAPP). This initial reaction condenses one DMAPP and two IPPs, resulting in the C_{15} farnesyl diphosphate (FPP), an intermediate that is sequentially elongated with IPP. FPP is thought to be synthesized exclusively by the prenyl diphosphate synthase (PDS) IspA. In *Staphylococcus aureus*, *ispA* mutants lack the golden carotenoid pigment staphyloxanthin. The fact that *ispA* can be inactivated in *S. aureus* and other bacteria is surprising given the reliance of lipid II on FPP and supports the hypothesis that an additional enzyme produces the critical isoprenoid precursor. We isolated pigmented *ispA* suppressor mutants harboring SNPs within a second PDS-encoding gene, *hepT*, suggesting that HepT and IspA have overlapping roles in *S. aureus* isoprenoid synthesis. Subsequent work determined that IspA and HepT support metabolic versatility, as a *hepT ispA* double mutant fails to aerobically respire, partially due to a lack of prenylated heme cofactors. The finding that a *hepT ispA* double mutant is viable supports a model whereby a third PDS compensates in the absence of *ispA* and *hepT* to produce lipid II precursors. Lastly, we show that *ispA* and *hepT* mutants exhibit colonization defects in a murine model of systemic infection, demonstrating that isoprenoid biosynthesis is a potential drug target for combating *S. aureus*.

Introduction

Isoprenoid synthesis is a highly conserved process present in virtually all living organisms and begins with the production of the universal five-carbon (C_5) precursors isopentenyl diphosphate (IPP) and dimethylallyl diphosphate (DMAPP) (116, 156). An initial condensation reaction of one DMAPP and one IPP produces geranyl diphosphate (GPP), to which a second IPP is immediately added to generate farnesyl diphosphate (FPP), a C_{15} isoprenoid that serves as a substrate for downstream cellular pathways (116). This initial condensation reaction and subsequent elongation reactions that add IPP units in a stepwise fashion, are carried out by enzymes called prenyl diphosphate synthases (PDSs) (116). Generally, bacteria harbor three PDSs: a short-chain PDS that catalyzes the initial condensation reaction between IPP and DMAPP to generate C_{10} GPP and then FPP; a medium-chain PDS that uses FPP and several additional IPP to produce medium-chain length isoprenoids; and a long-chain PDS, that also uses FPP and IPP to generate long-chain isoprenoids (157–163). Medium-chain isoprenoids range in length from C_{35} to C_{50} and support production of quinone respiratory cofactors (164, 165). Long-chain isoprenoids are C_{55} or greater and in bacteria include undecaprenyl phosphate (Und-P) which serves as a scaffold onto which glycan units are added to generate lipid II; an indispensable metabolite required for generating peptidoglycan (112, 165). Lipid II is essential for cell viability and is the target of several classes of antibiotics (112, 166–168). Therefore, a greater understanding of isoprenoid synthesis in bacteria will reveal fundamental mechanisms by which critical isoprenoid precursors are allocated to support cell envelope maintenance and metabolism.

In the Gram-positive pathogen *Staphylococcus aureus* FPP is a substrate for three reactions: condensation, elongation or prenylation, the covalent addition of an isoprenoid directly to a substrate. Condensation of two FPPs, generated by the short-chain PDS IspA, is catalyzed by

CrtM to generate dehydrosqualene, a C_{30} precursor for staphyloxanthin, the membrane localized carotenoid antioxidant that gives the pathogen its distinctive golden pigment (111). As such, *ispA* and *crtM* mutants are not pigmented (169, 170). Elongation reactions add IPP to FPP in a step wise fashion. At least two elongation reactions are active in *S. aureus*. The first is catalyzed by UppS, the enzyme that produces long-chain Und-PP, which serves as a lipid carrier for the transport of polysaccharides across the cytoplasmic membrane. Saccharide-based molecules generated by *S. aureus* include peptidoglycan, wall teichoic acid (WTA) and in some strains capsular polysaccharide (CP) (11, 112, 171). Importantly, each of these polysaccharide cell surface structures are either essential (peptidoglycan) or contribute to virulence (WTA and CP), making UppS an essential enzyme and a high priority target for therapeutic intervention (112, 172–174). Given the essentiality of UppS, it is surprising that the enzyme which produces the FPP substrate for its activity (IspA) is dispensable. Mutants lacking functional *ispA* have been generated in several different bacterial species including *S. aureus*, *E. coli*, *P. aeruginosa* and *B. subtilis* (115, 175–178). In *S. aureus ispA* mutants produce reduced quantities of FPP compared to WT, indicating that another PDS is capable of producing FPP (115). Therefore, clarifying the PDS enzymes that generate UppS substrates will lead to a better understanding of lipid carrier synthesis and peptidoglycan homeostasis.

The second elongation is carried out by HepT. HepT homologs in *B. subtilis* (HepT) and *E. coli* (IspB) produce the medium chain isoprenoids used in menaquinone (MK) synthesis (118, 160, 176, 179). Notably, *E. coli* also makes ubiquinone (UQ), which similarly incorporates medium chain length isoprenoids (180). MK and UQ function as electron carriers within the electron transport chain. *S. aureus* produces only MK, of which three species are synthesized that differ only in the length of the isoprenoid group, MK-7, MK-8 and MK-9 (113, 114). The number

refers to the C_5 isoprenoid moieties, thus MK-7, MK-8 and MK-9 have chain lengths of C_{35}, C_{40}, and C_{45}, respectively. Of note, some strains of *S. aureus* harbor HepT alleles that result in the production of a C_{50} MK-10 (113), which indicates that different *hepT* alleles influence the length of its isoprenoid product. These findings support a model whereby *S. aureus* HepT is required to generate MK, but direct experimental evidence of this model is lacking.

MK is a required cofactor for aerobic respiration, and *S. aureus* mutant strains impaired for MK synthesis are restricted to fermentative metabolism. This leads to a distinctive phenotype called the small colony variant (SCV), which usually coincides with increased antibiotic resistance (9, 114, 181, 182). In fact, MK auxotrophs are among the most common types of SCVs isolated from cystic fibrosis patients (81). Aminoglycoside treatment selects for SCVs because the antibiotic requires the proton motive force (PMF) to gain entry into the cell (134, 183, 184). In response, *S. aureus* develops inactivating mutations in the MK synthesis pathway, switching to fermentation and reducing the PMF (185). Notably, an *S. aureus hepT* mutant exhibited increased pigmentation but colony size or growth kinetics were not reported (170). Therefore, it is unclear whether mutation of *hepT* will induce the SCV phenotype. Additionally, whether HepT participates in other isoprenoid dependent pathways is uncertain, as HepT in *B. subtilis* and the *E. coli* HepT homologue IspB are essential for cell viability, suggesting medium chain PDSs may function beyond MK and UQ synthesis (186, 187). In fact, loss of heptaprenyl diphosphate synthase activity in *B. subtilis* was only tolerated when grown on media supporting cell wall-free (L-form) growth, indicating that this pathway may play a role in cell wall synthesis (188). The fact that *hepT* mutants are viable in *S. aureus* suggests that unique or redundant isoprenoid biosynthetic pathways exist in this species and presents an opportunity to study the physiological consequences of HepT inactivation, which is not possible in other bacterial species.

The third reaction, prenylation, also supports aerobic respiration through the covalent attachment of FPP to heme *b* to produce the modified heme cofactors heme *o* and heme *a*. Both prenylated heme cofactors are capable of supporting activity of the major terminal oxidase QoxABCD (28, 117, 189). Therefore, isoprenoid prenylation is essential for one of the two enzymes that perform the last step of aerobic respiration, the reduction of O_2 to H_2O (28). A second terminal oxidase, CydAB functions in the absence of QoxABCD leading to a branched respiratory chain; however, CydAB activity is not dependent on heme *o* or heme *a* (4, 28). Whether IspA produces FPP needed to generate heme *o* or heme *a* is uncertain. The *ispA* mutant exhibits slightly increased aminoglycoside (gentamicin) resistance and reduced ATP production suggesting electron transport chain activity is attenuated (115). However, direct evidence that IspA provides the isoprenoid precursors required to generate the modified heme cofactors needed for QoxABCD activity is not known. Overall, resolving the contributions of IspA and HepT towards generating isoprenoid metabolites in *S. aureus* will provide novel insight into three major pathways: carotenoid pigment production, cell envelope maintenance, and respiration.

In this study we show that isoprenoid synthesis supports metabolic versatility in *S. aureus* by demonstrating that IspA and HepT preferentially contribute to carotenoid pigment and MK synthesis, respectively. Interestingly, either enzyme is sufficient for the generation of prenylated hemes, heme *o* and heme *a*, indicating that both can produce the FPP needed for heme prenylation. The basis for this conclusion is the finding that a *hepT ispA* mutant is viable but restricted to fermentative metabolism despite supplementation with the C_{20} MK analogue MK-4. These results support a model whereby a third enzyme generates FPP that is specifically used to produce Und-PP for peptidoglycan synthesis. Additional experimentation focused on chemically complementing MK deficiency using MK-4 demonstrated the shorter MK analogue promotes

QoxABCD but not CydAB activity. This result suggests that MK isoprenoid chain length plays an important role in CydAB function, indicating that the different MK species modulate activity of the branched respiratory chain. Lastly, we show that *ispA* or *hepT* mutants exhibit colonization defects in a murine model of systemic infection, providing evidence that the isoprenoid biosynthetic pathway is a potential drug target. Overall, these results support a revised model of *S. aureus* isoprenoid synthesis whereby precursors generated by specific enzymes are used to produce staphyloxanthin, MK, or Und-PP, but prenylation of heme can be achieved using precursor from either IspA or HepT. Our data demonstrate that redundancy within the isoprenoid synthesis pathways of *S. aureus* supports the metabolic versatility and virulence of this important human pathogen.

Results

Pigmented *ispA* suppressor mutants contain nonsynonymous gain-of-function mutations in *hepT*

A previous study reported that *ispA* mutants lack pigmentation and exhibit increased resistance to gentamicin (115). We recapitulated these results using an agar-based assay whereby an overnight culture of the *ispA*::Tn mutant was spread onto a TSA plate supplemented with 3 µg/mL gentamicin. Interestingly, pigmented colonies could be observed at a rate of 0.047% across three independent trials. These strains demonstrated WT-like levels of staphyloxanthin production indicating that they are potential suppressor mutants (Fig. 3-1A). Whole genome sequencing analysis revealed nonsynonymous mutations in the gene encoding heptaprenyl diphosphate synthase, *hepT* (Table A-4). Notably, all three resistant pigmentation suppressor mutants (*ispA*::Tn^{115}, *ispA*::Tn^{144} and *ispA*::Tn^{164}) shared the same A72E amino acid change five residues preceding the **f**irst **a**spartate **r**ich **m**otif (FARM) (Fig. 3-1B). This amino acid position is highly

conserved in IspA and HepT homologs (190) and has been implicated in determining the length of the isoprenoid product (191). The non-pigmented gentamicin resistant control isolate harbored an amino acid change 93 amino acids downstream of the HepT FARM domain (A165T). Given the activity of HepT, it is likely that a *hepT* mutant does not produce MK and therefore cannot perform respiration, resulting in the observed gentamicin resistance. Consistent with this, the *hepT* mutant has a slower growth rate compared to WT (Fig. 3-1C) as it relies on fermentation to generate energy. Growth rate analysis of the *ispA*::Tn gentamicin resistant colonies showed similar doubling times to the *hepT*::Tn mutant (Fig. 3-1C), suggesting that the *hepT* mutations likely lead to reduced production of the medium-chain isoprenoids necessary for MK synthesis. In fact, the altered FARM domain of $HepT^{A72E}$ increases in similarity to the FARM domain of other PDSs that are known to synthesize short-chain isoprenoids (191), and might be performing an IspA-like role in producing FPP needed for pigmentation.

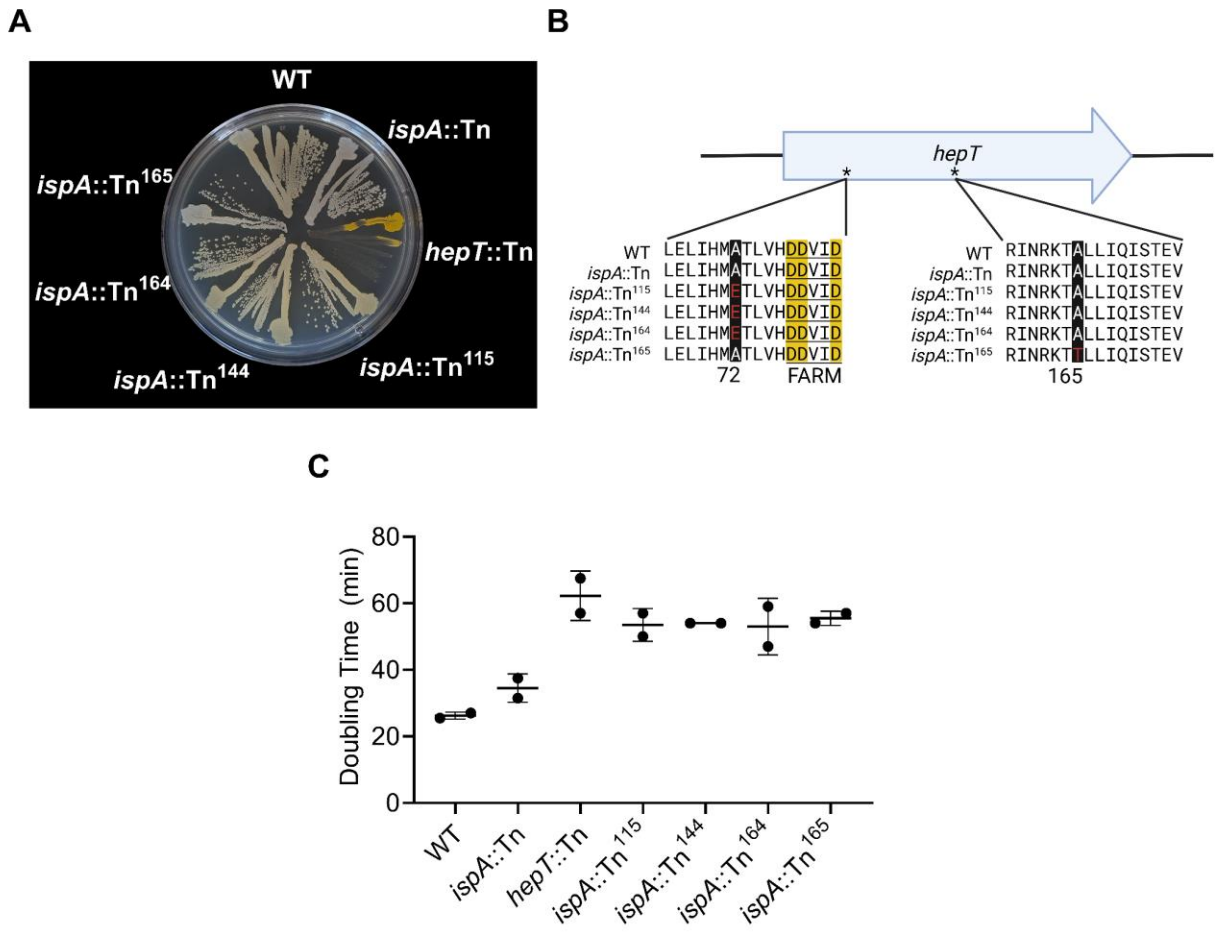

Figure 3-1. Pigmented ispA::Tn suppressors harbor SNPs within hepT.
(A) Indicated strains were streaked on TSA and incubated overnight. (B) Multiple alignment of the HepT amino acid sequence for the indicated strains. Conserved aspartic acid residues that comprise the first aspartic acid rich motif (FARM) domain are highlighted yellow. Black highlighted residues represent the amino acid position that was altered due to acquired mutations in the *ispA*::Tn gentamicin resistant mutants. (C) Doubling times of the indicated strains determined after incubation in TSB. Error bars represent one standard deviation from the mean.

Disruption of isoprenoid synthesis leads to downstream perturbations in the abundance of isoprenoid-derived metabolites

To determine the roles of IspA and HepT in the generation of downstream isoprenoid-containing metabolites, MK species, undecaprenyl phosphate (Und-P) and undecaprenol (Und-OH) were quantified via high-performance liquid chromatography (HPLC). The primary MK

species produced by WT was MK-8, followed by MK-7 and MK-9 (Fig. 3-2A), which is consistent with previous studies (113, 114). However, low levels of MK-5 and MK-6 were also detected in the WT, which, to the best of our knowledge, is the first report of *S. aureus* producing these MK species. Mutation of *ispA* resulted in increased production of longer chain MKs, with significantly higher production of MK-8 and MK-9 but decreased production of MK-7, while MK-5 and MK-6 were not significantly altered compared to the WT. Notably, *hepT*::Tn did not produce detectable levels of any MK species. Consistent with the hypothesis that the $HepT^{A72E}$ variant generates shorter chain isoprenoids, *ispA*::Tn^{115} produced significantly higher levels of MK-5 compared to the WT whereas MK-8 and MK-9 were not detected and MK-7 was significantly reduced (Fig. 3-2A). Notably, *hepT*::Tn contained significantly lower amounts of the lipid II precursor Und-P compared to WT (Fig. 3-2B). Additionally, all mutants demonstrated significantly lower quantities of Und-OH compared to WT, indicating both IspA and HepT may contribute to the production of precursors necessary for long-chain isoprenoid biosynthesis.

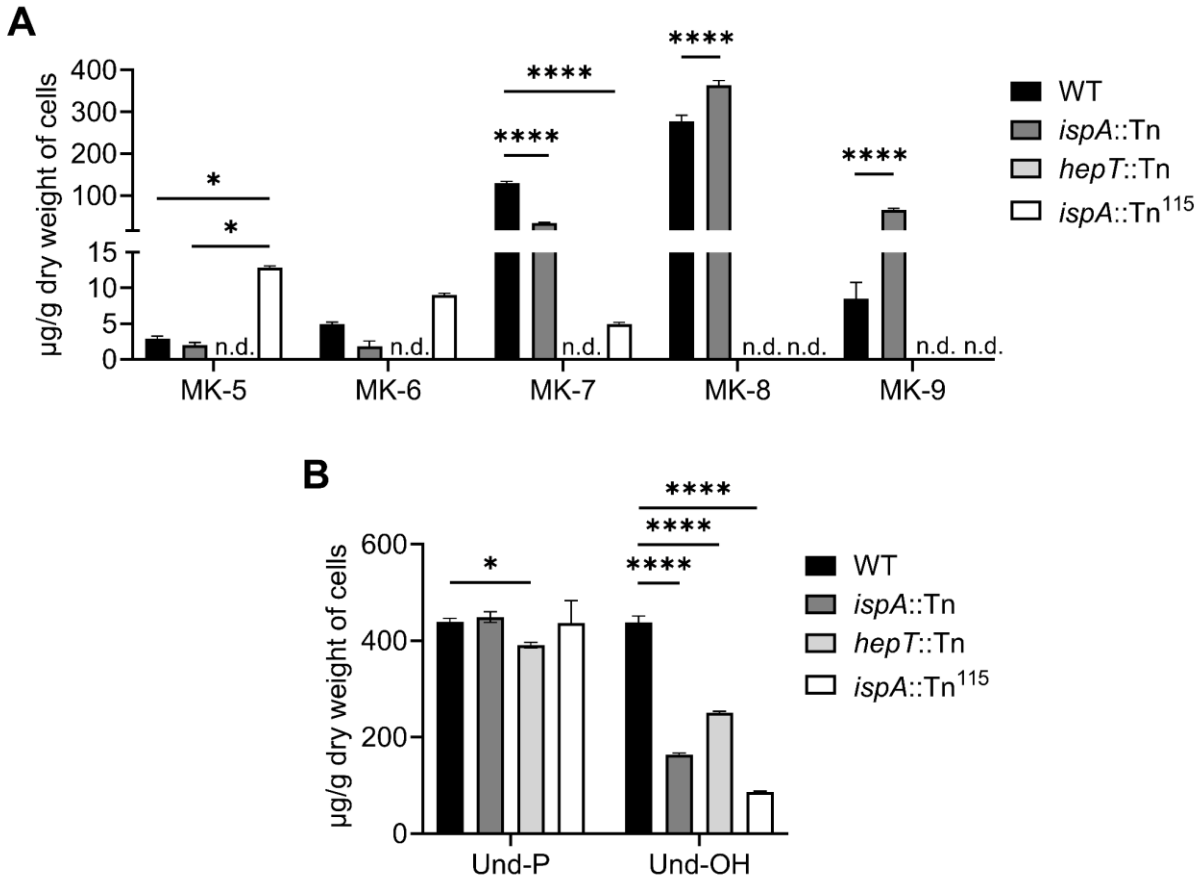

Figure 3-2. Mutating the PDS enzymes IspA and HepT alters the abundance of medium and long chain isoprenoid-containing metabolites.
A) High-performance liquid chromatography (HPLC) analysis of MKs extracted from whole cells. Error bars represent one standard deviation from the mean. Statistical significance was determined by two-way ANOVA with Tukey correction. * and **** represent *p*-values of <0.05 and <0.0001, respectively. n.d. (not detected) represents samples for which no MK was detected. B) HPLC analysis of undecaprenyl phosphate (Und-P) and undecaprenol (Und-OH) extracted from whole cells. Statistical analysis was determined by two-way ANOVA with Tukey correction. * and **** represent *p*-values of <0.05 and <0.0001 respectively. (A and B) Data are the average of three independent biological replicates performed in triplicate.

Simultaneous inactivation of *hepT* and *ispA* induces a small colony variant phenotype that is unresponsive to MK-4 supplementation

A consequence of inactivating *ispA* in *S. aureus* is reduced quantities of FPP, supporting a model whereby a second enzyme is capable of generating this indispensable precursor (115). Given that IspA and HepT are the only two enzymes that contain polyprenylsynthetase FARM domains in *S. aureus*, we hypothesized that simultaneous inactivation of both enzymes would result in synthetic lethality. An in-frame deletion of *hepT* was generated and subsequently transduced with φ85 propagated on the *ispA*::Tn mutant to yield the Δ*hepT ispA*::Tn double mutant. Surprisingly, the Δ*hepT ispA*::Tn double mutant was viable and displays growth kinetics similar to the Δ*hepT* single mutant and a respiration defective *menE*::Tn (MK deficient SCV) control strain (Fig. 3-3A). Supplementation of the growth medium with 12.5 μM MK-4 restored growth of the Δ*hepT* parental strain and *menE*::Tn control mutant to WT-like levels, indicating that respiration was restored in these mutants. This result suggests that the slower growth rate observed in these mutants is driven by a lack of MK that restricts cells to fermentation. However, MK-4 supplementation failed to stimulate increased proliferation of the Δ*hepT ispA*::Tn mutant, demonstrating that the strain is unable to aerobically respire. Genetic complementation of the Δ*hepT ispA*::Tn double mutant with plasmid-encoded *hepT* or *ispA* restored pigmentation and growth kinetics to that of the respective single mutant (Fig. 3-4A and B). These results confirm that the SCV phenotype observed in the Δ*hepT ispA*::Tn double mutant is not due second site mutations. Given the hyperpigmentation of the *hepT* mutant and the importance of *ispA* in staphyloxanthin production, we tested whether loss of the antioxidant carotenoid pigment was responsible for the respiration defect. A Δ*hepT crtM*::Tn double mutant was constructed and exhibited WT-like colony size compared to the SCV variant phenotype of the Δ*hepT ispA*::Tn

(Fig. 3-5A). Additionally, MK-4 supplementation restored proliferation of Δ*hepT crtM*::Tn (Fig. 3-5B), demonstrating that loss of pigmentation is not responsible for the Δ*hepT ispA*::Tn double mutant SCV phenotype or the failure of MK-4 supplementation to complement proliferation and aerobic respiration.

S. aureus predominantly produces lactate as a major fermentation end product (4, 23). To confirm that the Δ*hepT ispA*::Tn double mutant is restricted to fermentation regardless of MK supplementation, we quantified lactate production. WT and *ispA*::Tn mutants produced low amounts of L-lactate regardless of MK-4 supplementation (Fig. 3-3B), indicating that respiration is the primary energy generating pathway in these strains. The *menE*::Tn control SCV produced high levels of L-lactate that were significantly reduced upon MK-4 supplementation. This is similar to the Δ*hepT* single mutant and demonstrates that MK-4 induces respiration in these mutants. However, the Δ*hepT ispA*::Tn double mutant produced high levels of L-lactate that were not significantly reduced upon supplementation with MK-4 (Fig. 3-3B). Together, these results demonstrate that Δ*hepT ispA*::Tn is not capable of aerobic respiration, and is fermenting as the primary energy generating pathway.

Next, we sought to determine whether the failure of the Δ*hepT ispA*::Tn double mutant to respond to MK supplementation is due to a general respiration deficiency or if it is specific to aerobic respiration. To test this, the Δ*hepT ispA*::Tn mutant was cultured anaerobically in the presence or absence of MK-4 and the alternative terminal electron acceptor, nitrate (provided as KNO_3) as *S. aureus* is capable of anaerobic respiration when nitrate is supplied to the growth medium (22, 42). WT, *ispA*::Tn, Δ*hepT* and Δ*hepT ispA*::Tn proliferated to similar end-point optical densities (Fig. 3-3C). Addition of the terminal electron acceptor, KNO_3, increased the end-point optical density of the WT and *ispA*:Tn mutant, which produce MK and are therefore capable

of anaerobically respiring. Addition of both MK-4 and KNO_3 increased the end-point optical density of all strains, including the Δ*hepT ispA*::Tn double mutant (Fig. 3-3C). Together, these data show that the Δ*hepT ispA*::Tn double mutant is capable of anaerobic respiration via supplementation with MK-4, implying that the SCV phenotype is specific to aerobic respiration.

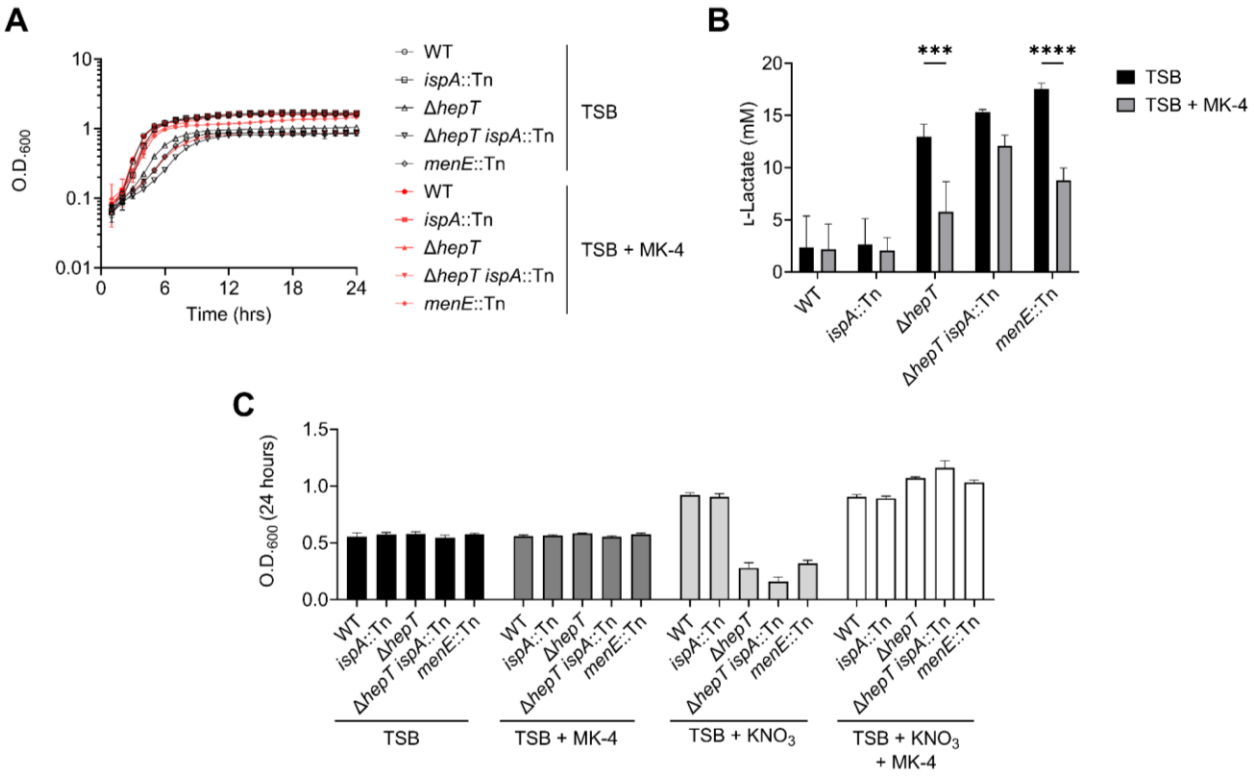

Figure 3-3. Simultaneous inactivation of hepT and ispA impairs aerobic respiration. (A) Growth curve analysis of the indicated strains in TSB with or without supplementation with 12.5 µM MK-4. Error bars represent one standard deviation from the mean. (B) The concentration of excreted L-Lactate was determined from cell-free supernatants of the indicated strain. Statistical significance was determined by two-way ANOVA analysis with Bonferroni correction. Error bars represent one standard deviation from the mean. *** and **** represent p-values of <0.001 and <0.0001 respectively. (C) Anaerobic terminal optical density at 24 hrs after incubation of the indicated strains cultured in TSB, TSB supplemented with MK-4, TSB supplemented with KNO_3 or TSB supplemented with both KNO_3 MK-4. Error bars represent one standard deviation from the mean.

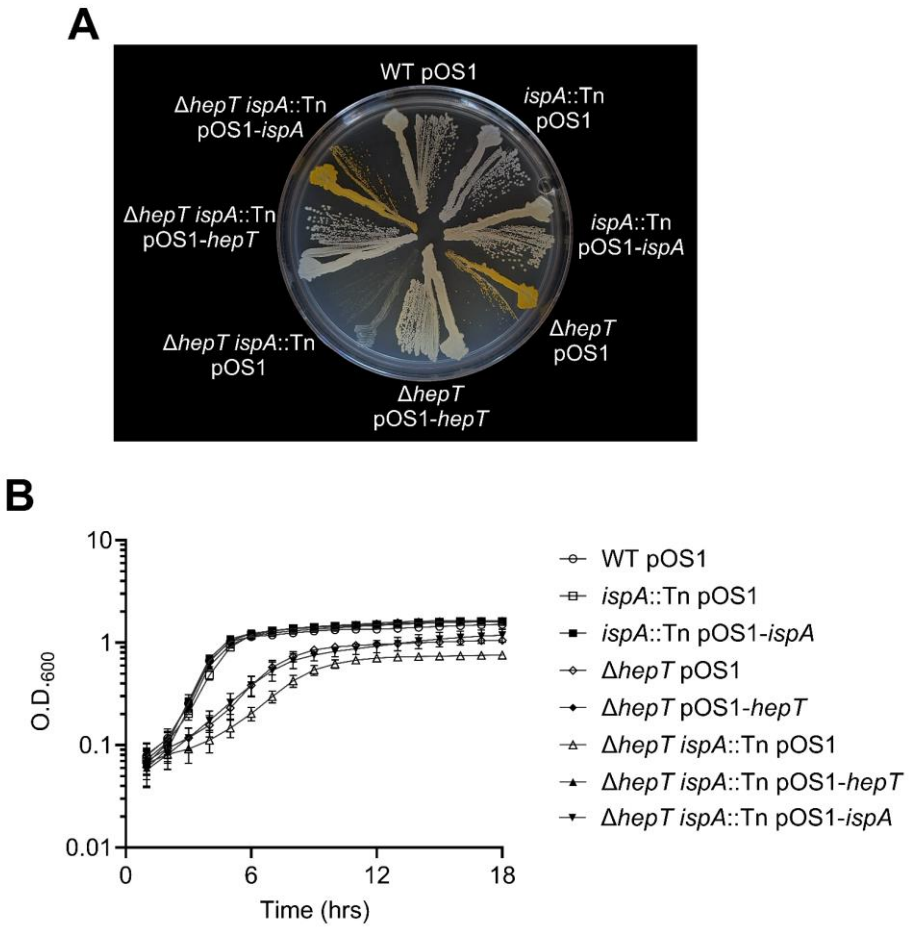

Figure 3-4. ΔhepT ispA::Tn harboring plasmid encoded copies of hepT or ispA exhibit phenotypes of corresponding single mutants.

A) An overnight incubation of the indicated strains were streaked onto TSA supplemented with 10 µg/mL chloramphenicol and 12.5 µM MK-4. (B) Growth curve analysis of the indicated strains grown in TSB supplemented with 10 µg/mL chloramphenicol. Data are the average of three independent biological replicates performed in technical triplicate. Error bars represent one standard deviation from the mean.

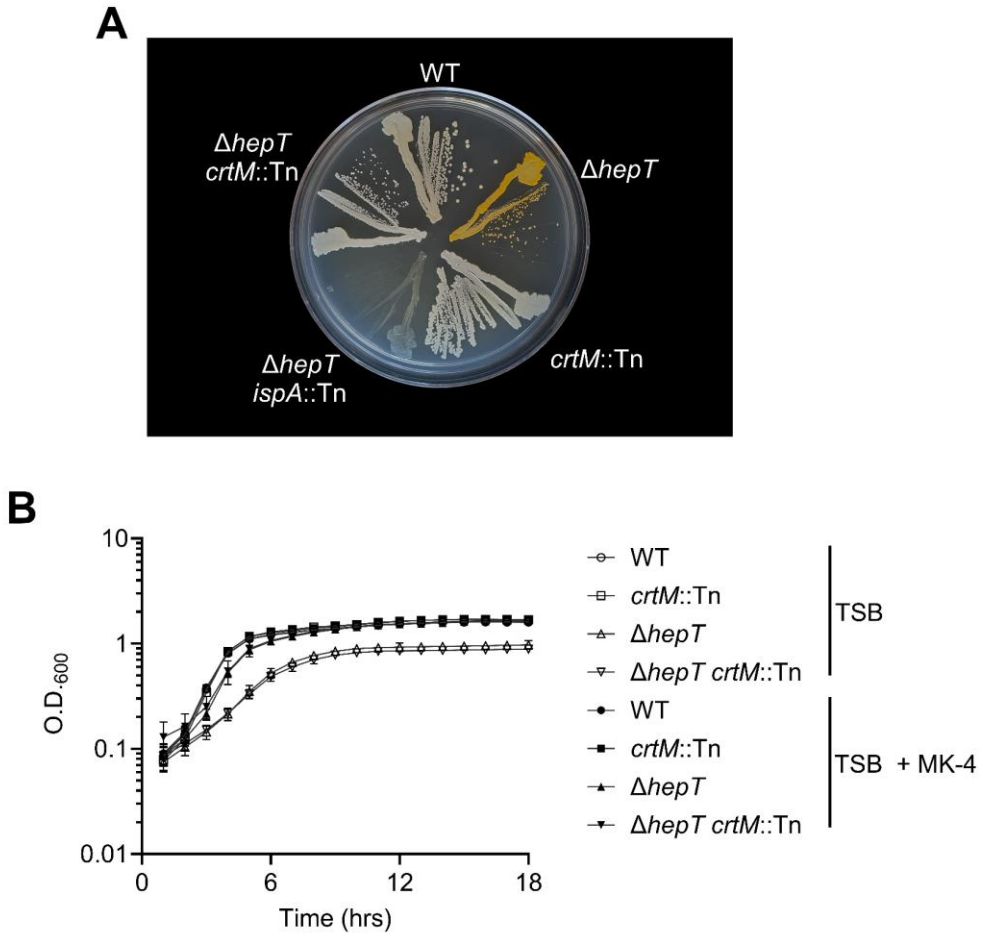

Figure 3-5. Loss of pigmentation does not induce the small colony variant phenotype or prevent MK-4 complementation of ΔhepT.
(A) The indicated strains struck for isolation on TSA supplemented with 12.5 µM MK-4 and incubated overnight. (B) Growth curve analysis of the indicated strains grown in TSB with or without supplementation with 12.5 µM MK-4. Data are the average of three independent biological replicates performed in technical triplicate. Error bars represent one standard deviation from the mean.

QoxABCD activity is impeded in the Δ*hepT ispA*::Tn double mutant via loss of prenylated heme cofactors

S. aureus utilizes a branched respiratory chain for aerobic respiration consisting of the QoxABCD and CydAB terminal oxidases, both of which require heme for their activity. The finding that the Δ*hepT ispA*::Tn double mutant respires anaerobically but not aerobically supports the hypothesis that both QoxABCD and CydAB are impeded in this strain. QoxABCD activity is

dependent on prenylated heme cofactors which are generated via the addition of FPP onto heme by CtaB to produce heme *o*. Heme *o* is further modified by the addition of a carbonyl group by CtaA to produce heme *a* (Fig. 3-6A). While QoxABCD requires prenylated hemes (heme *o* or heme *a*) for its activity, CydAB functions independently of these modified heme cofactors (28). To determine whether prenylated heme cofactors are produced in the Δ*hepT ispA*::Tn double mutant, hemes were extracted from overnight cultures and quantified via HPLC. In each strain, heme *b* was detected and used as an internal standard to normalize heme *o* and *a* abundance across samples. Mutation of *ispA* leads to a significant decrease in heme *o* and heme *a* abundance compared to the WT (Fig. 3-6B and C). Interestingly, disruption of MK synthesis via mutation of *menE* also leads to a significant decrease in heme *o* and heme *a* compared to WT and suggests that modified heme cofactor production is reduced during fermentative growth. Supplementation of the *menE*::Tn mutant with MK-4 partially restores heme *a* abundance, but not heme *o*. Similarly, the Δ*hepT* mutant also exhibits decreased amounts of prenylated hemes compared to WT, of which, only heme *a* was restored to WT-like levels upon MK-4 supplementation. Notably, the Δ*hepT ispA*::Tn double mutant does not produce detectable quantities of heme *o* or heme *a* (Fig. 3-6B and C), indicating that both HepT and IspA are capable of contributing to prenylated heme production. These findings demonstrate that QoxABCD is not active in the Δ*hepT ispA*::Tn double mutant due to an inability to produce prenylated heme cofactors.

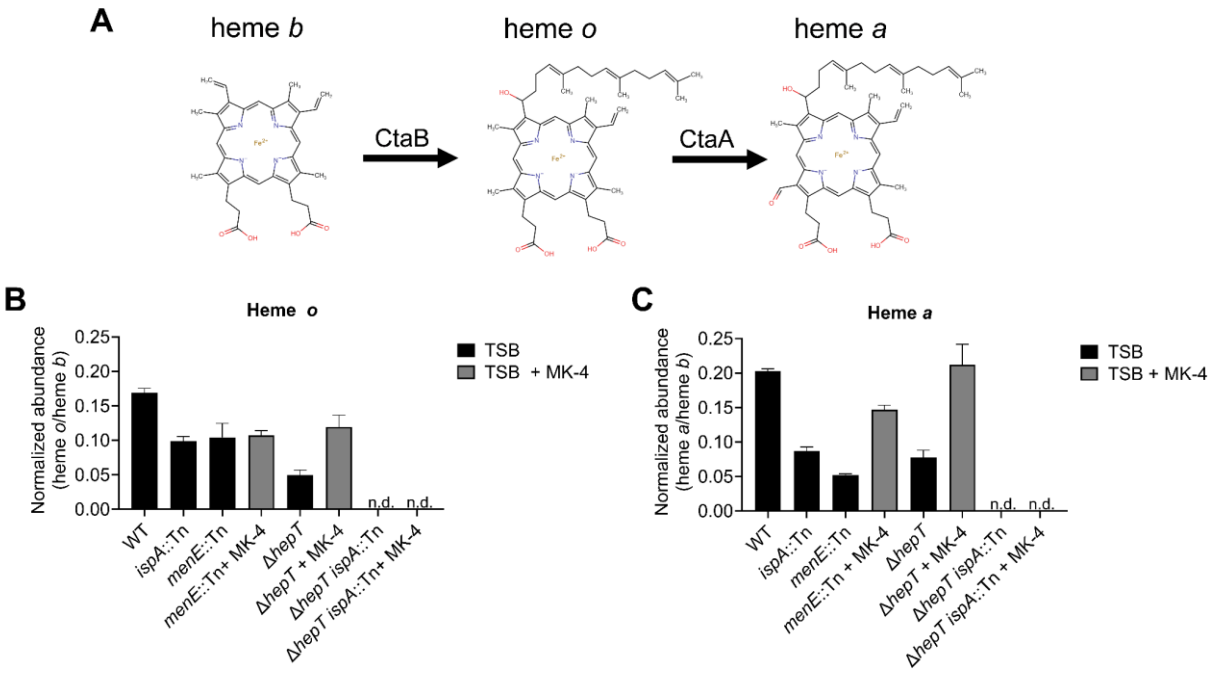

Figure 3-6. Both HepT and IspA are capable of contributing to the production of prenylated heme cofactors.
(A) An illustration of the prenylated heme synthesis pathway beginning with heme *b*. Heme *b* farnesylated by CtaB generating heme *o*. Heme *o* is modified by the addition of a carbonyl group to produce heme *a*. (B-C) High-performance liquid chromatography (HPLC) analysis of hemes extracted from whole cells. Heme *b* was used as an internal standard to which heme *o* (B) and heme *a* (C) were normalized for each sample. Data are the average of three independent biological replicates performed in triplicate.

CydAB function is not stimulated by MK-4

An inability to produce prenylated heme cofactors accounts for impairment of QoxABCD in Δ*hepT ispA*::Tn, but both CydAB and QoxABCD must be inactive to induce the SCV phenotype. Therefore, we reasoned that CydAB activity is not stimulated by MK-4. We demonstrate that *S. aureus* produces five MK species: MK-5, MK-6, MK-7, MK-8, and MK-9. Previous experiments used MK-4, an MK analogue that is not natively produced by *S. aureus*, to chemically complement MK deficiency (Fig. 3-3A and B). To determine whether MK-4 serves as an electron carrier substrate for CydAB, a Δ*menB qoxA*::Tn double mutant was generated. In this

strain respiration is dependent on CydAB and exogenous MKs. MK-4 supplementation of Δ*menB qoxA*::Tn did not promote significant proliferation after 24 h of incubation compared to the un-supplemented condition, which phenocopies Δ*hepT ispA*::Tn (Fig. 3-7A). Importantly, both Δ*menB* and Δ*menB cydA*::Tn, a strain restricted to QoxABCD for aerobic respiration, exhibited increased proliferation when supplemented with MK-4 (Fig. 3-7A). To determine if the shortened isoprenoid effects whether MK-4 can promote CydAB activity, the experiment was repeated using the MK analog menadione (MD), which lacks an isoprenoid moiety. Whereas MD also increased proliferation of Δ*menB* and Δ*menB cydA*::Tn, it failed to enhance proliferation of Δ*menB qoxA*::Tn, which again phenocopies Δ*hepT ispA*::Tn (Fig. 3-7B). Importantly, Δ*hepT* increased proliferation when supplemented with either MK-4 or MD, indicating that mutation of *hepT* alone is not responsible for the respiration phenotype observed in Δ*hepT ispA*::Tn. These data suggest that while Δ*hepT ispA*::Tn exhibits a defect in isoprenoid biosynthesis, its inability to perform aerobic respiration stems from the electron carrier preference of CydAB, which cannot effectively utilize MK-4. To provide further evidence of this, Δ*ispA qoxA*::Tn and Δ*hepT qoxA*::Tn were constructed. The Δ*ispA qoxA*::Tn mutant grew similarly to the WT, indicating that respiration is intact in this strain (Fig. 3-8A and B). However, Δ*hepT qoxA*::Tn displayed the SCV phenotype that also does not respond to MK-4 supplementation, phenocopying Δ*hepT ispA*::Tn (Fig. 3-8C and D). Together, these data show that the CydAB terminal oxidase cannot utilize MK-4 or MD as electron carriers.

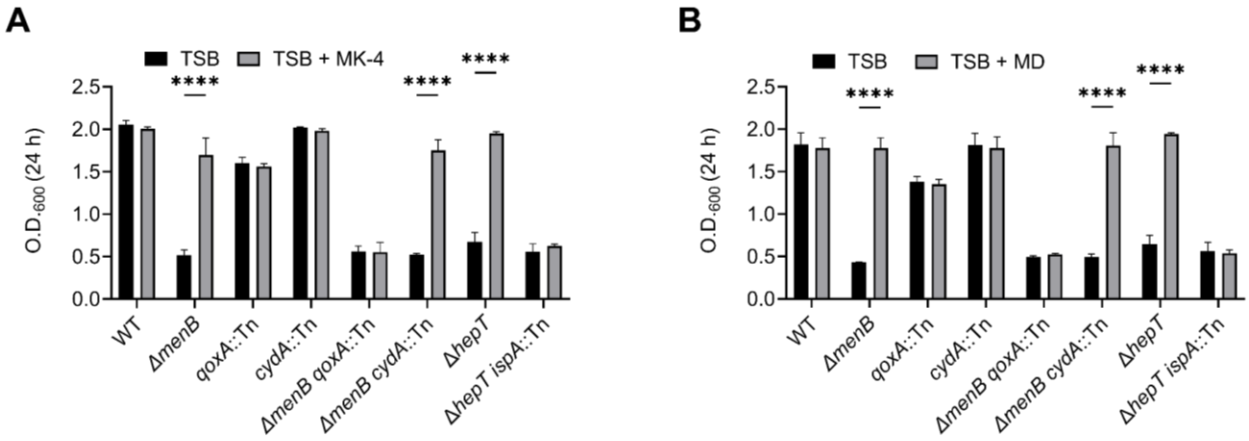

Figure 3-7. MK-4 and menadione fail to stimulate aerobic respiration in cells restricted to CydAB-dependent respiration.

(AB) O.D.$_{600}$ values were collected after 24 hours of incubation in TSB supplemented with either 12.5 µM MK-4 (A) or 2.5 µM menadione (MD) (B). Error bars represent one standard deviation from the mean. Statistical significance was determined via two-way ANOVA with Bonferroni correction. **** represents a p-value of <0.0001. Data are the average of three independent biological replicates performed in triplicate.

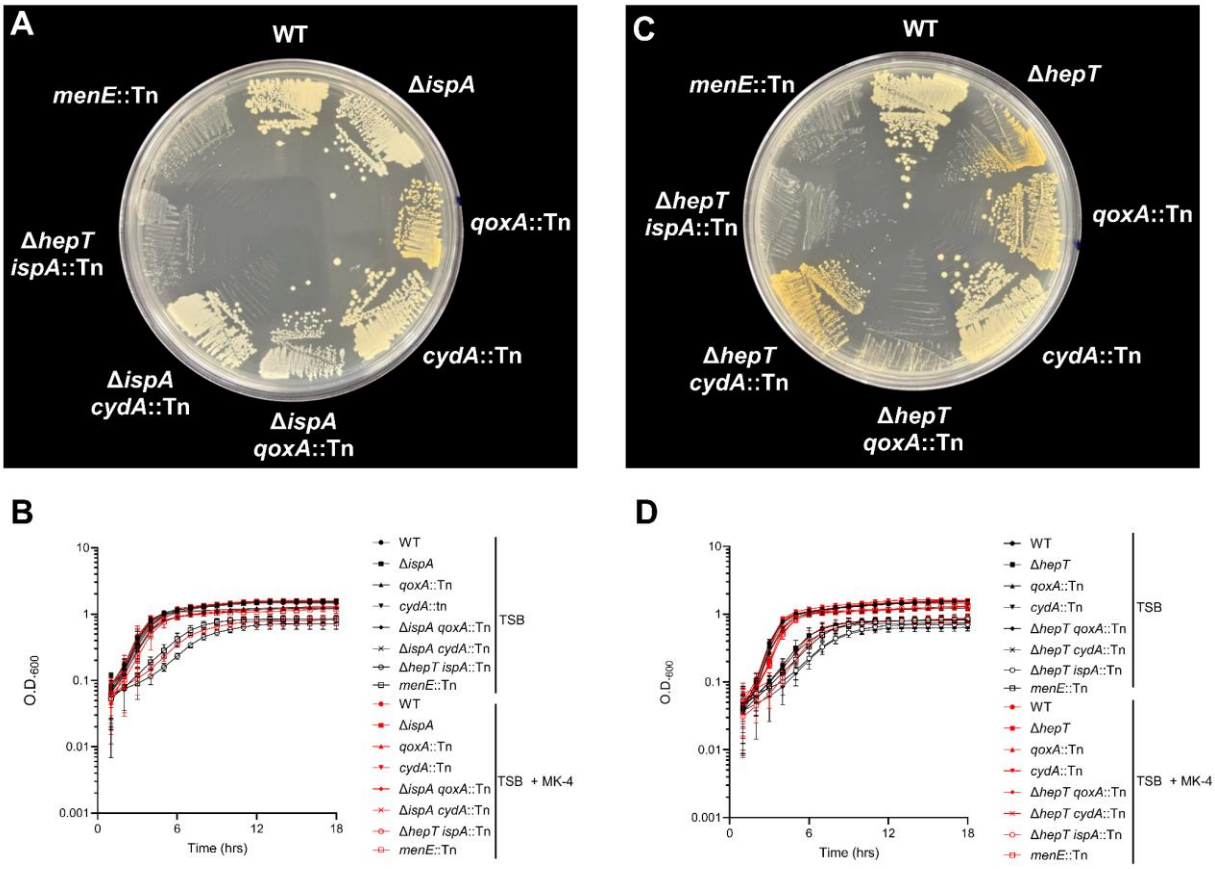

Figure 3-8. The ΔhepT qoxA::Tn double mutant phenocopies the ΔhepT ispA::Tn double mutant.
(AB) The indicated strains streaked onto TSA plates and incubated overnight. (CD) Growth curve analysis of the indicated strains. Cultures were grown in TSB (black symbols) or TSB supplemented with 12.5 µM MK-4 (red symbols). Error bars represent one standard deviation from the mean. Data are the average of three independent biological replicates performed in technical triplicate.

PDS activity supports host colonization

Isoprenoid biosynthesis contributes to three cellular pathways: carotenoid pigment production, cell envelope synthesis, and respiration. Importantly, each of these pathways have been shown to contribute to virulence or host colonization (4, 9, 169, 192, 193). Therefore, we sought to determine whether disruption of PDS function would impact fitness in a host. The heart, liver and kidneys of systemically infected mice were harvested 96 hours post infection and

enumerated for colony forming units. The *ispA*::Tn mutant had significantly reduced abundance in the heart, liver and kidneys, indicating that *ispA* plays a role in host colonization (Fig. 3-9A). Additionally, the *hepT*::Tn mutant had significantly reduced abundance in the heart and liver of systemically infected mice (Fig. 3-9B). However, the *menC*::Tn mutant, which is deficient for MK production, phenocopies the *hepT*::Tn mutant. This suggests that the colonization defect observed for the *hepT*::Tn mutant may be due to a loss of MK production, rather than a disruption in isoprenoid biosynthesis.

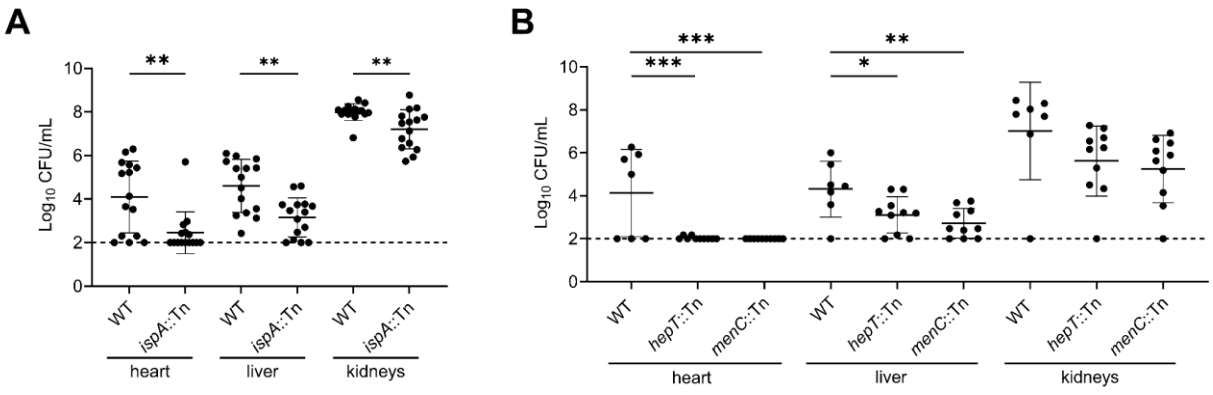

Figure 3-9. Disruption of isoprenoid synthesis impairs S. aureus colonization across multiple organs during systemic infection.
(A) Bacterial burdens of WT or *ispA*::Tn quantified after 96 hours of infection and represented as colony forming units (CFU) per milliliter (CFU/mL). Statistical significance was determined via unpaired Mann-Whitney test. (B) Bacterial burdens of WT, *hepT*::Tn and *menC*::Tn after 96 hours of infection represented as CFU/mL. Prior to infection, *hepT*::Tn and *menC*::Tn were supplemented with 12.5 µM MK-4 to achieve a WT-like inoculum. Statistical significance was determined via One-way ANOVA with Tukey correction. (AB) Error bars represent one standard deviation from the mean. *, ** and *** represent p-values of <0.05, <0.01 and <0.001 respectively.

Discussion

How bacterial isoprenoid synthesis is initiated in the absence of the short chain PDS, IspA, is a fundamental question. Our data shed light on this inquiry by demonstrating that functional redundancy sustains isoprenoid synthesis in *S. aureus*. We found that the medium chain PDS HepT

functions in three pathways: it is essential for MK synthesis but also plays a role in the lipid II cycle and supports production of prenylated hemes. While it has been hypothesized that HepT synthesizes the isoprenoid moieties used for MK synthesis (114, 118, 194), our results experimentally verify this function. We demonstrate that HepT inactivation results in the loss of MK-5, MK-6, MK-7, MK-8, and MK-9 providing direct evidence that HepT is needed for synthesis of these MK species. Cells lacking MK exhibit a distinct colony phenotype called the small colony variant (80, 81, 114, 125). SCV proliferation is limited due to a restricted metabolism that relies on lactic acid fermentation. Consistent with the lack of MK, *hepT* mutant growth is impaired compared to WT and the cells produce lactate, indicating that fermentation is the primary means by which the mutant cells generate energy. We also demonstrate the MK analogue, MK-4, chemically complements proliferation and reduces lactate production. Together these results support the conclusion that HepT is necessary for MK synthesis and respiration.

Isolation of pigmented *ispA* mutants encoding missense *hepT* mutations led us to hypothesize that HepT is also capable of condensing IPP and DMAPP to initiate isoprenoid synthesis. We predicted that simultaneous inactivation of *ispA* and *hepT* would be synthetically lethal as isoprenoid synthesis would not be initiated in this genetic background. Additional rationale for this prediction is provided by biochemical investigation of HepT and HepT homologues. *B. subtilis* HepT is capable of condensing IPP and DMAPP, although the reaction is inefficient (179). A similar result was described for the *E. coli* HepT homologue IspB, which is also capable of using IPP and DMAPP as substrates (176). Additionally, HepT and IspB are essential in *B. subtilis* and *E. coli* under standard growth conditions, respectively (186, 187), but *B. subtilis* can tolerate loss of HepT activity when cultured in a medium that supports proliferation of L-form cells that lack a cell wall (188). This finding implies that HepT also supports

peptidoglycan synthesis. Our results demonstrate that *S. aureus* is amenable to genetic inactivation of *hepT* in the presence or absence of *ispA*. However, Δ*hepT ispA*::Tn lacked pigmentation and was not able to respond to chemical complementation with the MK analogue MK-4. Subsequent experimentation demonstrated that Δ*hepT ispA*::Tn is impaired for aerobic respiration due to inactivity of both terminal oxidases, CydAB and QoxABCD. Terminal oxidases accept electrons from the quinone pool and reduce oxygen, thereby performing the last step of aerobic respiration. Our data show that QoxACBD impairment can be attributed to loss of prenylated heme cofactors while the inability of MK-4 to stimulate respiration in Δ*hepT ispA*::Tn is dependent on CydAB. The finding that MK-4 fails to chemically complement Δ*menB qoxA*::Tn conclusively showed that CydAB is restricted to the use of long chain MK, presumably MK-7 or greater. Further, it is unclear the role short chain MKs (MK-5 and MK-6) play in supporting respiration as these MK species are produced at significantly lower levels compared to the longer chain MKs (MK-7, MK-8, and MK-9). However, given the apparent preference of terminal oxidases for isoprenoid chain length of MKs, further investigation should be carried out to define the precise correlations between MK tail length, CydAB terminal oxidase activity, and the composition of the MK pool on cellular respiration.

Investigating Δ*hepT ispA*:Tn in the context of the single mutants demonstrated that HepT uniquely contributes to MK production while precursor for staphyloxanthin is provided exclusively by IspA. Interestingly, either enzyme can contribute to prenylated heme production. Both single mutants exhibit decreased prenylated heme cofactors compared to WT, but levels of heme *o* in the *hepT* mutant suggests a preference for HepT. These results reveal that HepT can function beyond MK synthesis. Consistent with this, we monitored levels of the lipid II precursors Und-P and Und-OH, which revealed decreased abundance of both metabolites in the *hepT* mutant.

Though Und-OH does not participate directly in the lipid II cycle (112), previous reports support a model whereby it serves as a reservoir for rapid conversion to Und-P via undecaprenol kinase when higher levels of Und-P are needed (195). In the *hepT* mutant, a depleted Und-OH reservoir implies the cell is attempting to maintain Und-P levels and demonstrates that HepT may provide substrates for UppS in the production lipid II precursors. Overall, the finding that Δ*hepT ispA*::Tn is viable provides strong evidence that another enzyme is capable of condensing IPP and DMAPP to produce the FPP needed for essential lipid II. Based on this supposition and our results, two models can be considered. In the first model, IspA, HepT, and the unknown PDS each produce FPP that is restricted to generate staphyloxathin, MK, and lipid II, respectively. Alternatively, the second model predicts that only IspA and the unknown PDS produce FPP, but FPP generated by the uncharacterized PDS is limited to the lipid II pathway or for use as a HepT substrate. Our data and the fact that HepT homologues are capable of condensing IPP and DMAPP *in vitro*, albeit at a limited rate, favor the first model (176, 179). Krute et al. hypothesized that HepT, UppS, or both can produce FPP to support growth of *ispA* mutant cells (115). However, studies of UppS substrate specificity in other bacterial species show that DMAPP, a necessary precursor for FPP synthesis, is not used as a substrate by this enzyme (161, 196). Discerning between these models requires further biochemical characterization of purified, recombinant *S. aureus* HepT and UppS to establish substrate specificities and reaction kinetics. Nonetheless, our data demonstrate that in addition to its importance in producing MK, HepT plays a multifunctional role by contributing to the isoprenoid dependent heme cofactor and lipid II precursor pathways.

Staphyloxanthin, MK, terminal oxidase activity, and aerobic respiration have been shown to be critical factors during *S. aureus* pathogenesis (4, 8, 9, 169). To determine the contributions of IspA and HepT to *S. aureus* host colonization we used the systemic mouse model of infection.

This analysis showed that the *hepT* mutant exhibited colonization defects in the heart and liver, which was phenocopied by the MK deficient *menC* mutant. This finding highly suggests that loss of MK production rather than disruption to isoprenoid biosynthesis drives the colonization defects displayed by the *hepT* mutant. On the other hand, the *ispA* mutant exhibited colonization defects in the heart, liver and kidneys. Disruption of isoprenoid biosynthesis has been previously established to reduce virulence, as mice treated with a chemical inhibitor of UppS exhibit increased survival compared to untreated mice in a model of systemic infection (197). Our data demonstrate that inhibiting isoprenoid synthesis at an earlier step in this pathway is also a viable strategy for reducing *S. aureus* infection.

S. aureus is a common nosocomial pathogen that is frequently resistant to antibiotics, making treatment difficult (198). Furthermore, the presence of antibiotic-resistant *S. aureus* in hospital settings can complicate surgical recovery and lead to increased mortality (199). By identifying biological pathways that support survival in the host, we reveal potential targets that could be used for drug development and therapeutic intervention. In this study, we showed that genetic disruption of isoprenoid biosynthesis impacted host colonization and impeded several downstream pathways that are known to support pathogenesis, revealing the potential of this pathway as a drug target. Additionally, our data support a redundant model of isoprenoid biosynthesis and showed that a high level of disruption in this pathway is tolerated by *S. aureus* but limits the pathogen's metabolic versatility. As isoprenoid biosynthesis is a highly conserved biological process that is active in other bacterial pathogens, developing strategies for targeting bacterial isoprenoid biosynthesis may impact treatment of a wide range of microbial pathogens.

Acknowledgments

We thank Dr. Elise Rivett for providing her expertise in heme quantification and the Dr.

Eric Hegg laboratory for allowing us to use their HPLC instrument. Funding for this study was provided by NIH 1R21AI144504-01. We acknowledge the Network on Antimicrobial Resistance in *S. aureus* (NARSA) and the Nebraska Transposon Mutant Library (NTML) screening array NR-48501, from which many of the transposons in this study were derived, as indicated by NE in Table A-5.

Materials and Methods

Bacterial strains, plasmids and culture conditions

S. aureus strain JE2 was used as the WT strain in this study. All *S. aureus* mutants were generated in the JE2 WT background as listed in Table A-5. Transposon mutagenesis was carried out by propagating φ85 on the appropriate strain from the Nebraska Transposon Mutant Library (NTML) and transduced into a recipient strain as described previously (170, 200). However, for generating the Δ*hepT ispA*::Tn double mutant we found no colonies were obtained when plating on TSA (Remel) supplemented with 10 µg/mL erythromycin and 40 mM sodium citrate. Instead, plating on TSA supplemented with 10 µg/mL erythromycin without sodium citrate yielded colonies. In-frame deletions were generated via an allelic exchange protocol with the pKOR1mcs-Δ*hepT* plasmid as described previously and confirmed via PCR (201, 202). The previously generated pKOR1-Δ*menB* plasmid was used to generate the Δ*menB* deletion mutant in the JE2 background (114). Cloning and PCR confirmation of mutants was performed using primers listed in Table A-6. All overnight cultures were started from single colonies in 5 mL TSB (Fisher Scientific) and incubated overnight at 37°C at 225 rpm unless stated otherwise. Mutants deficient for MK synthesis were supplemented with 12.5 µM MK-4 in overnight cultures. All strains harboring the pOS1 plasmid were grown in the presence of 10 µg/mL chloramphenicol.

Whole-genome sequencing and analysis

Genomic DNA was extracted from 1 mL of the overnight cultures using a Wizard® Genomic DNA purification kit (Promega). Genomic DNA was sequenced via Illumina sequencing at the Duke University Sequencing and Genomic Technologies core facility. Genomic analyses, including paired-end read trimming, mapping, and single nucleotide polymorphism (SNP) calling were performed using Geneious Prime version 2024.0.5. The genome of *S. aureus* strain USA300_FPR3757 (GenBank accession number: CP000255.1) was used as a reference genome to which sequencing data was mapped.

Quantification of isoprenoid derived metabolites via high-performance liquid chromatography mass spectrometry (HPLC-MS)

MKs and C_{55} isoprenoids were extracted and analyzed as described previously with slight modifications (176). *S. aureus* cultures were grown in 50 mL of TSB at 37 °C with shaking at 225 rpm until stationary phase. Cultures were pelleted and resuspended in 2 mL of methanol:0.3% NaCl (10:1, v/v). Vitamin K_1, solanesol and solanesyl phosphate were added as internal standards. To extract MKs and Und-OH, hexane was added to the cell suspension, vortexed, and the upper phase was collected. Remaining Und-OH and Und-P in the aqueous layer were treated with alkali by adding 1 mL 60% KOH and boiled for 60 minutes. Diethyl ether was added and vortexed, then collected after phase separation. The collected diethyl ether was washed with 5% acetic acid.

The hexane solution containing MKs and polyprenols was loaded onto a 0.4-g column of neutral alumina (grade III). MKs were eluted with 2.4% diethyl ether in hexane, and polyprenols were eluted with 10% diethyl ether in hexane. MKs and polyprenols were run on an LCMS-2010 (Shimadzu Co.) using a STR ODS_II column (Shinwa Chemical Ind. Ltd.). A 2-propanol:methanol (1:1, v/v) mixture was used as the mobile phase at a flow rate of 0.1 mL/min.

The diethyl ether extract was divided in half. One half was dried under nitrogen gas and the remaining residue was resuspended in hexane. The hexane solution was loaded onto a neutral alumina column, and polyprenols were eluted with 10% diethyl ether in hexane as described above. The other half of diethyl ether extract was dried under nitrogen gas and the remaining residue was resuspended in chloroform:methanol (2:1, v/v). The chloroform:methanol (2:1, v/v) solution containing polyprenyl phosphates derived by alkaline hydrolysis was loaded onto an ion exchange cartridge (Supelclean LC-NH_2). Polyprenyl phosphates were eluted with a chloroform:methanol:water (2:0.9:0.1, v/v/v) solution containing 0.1 M ammonium acetate and analyzed via HPLC using a STR ODS_II column with 2-propanol:methano (1:1, v/v) containing 5 mM phosphoric acid.

Growth curve analysis and end-point optical density reading

Overnight cultures were pelleted and resuspended in 137 mM NaCl, 2.7 mM KCl, 10.1 mM Na_2HO_4P, 1.8 mM KH_2O_4P phosphate buffered saline pH 7.4 (PBS) and placed on ice. Resuspended cultures were normalized to an $O.D._{600}$ of 1.0. A volume of 150 µL growth medium was dispensed into each well of a 96-well plate and 1.5 µL of the normalized culture was used to inoculate each well. The plate was incubated in a Stratus (Cerillo) plate reader at 37°C with shaking at 300 rpm.

For growth analysis where end-point optical density was collected, a 96-well plate was prepared and incubated as described above. After the designated incubation time, the plate was removed from the stratus plate reader and each well was carefully pipetted up and down to ensure all cells were resuspended. A single time point was then collected using an H1 Synergy (Biotek) plate reader.

Measuring L-lactate production

The EnzyCrhom^{TM} L-lactate assay kit (ECLC-100, BioAssay Systems) was used to assess L-lactate production in *S. aureus* cultures. Overnight cultures were pelleted and normalized to an $O.D._{600}$ of 1.0 in PBS and placed on ice. Normalized cultures were subcultured 1:100 in 5 mL fresh TSB and incubated at 37°C with shaking at 225 rpm for 15 h. Cultures were then pelleted and the supernatant was collected and sterile filtered and stored at -20°C. Sterile supernatants were diluted 1:10 in sterile Milli-Q water and 20 µL was dispensed into a well of a 96-well plate. The reaction buffer was prepared by mixing the following reagents from the L-lactate assay kit: 60 µL assay buffer, 1 µL enzyme A, 1 µL enzyme B, 10 µL NAD and 14 µL MTT. In a 96-well plate 20 µL of the diluted supernatant was added to a well for each sample. An 80 µL volume of reaction buffer was added to each well and mixed briefly by pipetting up and down. The initial $O.D._{565}$ was measured immediately after mixing using an H1 Synergy plate reader and then the plate was incubated at room temperature for 20 minutes. The $O.D._{565}$ was measured again, and the initial $O.D._{565}$ measurement was subtracted from the second measurement to yield the sample values. The sample values were compared to a standard curve (prepared as described in the L-lactate assay kit) to determine L-lactate concentrations.

Heme quantification via high-performance liquid chromatography (HPLC)

In a 125 mL Erlenmeyer flask, 20 mL of TSB was inoculated with a single colony and grown overnight at 37°C with shaking at 225 rpm. Cultures were pelleted and resuspended in 200 µL molecular biology grade water (Cytiva: SH30538.03). A volume of 100 µL of the cell suspension was transferred to a 1.5 mL Eppendorf tube. An acid:acetone solution was prepared which consisted of 5 parts 12 M HCl to 95 parts acetone. A 150 µL volume of acid acetone was added to the cell suspension and mixed briefly by vortexing. The mixture was incubated on ice for

10 minutes and vortexed for 20 seconds. The mixture was further incubated for 10 minutes and then vortexed for 20 seconds. The cells were pelleted and the supernatant was collected. The supernatant was centrifuged again and the resulting supernatant was transferred to an HPLC injection vial.

Hemes were analyzed with an Agilent 1260 Infinity HPLC system using an InfinityLab Poroshell EC-C18 reverse-phase column (Agilent: 699975-902) coupled with a diode array detector (Agilent: G1315D). A 10 µL volume of sample was injected and hemes were separated using a gradient of solvent A (0.1% v/v trifluoroacetic acid in Milli-Q water) and solvent B (0.1% v/v trifluoroacetic acid in acetonitrile). The gradient progressed as follows: 25% solvent B (0.00-2.67 min.), 25%-55% solvent B (2.67-4.33 min.), 55%-75% solvent B (4.33-11.00 min.), 75%-100% solvent B (11.00-12.67 min.), 100% solvent B (12.67-20.00 min.), and a gradient returning to 25% solvent B (20.00-23.00 min.). Using this method, heme *b* elutes at 6.8 minutes, heme *a* at 10.8 minutes and heme *o* at 12 minutes. Hemes were detected by measuring absorbance at 400 nm and identified by comparing retention time and the absorbance maximum (203). HPLC chromatograms were used to determine the area under the peak for each of the heme species. Normalized heme abundance was determined by dividing the peak area of hemes *o* and *a* by the peak area of heme *b*.

Systemic mouse infections

Overnight cultures were subcultured 1:100 in 5 mL fresh TSB and incubated at 37°C with shaking at 225 rpm for 3 h. Cultures were pelleted at 4°C and washed once in 12 mL of Dulbecco's PBS (DPBS, Sigma-Aldrich: D8537). Resuspended cultures were pelleted again and normalized to an $O.D._{600}$ of 0.4 in DPBS and kept on ice. Eight-week-old female BALB/c mice (Jackson Laboratories) were retro-orbitally infected with 10^7 CFU of the indicated *S. aureus* strain. Mice

were sacrificed 96 h post-infection, and the heart, liver, and kidneys were harvested. Heart and Kidneys were homogenized via bead beating (1.5 mL RINO lysis beads, NextAdvance Inc.) in 500 uL DPBS using a Bullet Blender Storm24 (NextAdvance Inc.). Once homogenized, 500 uL DPBS was added to the lysate. Livers were manually homogenized in a Whirl-pak (Nasco) containing 1 mL DPBS. Organ homogenates were serially diluted in DPBS and plated on TSA for enumeration. All infections were performed at Michigan State University under the principles and guidelines described in the *Guide for the Care and Use of Laboratory Animals* with the protocol approved by Michigan State University Institutional Animal Care and Use Committee (IACUC): PROTO202200474.

Chapter 4: Identifying small molecule inhibitors of the fatty acid kinase (FAK) system in *Staphylococcus aureus*.

Abstract

Fatty acids (FAs) are essential for the generation of the phospholipids that comprise the cell membrane. Some bacterial pathogens, such as *Staphylococcus aureus*, possess the fatty acid synthesis type II (FASII) pathway, which endogenously synthesizes FAs, and the fatty acid kinase (FAK) system, which acquires exogenous FAs. Antimicrobials that target the FASII pathway are in use, however their effectiveness against bacterial species possessing the FAK system is limited, because the FAK system is capable of supporting cell membrane synthesis in FA rich environments, thus bypassing the FASII pathway. Therefore, the efficacy of FASII pathway inhibition would be increased with concomitant targeting of the FAK system. However, FAK system inhibitors have not been identified. In this study, a *S. aureus* mutant deficient for the FASII pathway was used in a high-throughput screen to identify potential inhibitors of the FAK system. One compound, MSU-40452, displayed exceptionally selective activity against the FASII deficient mutant, while little activity was observed against the WT. The effectiveness of MSU-40452 against WT increased when the staphylococci were also exposed to the known FASII inhibitor triclosan. This result suggests that simultaneous inactivation of FASII and FAK is a viable antimicrobial strategy.

Introduction

Antimicrobial resistance is a growing problem worldwide. It is estimated that by 2050, 10 million deaths per year will be attributed to antibiotic resistant bacterial pathogens (204). At the same time, the rate of developing new classes of antibiotics has decreased significantly, with only four antibiotics representing new classes approved for clinical use since 1970 (205, 206). Therefore, new antibiotics with novel mechanisms of action are needed to combat the threat of antimicrobial resistance. The bacterial cell membrane represents a prime target for the development of antibiotic therapies. In fact, the newest antibiotic approved by the FDA with a novel mechanism of action

(daptomycin) targets the cell membrane by integrating into the lipid bi-layer in a phosphatidyl glycerol dependent manner (207). Production of phosphatidyl glycerol and other phospholipids which comprise the cell membrane is essential and depends on fatty acids (FAs) (208). Endogenous synthesis of FAs in bacteria is carried out by the fatty acid synthesis type II (FASII) pathway, which is unique from the fatty acid synthesis type I (FASI) pathway used by humans, making it a druggable target (208–211).

The FASII pathway consists of two stages: initiation and elongation. In the initiation stage acetyl-CoA is converted to malonyl-CoA by the AccABCD complex (Fig. 4-1). Subsequently, malonyl-CoA is transferred to acyl carrier protein (ACP) by FabD. The first step of elongation is carried out by either FabF or FabH, which decarboxylate malonyl-ACP to generate β-ketoacyl-ACP (212–214). A reduction reaction is carried out by FabG using an electron from NADPH to produce β-hydroxyacyl-ACP, which undergoes a dehydration reaction catalyzed by FabZ to generate *trans*-2-enoylacyl-ACP (215, 216). Next, FabI reduces *trans*-2-enoylacyl-ACP to make acyl-ACP (211, 217, 218). From here, the elongation stage can cycle again to elongate the acyl chain by another two carbons, or the acyl-ACP can enter the phosphatidic acid synthesis pathway for incorporation into phospholipids (208). Notably, FAs synthesized in this way are comprised of even numbered carbon chain lengths. However, many bacterial species, such as the human pathogen *Staphylococcus aureus*, are capable of producing odd-numbered chain length FAs for incorporation into phospholipids (219). This is due to the presence of the branched chain fatty acid synthesis pathway, which uses leucine, isoleucine or valine to make isobutyryl-CoA, 2-methylbutyryl-CoA and isovaleryl-CoA, respectively (Fig. 4-1). These branched chain precursors feed into the FASII pathway, with the incorporation of isobutyryl-CoA or 2-methylbutyryl-CoA leading to odd numbered chain length FAs (219, 220).

There are three antimicrobial compounds which inhibit the FASII pathway that are currently in use or in development: triclosan, afabicin and isoniazid (221–223). However, the efficacy of these FASII inhibitors is limited due to the presence of a FASII bypass mechanism in many bacterial pathogens, including *S. aureus* (224). The fatty acid kinase (FAK) system utilizes exogenous FAs for incorporation into phospholipids and is capable of sustaining proliferation in the absence of the FASII pathway (224). Exogenous FAs are thought to diffuse into the cell membrane, where they are bound and removed by either FakB1 or FakB2 (Fig. 4-1) (225, 226). Protein bound FAs are phosphorylated by FakA (225, 227). Once phosphorylated, the FA can be used by PlsY for attachment to a glycerol phosphate backbone in the production of phospholipids (228). Theoretically, simultaneous inhibition of both the FASII pathway and FAK system would impede bacterial proliferation. However, inhibitors of the FAK system have not been reported.

This chapter explores a high-throughput chemical screen strategy to identify inhibitors of the FAK system in *S. aureus*. The isolation of an *accB* mutant that is deficient for endogenous FA synthesis and is therefore reliant on exogenous FAs and the FAK system was developed by Delekta et al. (229). This strain will be referred to as ΔFASII throughout and was used to screen chemical libraries at the Michigan State University Assay Development and Drug Repurposing Core (ADDRC) for growth inhibition. Comparison of growth inhibitors for their activity against WT identified unique inhibitors of the ΔFASII mutant and represent potential inhibitors of the FAK system.

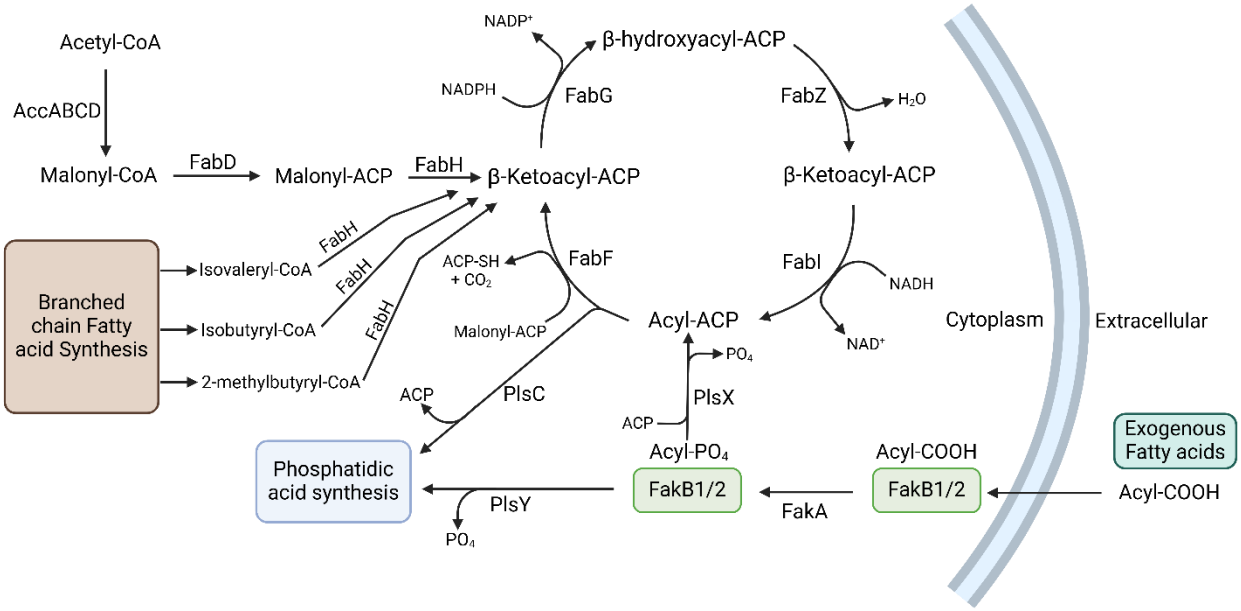

Figure 4-1. Fatty acid synthesis in *Staphylococcus aureus*.
A figure depicting the FASII, FAK and branched chain fatty acid synthesis pathways in *S. aureus*. Abbreviations: acyl carrier protein (ACP), Coenzyme A (CoA). ACP-SH refers to an ACP which is not bound to a fatty acid precursor in which the sulfhydryl group of the active site within ACP is exposed. Acyl-COOH is a generic representation of fatty acids which can be various lengths. Figure made in Biorender.

Results

Development of a FAK inhibitor screening platform

As a first step to designing a screening methodology, the ΔFASII mutant was validated for FA auxotrophy in brain heart infusion (BHI) broth with or without supplementation of FAs. The FA mixture used for supplementation consisted of a 1:1:1 ratio of myristic acid (14:0), palmitic acid (16:0), and oleic acid (18:1) at a final concentration of 16.65 µM of each FA (49.95 µM total FAs). Importantly, this FA mixture has been demonstrated previously to support the growth an *S. aureus* FA auxotroph (229). A considerable lag phase was observed for the ΔFASII mutant when supplemented with FAs, however after 21 hours of growth it reached an optical density comparable to the WT (Fig. 4-2A). Interestingly, the addition of FAs was inhibitory towards WT which caused an increased lag phase and a lower optical density in stationary phase. Importantly, the ΔFASII

mutant did not exhibit growth in BHI alone (Fig. 4-2A), demonstrating that this mutant is auxotrophic for FAs.

The lack of proliferation in the absence of FAs for the ΔFASII mutant simulates what would be expected of a theoretical compound that inhibits the FAK system. Therefore, the signal of a positive hit in a high throughput chemical screen would be inhibition of growth as quantified by optical density at 600 nm ($O.D._{600}$). However, when screening thousands of compounds it is essential to have a large difference between the positive control (growth inhibition) and the negative control (growth) so that single data point measurements can be reliably discerned from variation within the chemical screen. The Z-prime factor (Z' factor) is a quantifiable method of determining the quality of a screening assay by comparing the mean and standard deviation of a positive control to the mean and standard deviation of a negative control. To determine if a proliferation assay is a viable screening method, the ΔFASII mutant was grown in three different conditions: BHI, BHI + FAs and BHI + FAs + chloramphenicol (Cm) in a 96 well plate for 24 hours and the $O.D._{600}$ was measured. Consistent with the growth curve analysis, the ΔFASII mutant did not grow in the absence of FAs, but displayed robust growth when FAs were provided, though it was less than the WT (Fig. 4-2B). As a positive control for inhibition of FA-dependent growth, chloramphenicol inhibited proliferation of the ΔFASII mutant. Z' factor analysis was performed to compare the growth of the ΔFASII mutant supplemented with FAs to that of the un-supplemented and FA + Cm conditions. A Z' factor score of 0.946 was obtained for the ΔFASII + FAs vs. ΔFASII + FAs + Cm condition, while a similar score of 0.927 was calculated for the ΔFASII +FAs vs. ΔFASII un-supplemented conditions. A Z' score between 0.5 and 1.0 represents an "excellent assay" in which the positive and negative controls are sufficiently separated to enable interpretation of data points that fall between them (230). Therefore, a growth vs. no growth assay with a single timepoint

reading at 24 hours is a sufficient method for a high throughput chemical screen so long as the positive and negative controls are included.

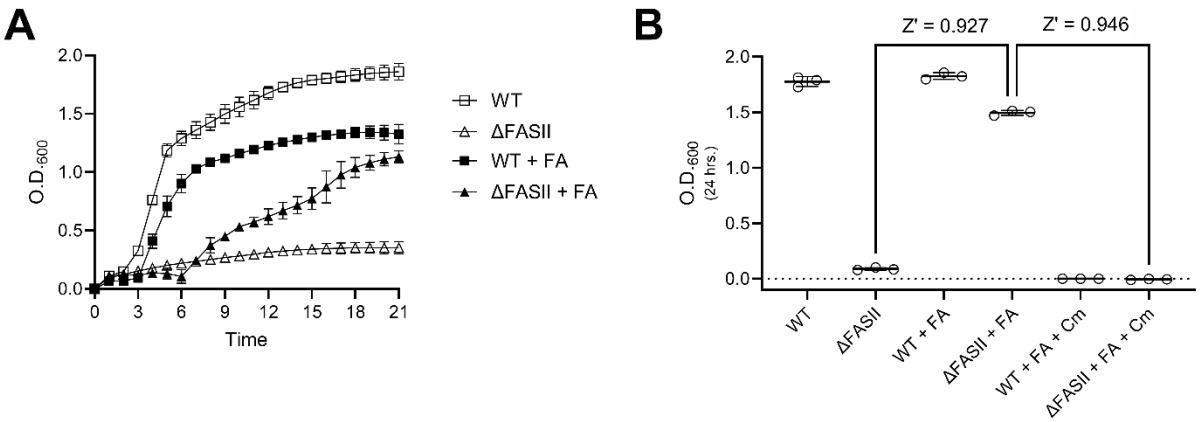

Figure 4-2. The ΔFASII mutant is auxotrophic for exogenous fatty acids which enables a growth versus no growth assay for chemical screening.
(A) Growth kinetics analysis of the WT and ΔFASII mutant in BHI broth either un-supplemented or with Fatty acid (FA) supplementation. (B) 24 hour end point optical density readings of the WT and ΔFASII mutant in BHI broth with the indicated supplementations. Abbreviations: Z' factor (Z'), chloramphenicol (Cm). (A and B) Data represent the average of three independent experiments performed in technical triplicate.

Selection of chemical libraries to screen against ΔFASII

The characteristics of the individual compounds within a chemical library are important to consider when selecting a set of chemicals to screen. The MSU ADDRC has 6 chemical libraries which are highly relevant to screen against the ΔFASII mutant: PKIS, Prestwick, NCI, NCATS_MIPE, LOPAC and Maybridge libraries. The PKIS library consists of 558 compounds known to inhibit kinase activity, which is especially relevant to inhibition of the FAK system due to the kinase activity of FakA. Furthermore, the PKIS library has been previously screened against the WT, which will enable the identification of inhibitors that are unique to the ΔFASII mutant. However, a drawback to this library is that the compounds are proprietary and not available for

purchase of fresh powder. Nevertheless, screening the PKIS library is beneficial as potential hits from this library can be synthesized if needed. The Prestwick, NCI, LOPAC and NCATS_MIPE libraries are all annotated libraries containing pharmacologically active chemicals which together consist of 4,584 compounds, some of which are known kinase inhibitors. Lastly, the Maybridge library is an un-annotated library of 23,552 drug-like compounds. Similar to the PKIS library, the Maybridge library has been previously screened against the WT strain and will enable comparison of compounds that inhibit the ΔFASII mutant but not the WT. In total, these selected libraries consist of 28,694 compounds.

Initial screening of the Maybridge library identifies selective inhibitors of the ΔFASII mutant

The activity of each compound in the Maybridge library was plotted for its percent inhibition of the ΔFASII mutant vs. the WT (Fig. 4-3). Parameters to define hits that are selective toward inhibition of the ΔFASII mutant were arbitrarily set at ≤20% WT activity and ≥40% ΔFASII activity represented as vertical and horizontal dashed lines in figure 4-3, respectively. 100 compounds were found to fall within these parameters and will be referred to as "unique ΔFASII inhibitors" (Table A-7). Interestingly, some compounds also exhibited a high level of activity against both the ΔFASII mutant and the WT, which suggests these compounds may be generally anti-staphylococcal (Fig. 4-3) and should be followed up on in future investigations.

Structural analysis of the compounds within the Maybridge library was carried out using the classification tool ClassyFire (231). Of the 23,552 Maybridge compounds 19,642 (83.4%) could be categorized at the sub-class level of classification. This analysis revealed the Maybridge library contains 303 compound sub-classes, the top 50 of which represent 80.8% of the classified compounds. The ClassyFire tool was able to categorize 77 of the 100 (77%) unique ΔFASII

inhibitors at the sub-class level. Comparison of the unique ΔFASII inhibitor sub-classes to those of the Maybridge library revealed an over representation of N-phenylureas and N-phenylthioureas compared to their abundance in the library (Fig. 4-4A). Pyrazoles, trifluoromethylbenzenes and ethers were also found to be overrepresented in the unique ΔFASII inhibitors, however this was less striking compared to N-phenylureas and N-phenylthioureas.

The base structure of N-phenylureas and N-phenylthioureas are similar, differing only in the presence of a carbonyl group (N-phenylurea) or thiocarbonyl group (N-phenylthiourea) (Fig. 4-4B). Chemicals belonging to the N-phenylurea and N-phenylthiourea sub-classes have been used in the development of pesticides and herbacides (232, 233), though studies describing their effects on bacteria are limited. One study reported the antimicrobial activity of various N-phenylureas, however the MIC for *S. aureus* was in the range of ~130 µM to ~490 µM (234), which is far above the 7.5 µM concentration at which the Maybridge library was screened. Further, no reports of the effects of N-phenylureas or N-phenylthioureas on FA synthesis have been published.

To confirm the activity of the unique ΔFASII inhibitors a dose response assay was performed using the same compound stocks as the initial screen. All N-phenylureas and N-phenylthioureas were included in the follow up with the addition of other compounds which displayed a high level of activity against the ΔFASII mutant but not the WT in the initial screen. Many of the compounds exhibited either no activity or a high degree of activity against both the WT and ΔFASII and thus were ruled out as unique ΔFASII inhibitors (Fig. 4-5A to R). Furthermore, some compounds displayed selective activity for the ΔFASII mutant only at the highest concentration tested, while others inhibited growth of ΔFASII in a dose dependent manner (Fig. 4-5S to AG), indicating that these are inhibitors of the ΔFASII mutant and may inhibit the FAK system. Nine of these selective compounds were chosen for purchase of fresh powder: MSU-22374,

MSU-15890, MSU-28435, MSU-22522, MSU-24281, MSU-32348, MSU-34372, MSU-30863, and MSU-28105.

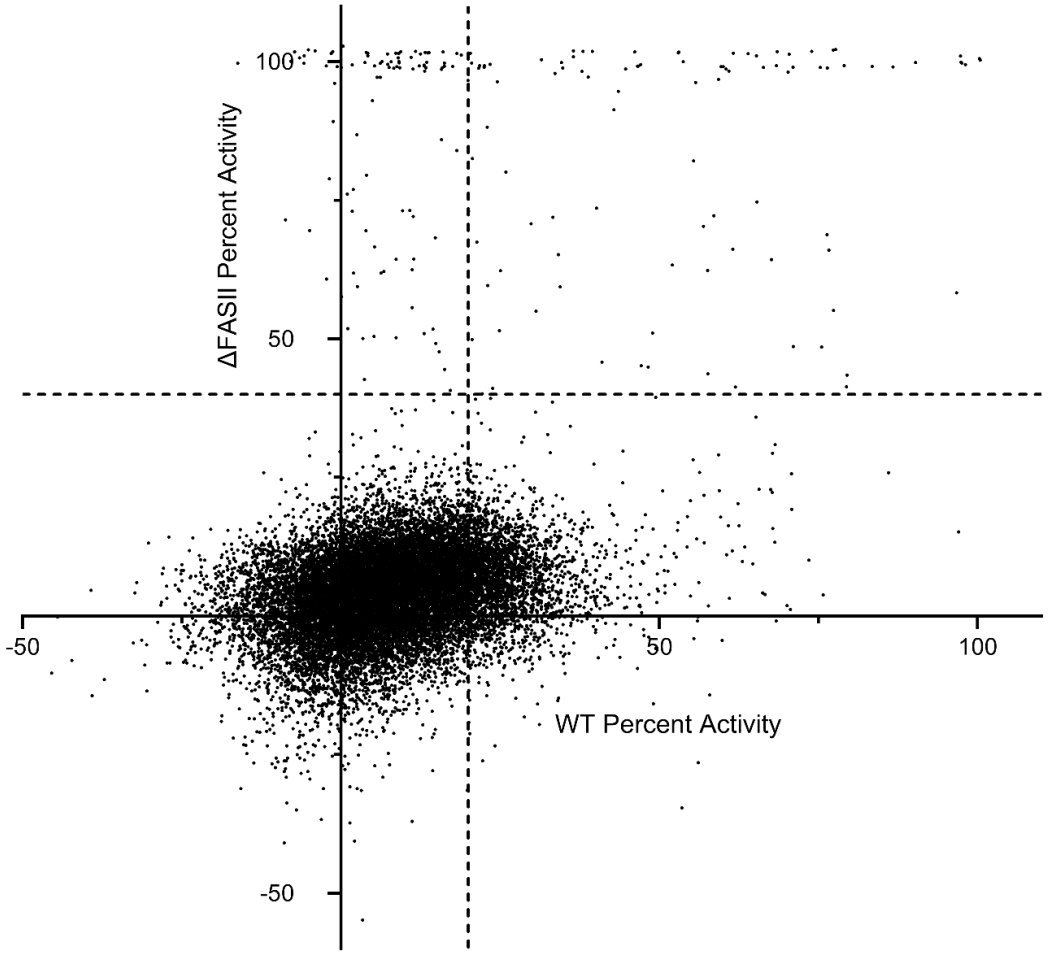

Figure 4-3. Screening of the Maybridge Library identifies unique inhibitors of the ΔFASII mutant.
The percent activity (percent inhibition compared to untreated control) is plotted on the x- and y-axis for the WT and ΔFASII mutant, respectively. Each point represents an individual compound. The vertical dotted line is set at 20% WT activity and the horizontal dotted line is set at 40% ΔFASII activity, where unique ΔFASII mutant inhibitors are defined as above the horizontal line and left of the vertical line.

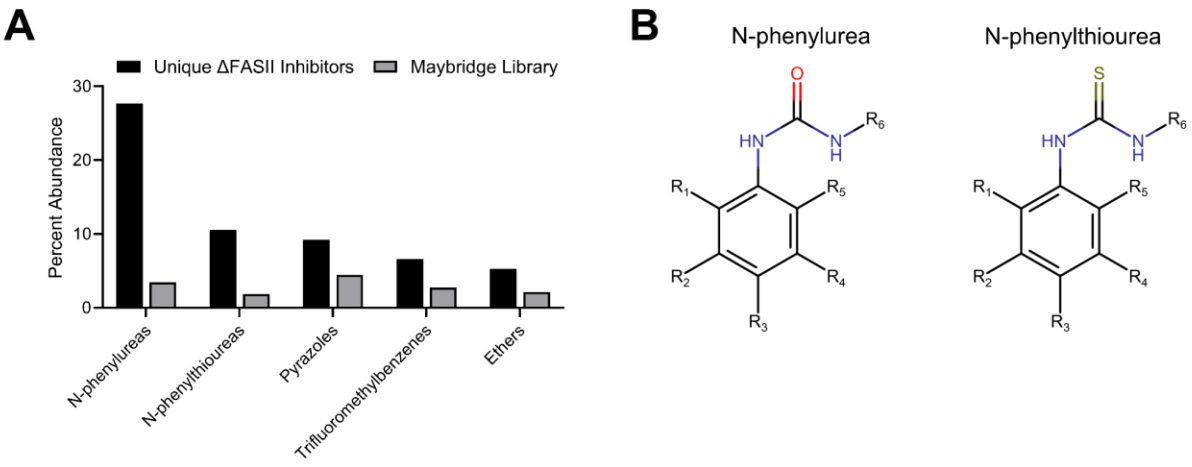

Figure 4-4. N-phenylureas and N-phenylthioureas are overrepresented in unique ΔFASII inhibitors compared to their abundance in the Maybridge Library.
(A) A bar graph depicting the percent abundance of chemical sub-classes for either unique ΔFASII inhibitors (black) or the Maybridge Library. (B) The most basic form of either an N-phenylurea (left) or an N-phenylthiourea (right). Importantly, these compounds can be modified by the addition of other chemical groups, as represented by "R_n".

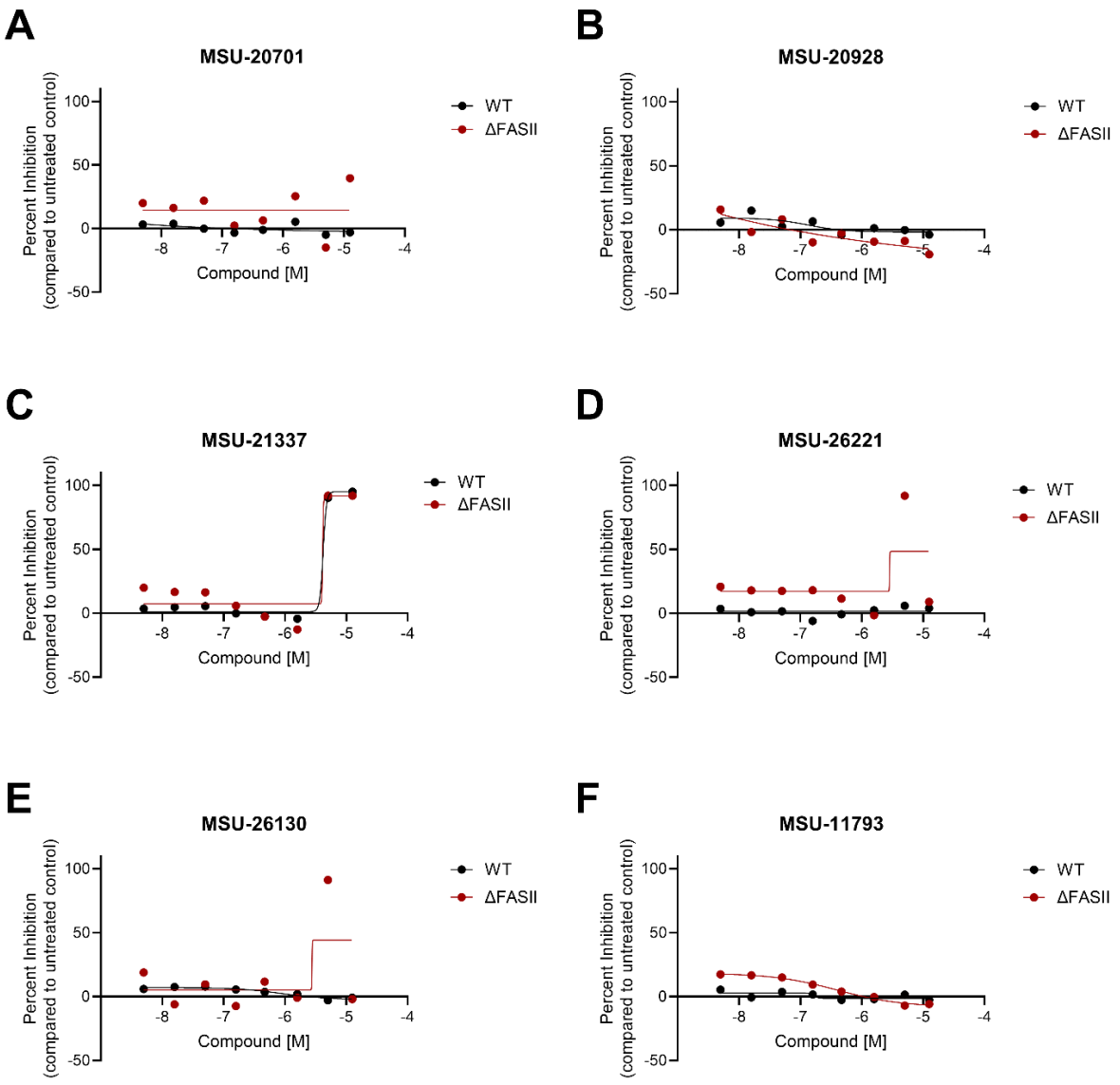

Figure 4-5. Dose response follow up of selected Maybridge compounds.
(A-AG) Graphs represent the dose response follow up of the unique ΔFASII inhibitors. Compounds used for the dose response follow up were taken from the same stocks used for the initial screen of the Maybridge library. Dose response curves were calculated using the variable four slope parameter in GraphPad Prism. (A-R) Compounds which displayed no inhibitory activity or displayed activity against both the WT and the ΔFASII mutant. (S-AG) Compounds which displayed selective activity for the ΔFASII mutant.

Figure 4-5 (cont'd)

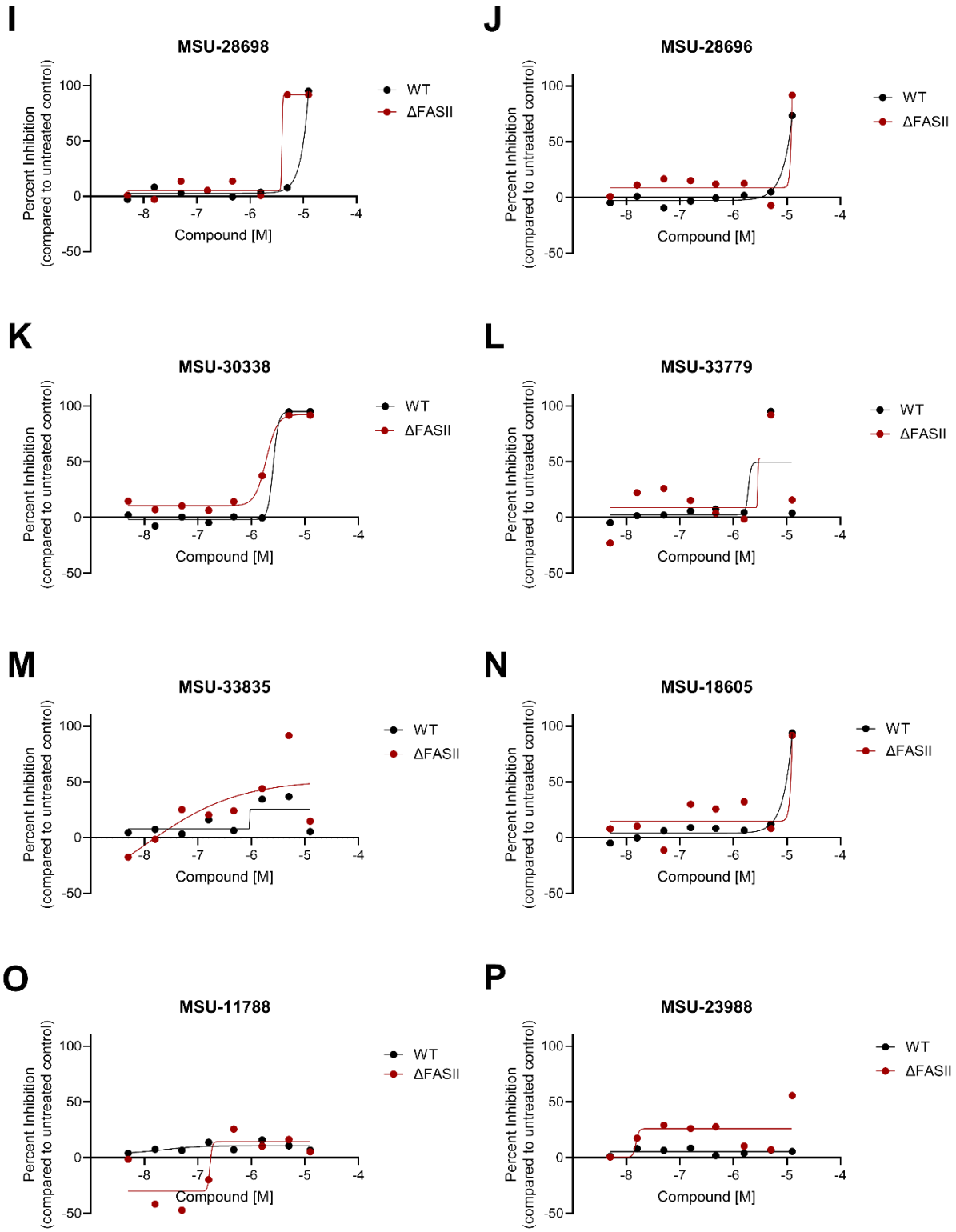

Figure 4-5 (cont'd)

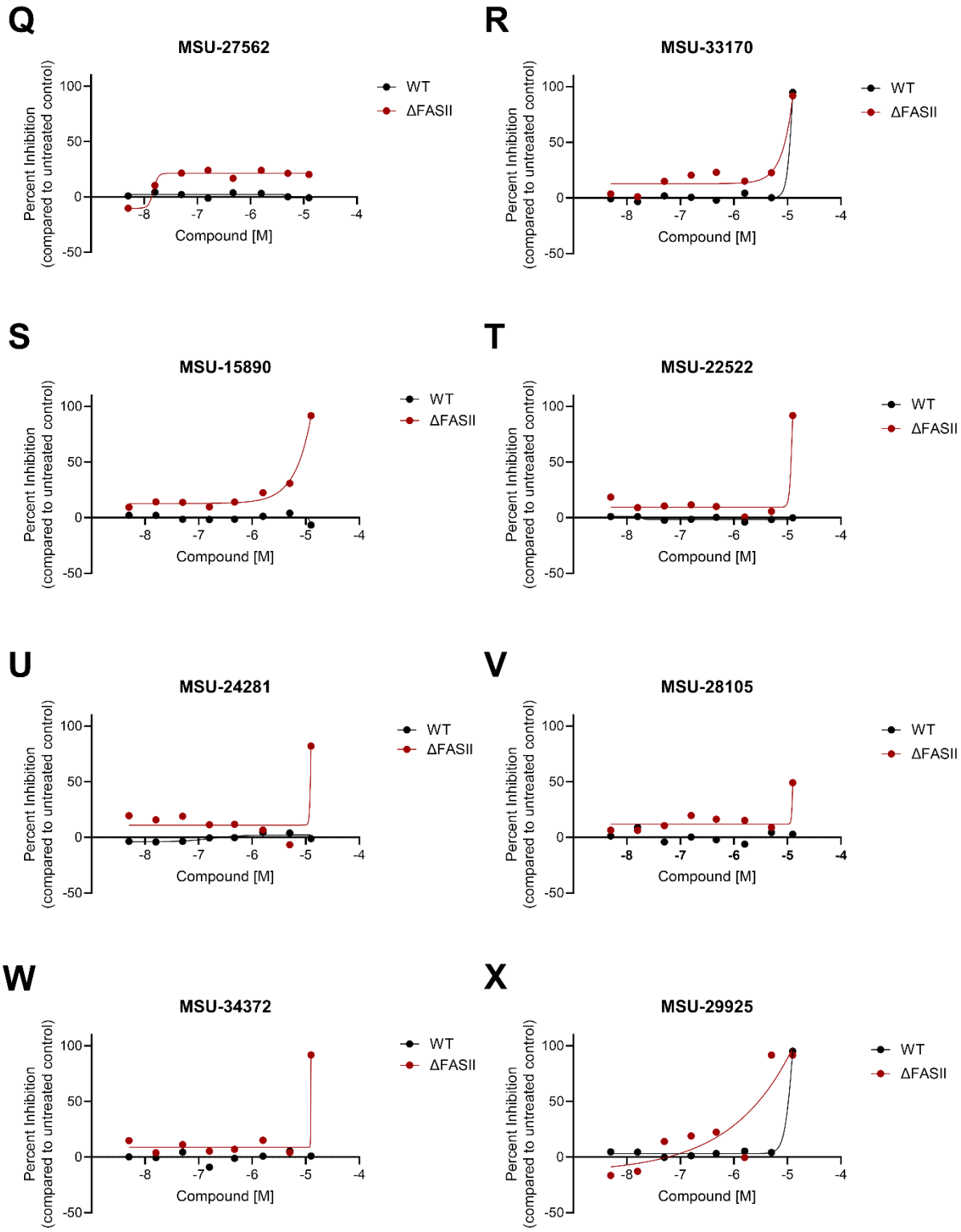

Figure 4-5 (cont'd)

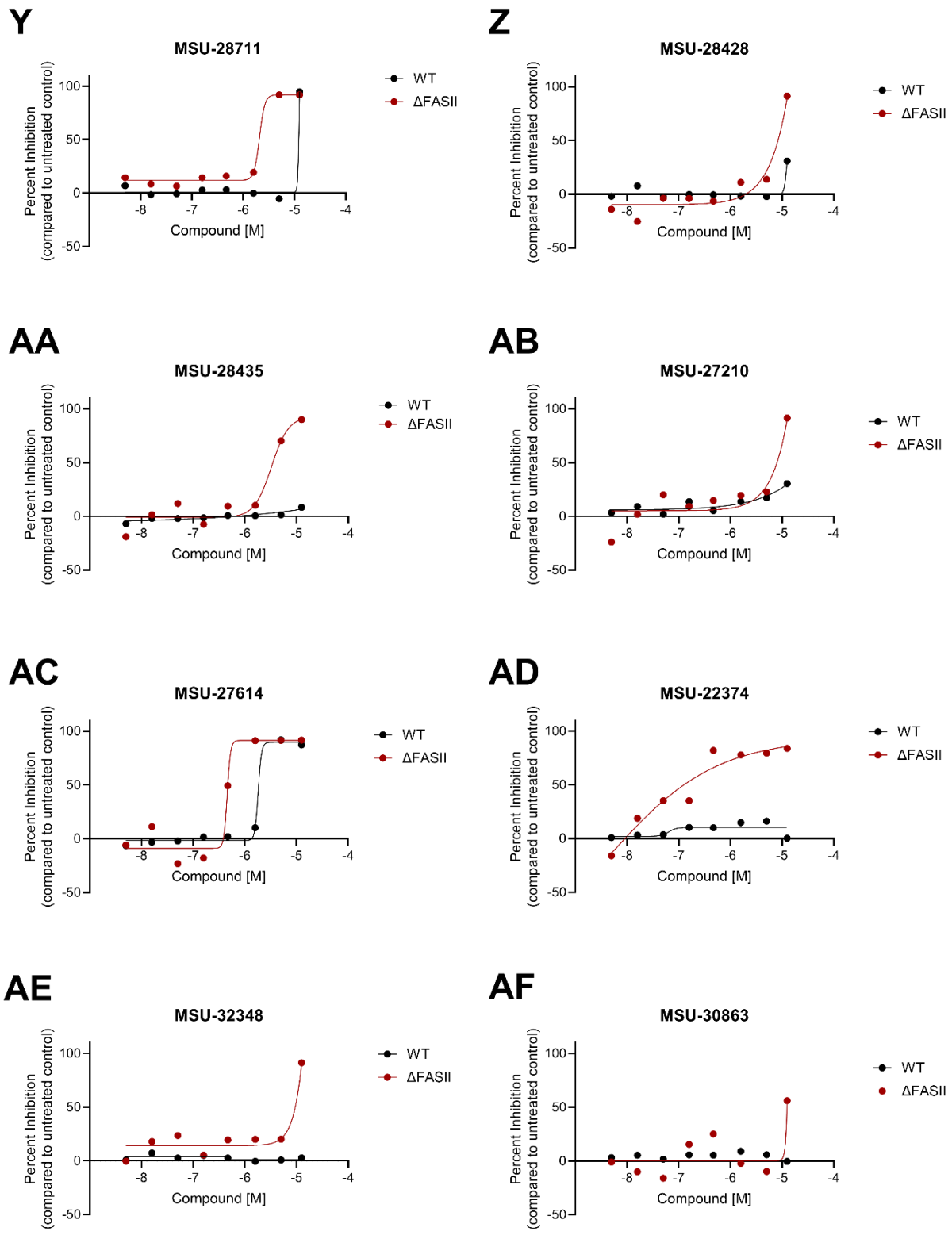

Figure 4-5 (cont'd)

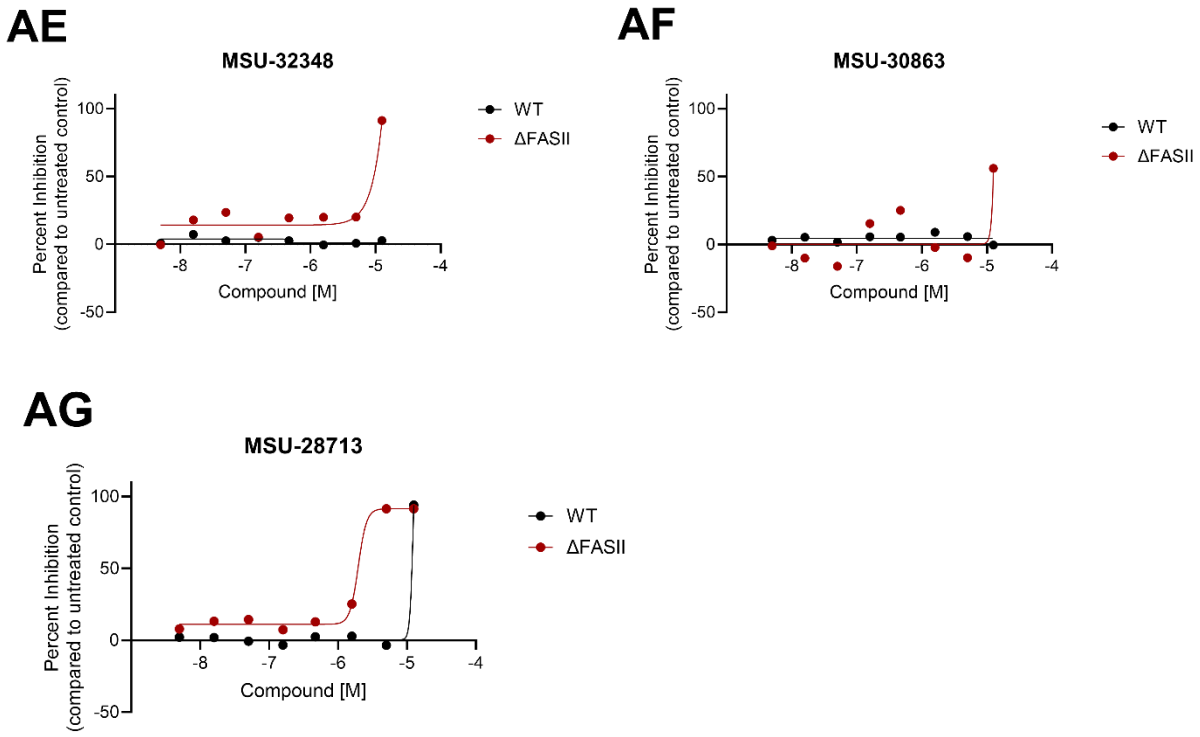

Screening of the PKIS library identifies one unique inhibitor of the ΔFASII mutant

The PKIS library was screened for activity against the ΔFASII mutant and compared to the results of the WT. Using the same parameters to define unique ΔFASII inhibitors as were used for the Maybridge library identified a single compound (Fig. 4-6). Given that compounds from the PKIS library are not available for purchase of fresh powder and that unique ΔFASII mutant inhibitors were identified in the Maybridge library and libraries described below, a dose response follow up was not performed. Similar to the Maybridge library, compounds that inhibit both the WT and the ΔFASII mutant were identified (Fig. 4-6 upper right corner) and may be generally anti-staphylococcal. Also of note is a cluster of compounds which appears to have a high degree of activity for the WT but little to no activity for the ΔFASII mutant (Figure 4-6, bottom right). This suggests that loss of FASII activity has a protective effect against these compounds.

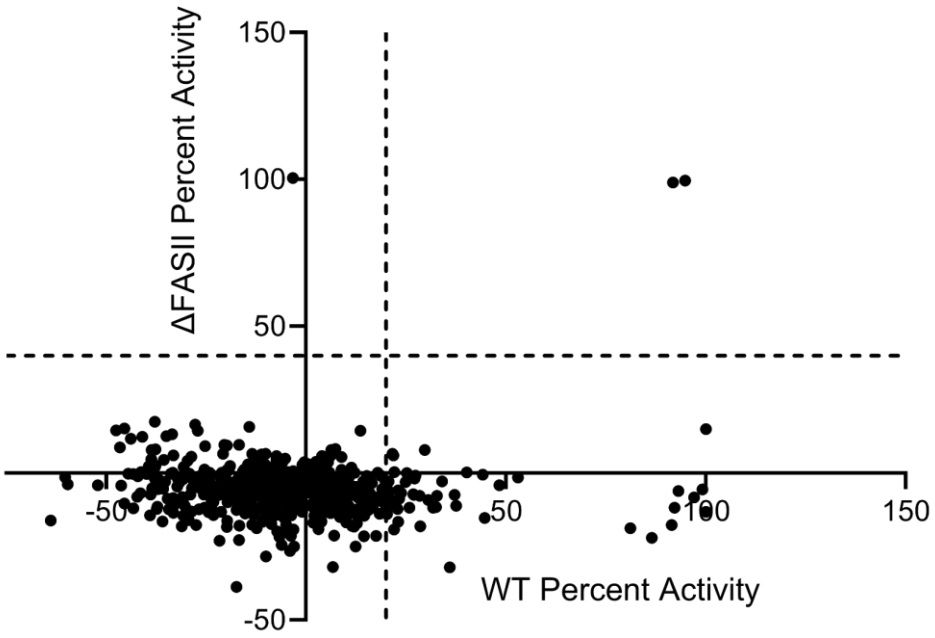

Figure 4-6. Unique inhibitors of the ΔFASII mutant were not identified in the PKIS library.
The percent activity of the WT and ΔFASII mutant from the PKIS library. The vertical dotted line is set at 10% WT activity and the horizontal dotted line is set at 40% ΔFASII activity, where unique ΔFASII mutant inhibitors are defined as above the horizontal line and left of the vertical line.

Screening of LOPAC, NCI, NCATS_MIPE and Prestwick libraries

The remaining libraries do not have WT data points for comparison of the ΔFASII screening results. However, the LOPAC, NCI, NCATS_MIPE and Prestwick libraries are annotated for their known activity. Therefore, compounds which are known to be antimicrobial (β-lactams, macrolides, glycopeptides, etc.) can be excluded from further investigation as they are likely not inhibitors of the FAK system. A cutoff of 40% or greater was arbitrarily set to define a compound as having activity against the ΔFASII mutant (Fig. 4-7, horizontal dotted line). Using these parameters 117 compounds were found to inhibit growth of the ΔFASII mutant. Structural analysis could not be performed on these libraries, as the majority of the compounds in these libraries are too structurally complex for the ClassyFire tool to categorize. Of the 117 identified inhibitors, 21

of them were found to have no prior reports of antimicrobial activity (Table A-8). These 21 compounds were followed up with a dose response analysis using the same compound stocks that were used for the initial screening. Similar to what was observed for the Maybridge library, many of the compounds either did not exhibit any activity or showed similar activity between the WT and the ΔFASII mutant (Fig. 4-8A to Q). Four of the compounds demonstrated activity that was selective toward the ΔFASII mutant (Fig. 4-8R to U).

The dose response of MSU-40452, of the NCATS_MIPE library, was particularly impressive, as it displayed an $I.C._{50}$ in the nanomolar range while the WT was unaffected (Fig. 4-8U). Furthermore, MSU-40452 is annotated as an IKK inhibitor, which belongs to a class of molecules that inhibit the phosphorylation of NF-κB; a proinflammatory transcription factor in humans (235, 236). Given that MSU-40452 is a known kinase inhibitor, and it displayed exceptional selectivity toward the ΔFASII mutant, it was chosen for the purchase of fresh powder to further validate these results.

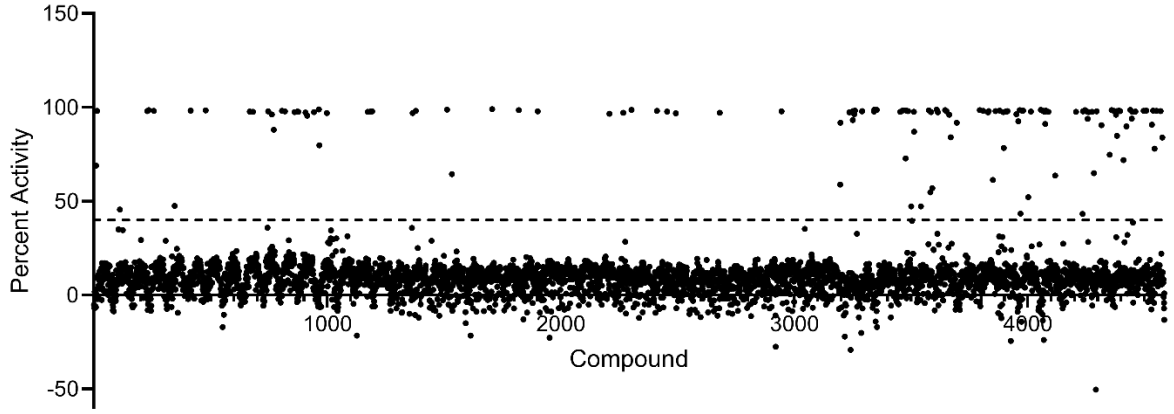

Figure 4-7. Screening the LOPAC, NCI, NCATS_MIPE and Prestwick library identified inhibitors of the ΔFASII mutant.

The percent activity (percent inhibition compared to an untreated control) of compounds from the LOPAC, NCI, NCATS_MIPE and Prestwick libraries screened against the ΔFASII mutant. The horizontal dotted line represents 40% inhibition, above which a compound was considered to have activity against the ΔFASII mutant. The x-axis represents the total amount of compounds screened in these libraries (4,584).

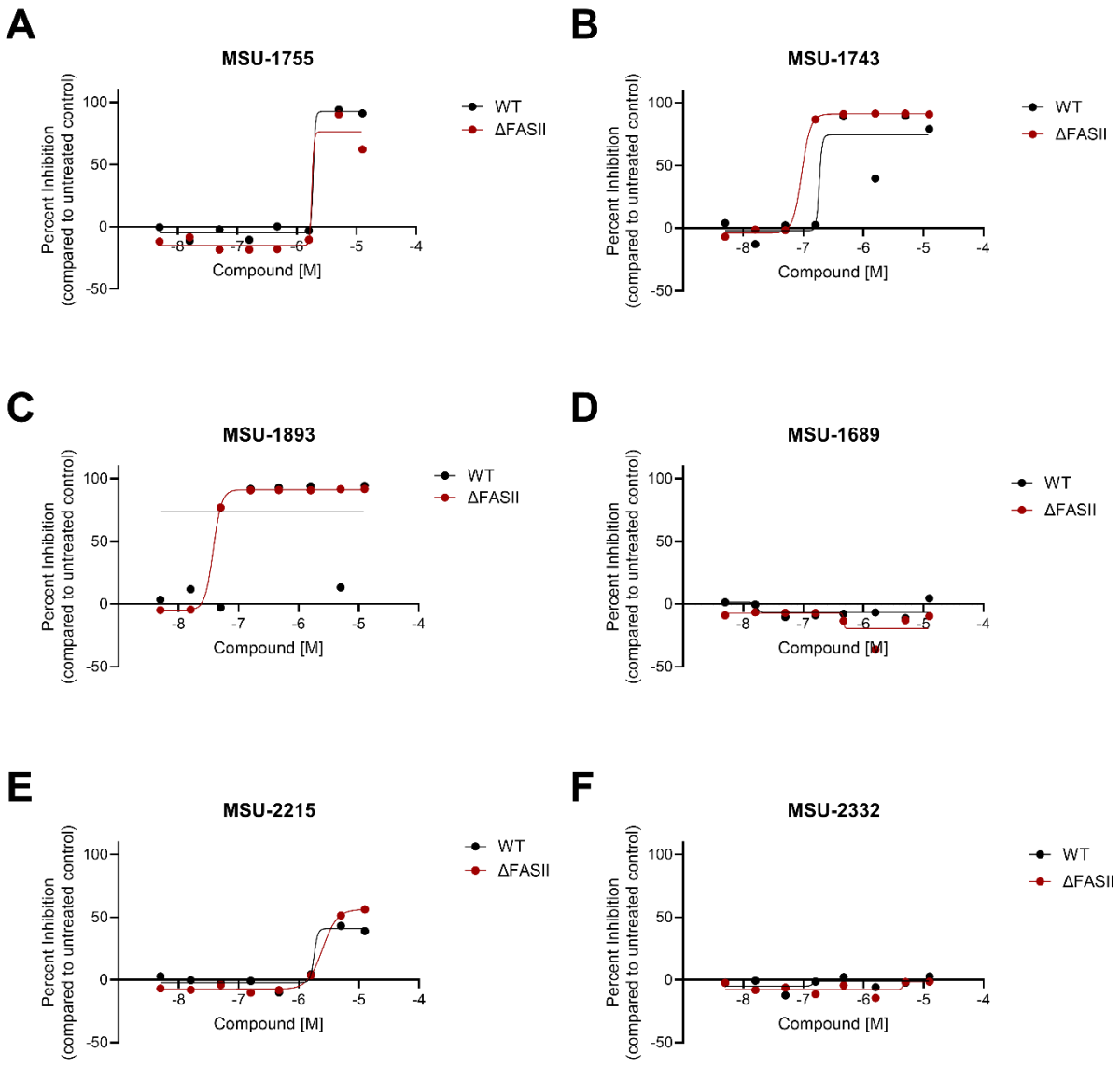

Figure 4-8. Dose response follow up of selected compounds from the LOPAC, NCI, NCATS_MIPE and Prestwick libraries.

(A-U) Graphs represent the dose response follow up of the selected ΔFASII mutant inhibitors where the percent inhibition is plotted on the y-axis and the concentration (M) of the compound is plotted on the x-axis. Compounds used for the dose response follow up were taken from the same stocks used for the initial screen of the LOPAC, NCI, NCATS_MIPE and Prestwick libraries. Dose response curves were calculated using the variable four slope parameter in GraphPad Prism. (A-R) Compounds which displayed no inhibitory activity or displayed activity against both the WT and the ΔFASII mutant. (S-U) Compounds which displayed selective activity for the ΔFASII mutant.

Figure 4-8 (cont'd)

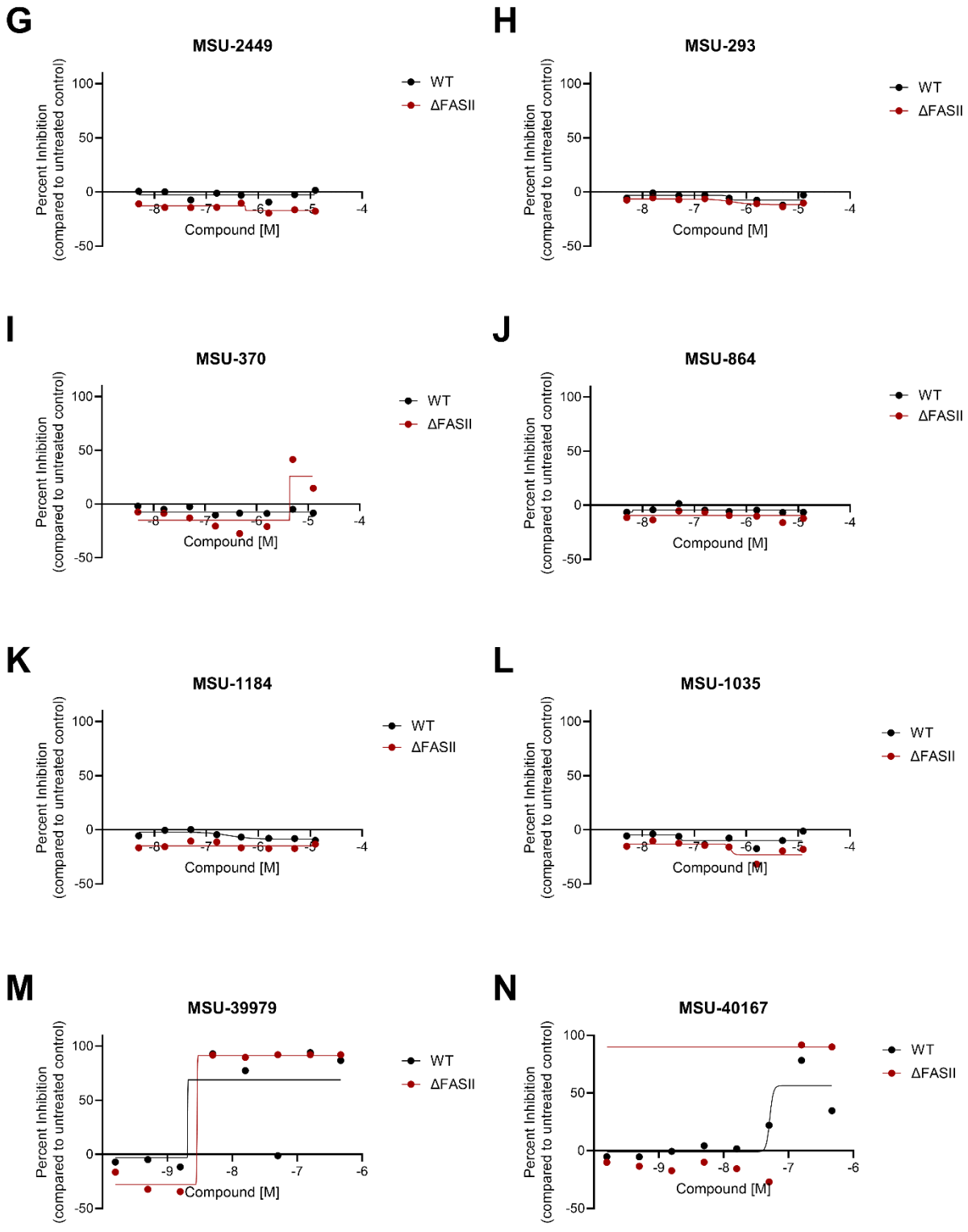

Figure 4-8 (cont'd)

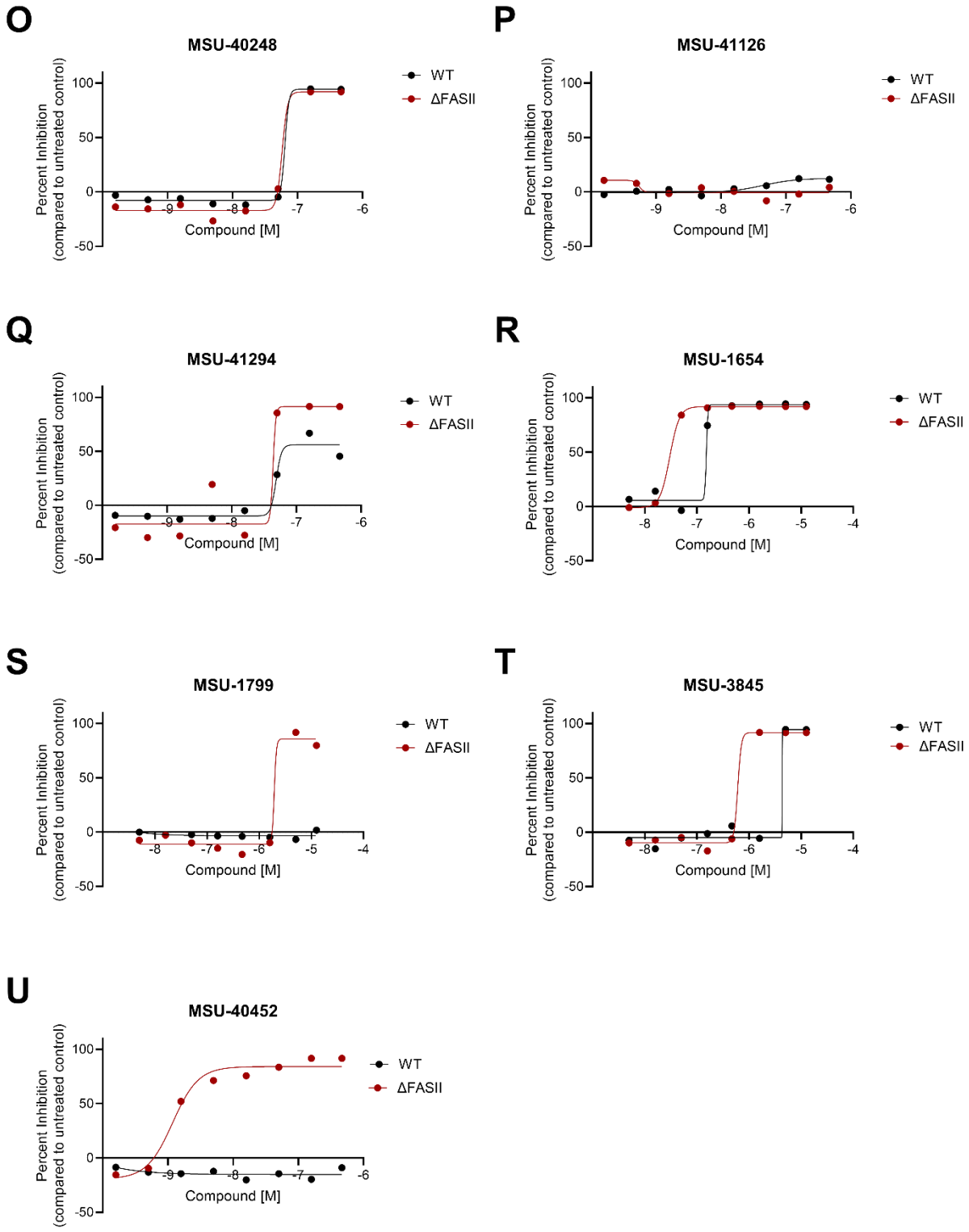

MSU-40452 is a selective inhibitor of the ΔFASII mutant and works synergistically with the FASII inhibitor triclosan

In total, fresh powder for ten compounds was purchased for validation of their activity against the ΔFASII mutant. Dose response analysis was performed and revealed many compounds either have no activity against the WT and ΔFASII mutant or to have similar activity against the WT and ΔFASII mutant (Fig. 4-9A to E). Four compounds displayed greater activity against ΔFASII than the WT (Fig. 4-9F to I). Though MSU-22374 exhibited selective activity against the ΔFASII mutant it never reached 100% inhibition, even at a concentration of 100 μM (Fig. 4-9F). Both MSU-24281 and MSU-15890 displayed greater activity against the ΔFASII mutant, however growth of WT reached 100% inhibition for these compounds at higher concentrations. Conversely, MSU-40452 displayed selective activity against the ΔFASII mutant, with an $I.C._{50}$ of 0.144 μM and reached 100% inhibition at 2.5 μM (Fig. 4-9I). Growth of the WT was reduced, but never reached greater than 54% inhibition, even at the highest concentration of 100 μM. It is important to note that not only does MSU-40452 display greater selectivity toward the ΔFASII mutant, it also exhibits greater potency. Whereas the dose response assays for other compounds started at 100 μM, the dose response for MSU-40452 began at only 10 μM.

Triclosan is a known inhibitor of the FASII pathway and exerts its antimicrobial activity by forming a complex with NAD^+ in the active site of FabI; an enzyme in the elongation stage of FA synthesis (237). The efficacy of FASII inhibitors is limited due to the ability of *S. aureus* to acquire host derived FAs via the FAK system (238). Therefore, a dual therapy strategy that targets both endogenous FA synthesis and exogenous FA acquisition will be necessary to treat *S. aureus* infections. To assess the viability of this treatment strategy a synergy assay was performed using triclosan and MSU-40452. Different combinations of these compounds were tested for their ability

to inhibit growth of the WT supplemented with FA, and the combinatory effect was determined using the combination index (CI), which quantitatively determines drug interactions as synergistic (<1), additive (=1), or antagonistic (>1) (239). The MIC of triclosan alone was 0.25 μM for the WT (Fig. 4-10). However, the addition of only 0.009766 μM MSU-40452 lowered the MIC of triclosan to 0.125 μM and yielded a CI value of 0.504, indicating a synergistic effect. The MIC of triclosan was further lowered to 0.0625 μM when in combination with 0.3125 μM MSU-40452, a combination that also exhibited synergism (CI=0.375). However, an antagonistic effect was observed at lower concentrations of triclosan and high concentrations of MSU-40452. Whereas the MIC of MSU-40452 alone was 2.5 μM, the addition of 0.015625 μM triclosan increased the MIC to 10 μM (CI=4.063) (Fig. 4-10). A similar, but not as drastic effect was observed at 0.3125 μM triclosan, which raised the MIC of MSU-40452 to 5 μM (CI=2.125). The overall interaction between these two compounds indicates that a dual therapy strategy would require a high concentration of triclosan in combination with a low concentration of MSU-40452 to achieve the synergistic effect.

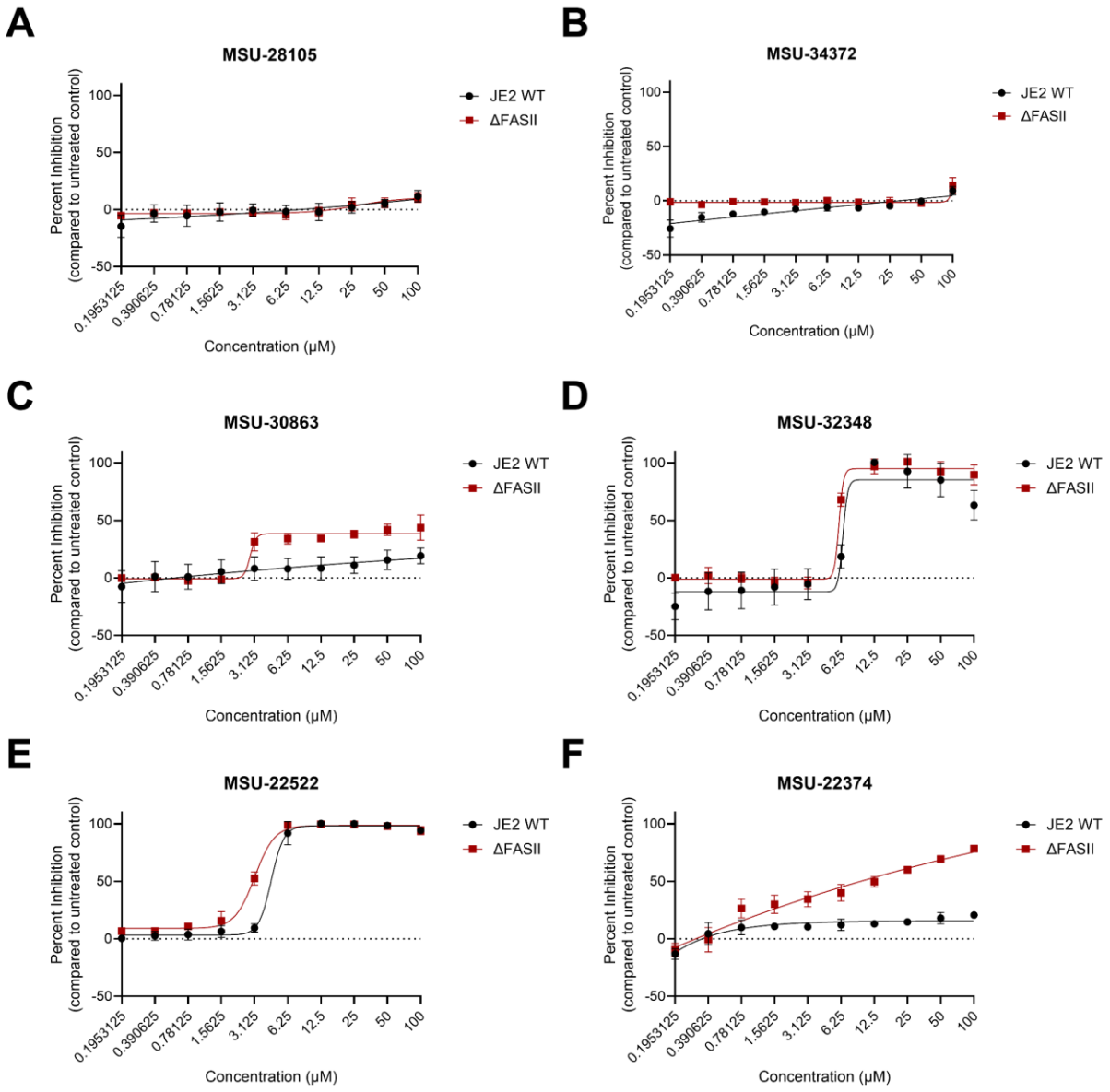

Figure 4-9. Dose response of analysis of purchased compounds.
(A-I) Graphs represent the dose response follow up of the compounds selected for purchase of fresh powder. The percent inhibition is plotted on the y-axis and the concentration (μM) of the compound is plotted on the x-axis. Dose response curves were calculated using the variable four slope parameter in GraphPad Prism. (A-E) Compounds which displayed no inhibitory activity or displayed activity against both the WT and the ΔFASII mutant. (F-I) Compounds which displayed selective activity for the ΔFASII mutant. Data represent the average of three biological replicates performed in technical triplicate.

Figure 4-9 (cont'd)

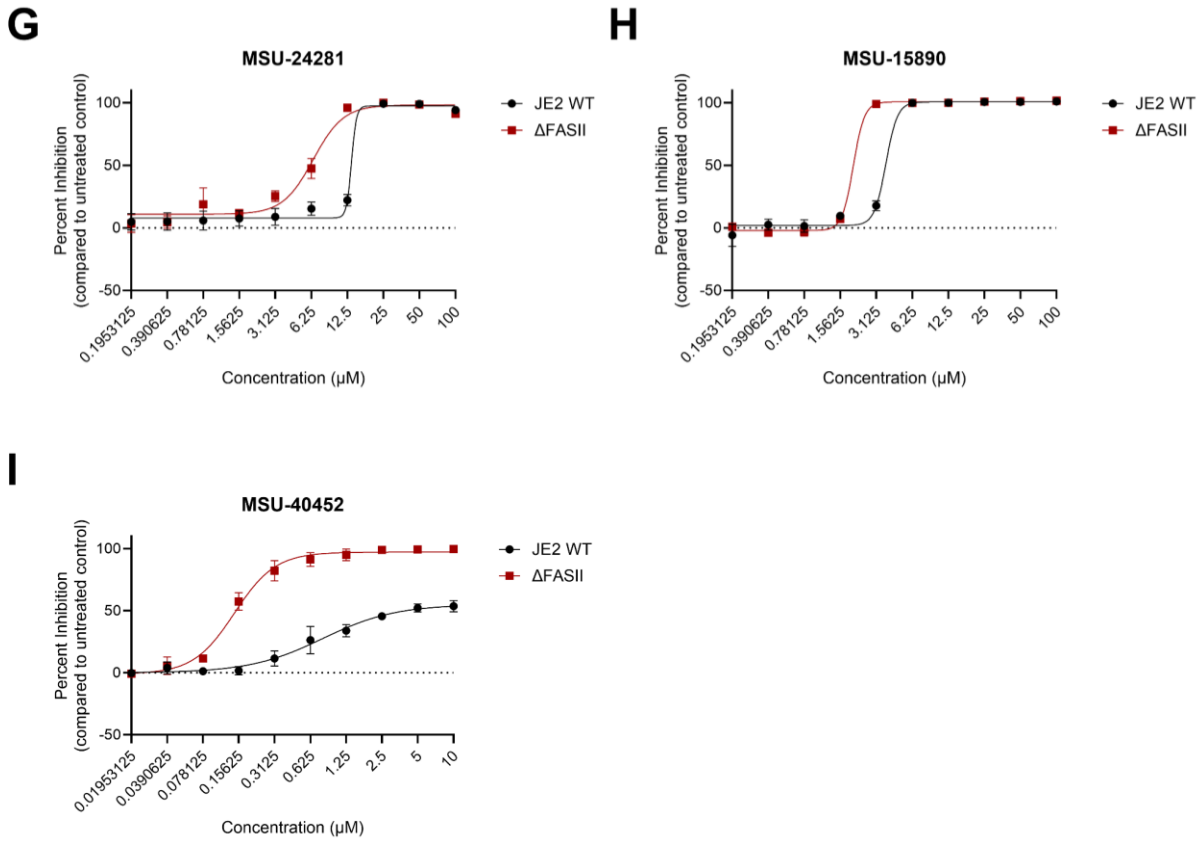

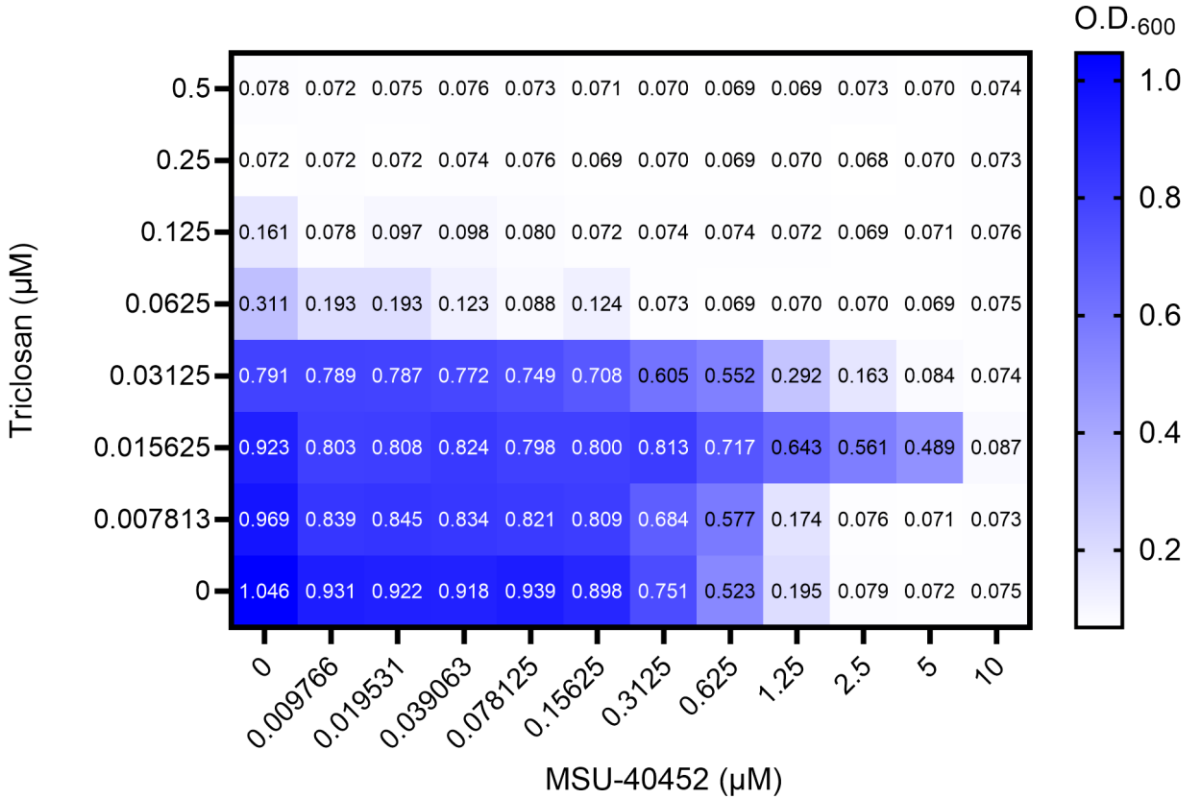

Figure 4-10. Triclosan and MSU-404052 display both synergistic and antagonistic effects when used in combination.
The results of a checkerboard assay displayed as a heat map. Individual values represent the measured optical density at 600 nm ($O.D._{600}$), where dark blue represents a high $O.D._{600}$ value (more growth) and lighter blue represents a low $O.D._{600}$ value (less growth). Data represent the average of three independent biological replicates.

Generation of mutants resistant to MSU-40452

As a first step toward elucidating the mechanism of action for MSU-40452, a method was developed for the isolation of resistant clones with the hypothesis that whole genome sequencing of resistant strains may reveal potential targets of this compound. A single colony of ΔFASII was used to inoculate BHI + FAs and serially passaged in increasing concentrations of MSU-40452. For each passage, BHI without FA supplementation was inoculated as a control to ensure FA auxotrophism was maintained. After the final passage, the culture was struck for isolation on BHI agar + FA to isolate an individual colony which was named ΔFASII Clone 1. Subsequent dose response analysis confirmed that ΔFASII Clone 1 displayed increased resistance compared to the ΔFASII parental strain (Fig. 4-11). The maximum level of

ΔFASII Clone 1 growth inhibition compared to the untreated control was ~44% at 10 μM MSU-40452; a level of resistance that is greater than even the WT, which displayed a similar level of inhibition at only 2.5 μM (Fig. 4-9I). These data demonstrate that serially passaging ΔFASII in the presence of MSU-40452 is a viable strategy for the isolation of resistant mutants which can be used for whole genome sequencing to identify mutations that may be responsible for the observed resistance phenotype.

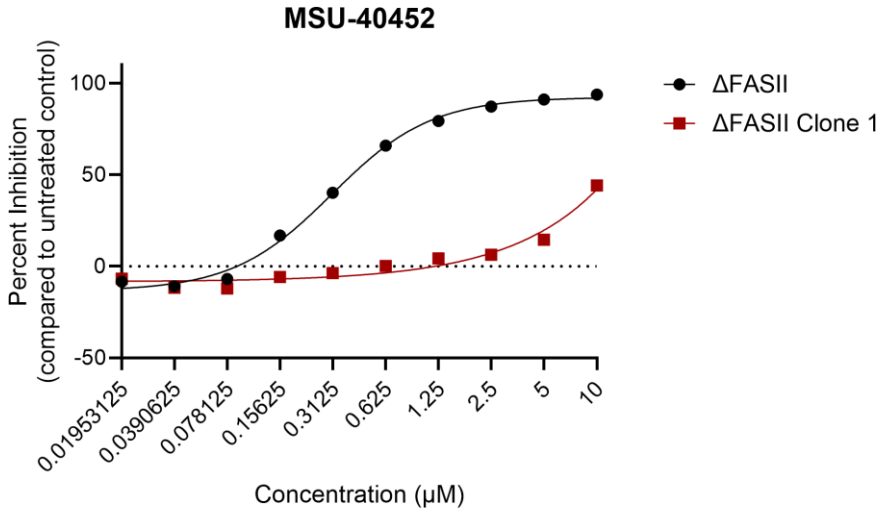

Figure 4-11. ΔFASII Clone 1 exhibits increased resistance to MSU-40452 compared to the ΔFASII parental strain.
Dose response analysis of ΔFASII and ΔFASII Clone 1 against MSU-40452. The percent inhibition is plotted on the y-axis and the concentration (μM) of the compound is plotted on the x-axis. Dose response curves were calculated using the variable four slope parameter in GraphPad Prism. Data represent the average of one biological replicate performed in technical triplicate.

Discussion

The increasing prevalence of antibiotic resistance highlights the need for development of antimicrobials with novel mechanisms of action (204). To this end, we screened chemical libraries for growth inhibitors of the ΔFASII mutant that had little or no activity against the WT. This approach enriched hit compounds for potential FAK system inhibitors, and dose response analysis identified three categories of compounds that: 1) demonstrated greater activity against ΔFASII than the WT, 2) exhibited similar inhibitory activity against both the WT and ΔFASII mutant, and 3)

displayed no activity against the WT or ΔFASII mutant. Four compounds (MSU-24281, MSU-15890, MSU-22374, and MSU-40452) were verified to exhibit greater activity against ΔFASII than the WT via dose response analysis using fresh powder. However, two of these compounds, MSU-24281 and MSU-15890, also inhibited the WT at high concentrations (Fig. 4-9G and H). Mutants deficient for the FAK system grow similar to the WT (240). Therefore, a compound that inhibits the FAK system should have little to no effect on WT growth. There are two possible mechanisms that can explain the activity of MSU-24281, and MSU-15890 against the WT. 1) These compounds are FAK system inhibitors, but have off target effects that lead to inhibition of the WT, or 2) the mode of action is independent of the FAK system and the ΔFASII mutant happens to be more sensitive than the WT. Regardless of the mechanism, it is intriguing to consider that disruption of the FASII pathway sensitizes *S. aureus* to these compounds, and raises the question of whether inhibition of the FASII pathway could be used as a strategy to reduce resistance to other antimicrobials.

Two other compounds, MSU-22374 and MSU-40452, displayed significantly greater activity against ΔFASII than the WT (4-9F), however the former compound never reached 100% growth inhibition of ΔFASII. A possible explanation for this observation is that MSU-22374 may have low affinity for its target or may be limited in its ability to cross the cell membrane. The selectivity of this compound against ΔFASII is the same dynamic that would be expected for a FAK system inhibitor. Therefore, it is worth further investigation to identify the target of MSU-22374 and subsequently optimize the compound to increase potency. On the other hand, MSU-40452 completely inhibited growth of ΔFASII at low concentrations while only inhibiting ~50% growth of the WT at the highest concentration tested (Fig. 4-9I). The high degree of potency displayed by MSU-40452 made it an ideal candidate for combination therapy with FASII inhibitors. A synergy

assay with MSU-40452 and the FASII inhibitor triclosan demonstrated that these two compounds complement the others activity synergistically. However, at low concentrations of triclosan and high concentrations of MSU-40452 an antagonistic effect was observed. Antagonism is often exhibited in drug combinations in which one antibiotic is bacteriostatic, and the other is bactericidal (241). This phenomenon is likely explained by the observation that many antibiotics are only effective on actively dividing cells (242). Therefore, the cessation of cell division caused by a bacteriostatic drug would reduce the efficacy of the bactericidal drug when used in combination. It has been established that triclosan exhibits bacteriostatic effects at low concentrations and bactericidal effects at high concentrations (243, 244), which may explain the transition from synergism to antagonism with MSU-40452 as the concentration of triclosan decreases. Accordingly, the development of a dual therapy treatment targeting bacterial FA synthesis will need to take into consideration the bacteriostatic-bactericidal antagonistic interactions of candidate compounds to ensure efficacy. Additionally, the isolation of ΔFASII Clone 1 demonstrated that generation of MSU-40452 resistant strains is possible. To begin elucidating the mechanism of action a panel of MSU-40452 resistant strains should be generated in the ΔFASII background. Whole genome sequencing of these resistant strains may reveal commonly mutated genes which would serve as a starting point of investigation.

Initial screening of the Maybridge and PKIS libraries identified groups of compounds that inhibited both the WT and ΔFASII mutant similarly. The goal of this study was to identify unique inhibitors of the ΔFASII mutant, so these compounds were not included in follow up analysis. However, some compounds that were identified as unique ΔFASII inhibitors in the initial chemical screening displayed inhibitory activity against WT and ΔFASII in the dose response follow-up. These compounds include MSU-22522 (Fig. 4-9E) and MSU-32348 (Fig. 4-9D), which may be

anti-staphylococcal or generally antibacterial and warrant further investigation to determine their spectrum of activity and evaluate their potential as antimicrobial agents.

Structural analysis of compounds in the Maybrige library identified the N-phenylurea and N-phenylthiourea subclasses as a potential family of FAK system inhibitors. Because of this, compounds belonging to these subclasses were given priority over other compound subclasses for dose response characterization. However, the follow up analysis invalidated the majority of N-phenylureas and N-phenylthioureas as FAK system inhibitors. Consequently, many compounds which displayed considerable selective activity against ΔFASII in the initial screen were not included in the dose response follow up. To ensure that promising compounds with selective activity against ΔFASII are not overlooked, the putative ΔFASII inhibitors initially identified in the screening of the Maybridge library should be re-evaluated and a more structurally diverse set should be selected for validation of activity.

The *S. aureus* cell membrane is an essential structure for viability and the pathways supporting its synthesis are unique from those of the human host. Thus, these pathways can serve as druggable targets for the treatment of *S. aureus* infections. However, the effectiveness of current antimicrobials targeting endogenous FA synthesis is limited in FA rich host environments due to the FAK system (224). Here, we described a chemical screen that identified several compounds which may target the FAK system; serving as an essential first step toward developing a dual treatment strategy inhibiting synthesis of the cell membrane. FA synthesis is a highly conserved pathway in bacteria, thus developing a therapeutic regiment in which the FASII pathway and FAK system are simultaneously inhibited has the potential to impact the treatment of infections caused by a wide range of bacterial pathogens.

Materials and Methods

Bacterial strains and growth conditions

The bacterial strains used in this study are described in Table 4-1. The ΔFASII mutant was supplemented with fatty acids consisting of myristic acid, palmitic acid and oleic acid at a final concentration of 16.65 µM of each fatty acid (49.95 µM total fatty acid). Routine culturing of strains was carried out on TSA with or without fatty acid supplementation unless otherwise specified. Agar plates were incubated at 37 °C. Overnight cultures were started from single colonies in BHI broth with or without fatty acid supplementation and incubated at 37 °C with shaking at 225 rpm.

Table 4-1. Bacterial strains used in this study

Name	Relevant genotype and phenotype	Source
JE2	USA_300, Wild type (WT)	(170)
ΔFASII	AH1263, USA_300, *accB*, fatty acid axuotroph	(229)

Screening of chemical libraries

Overnight cultures of the ΔFASII mutant were normalized to an $O.D._{600}$ of 1.0 in PBS. BHI supplemented with fatty acids was inoculated 1:100 with the normalized cultures. Screening of libraries was carried out by MSU ADDRC. Compounds from the libraries were screened at a concentration of 7.5 µM in 384-well plates. The plates were incubated at 37 °C with shaking for 24 hours, after which the $O.D._{600}$ was measured.

Structural analysis of Maybridge library compounds

Structural analysis was carried out using the simplified molecular input line entry system (SMILES) string for each compound in the Maybridge library. SMILES strings were analyzed using the R package classyfireR, which uses API access to obtain structural information from the

ClassyFire chemical classification tool (231). Compounds were classified to the sub-class level of classification, as this level of detail provides a high degree of information without creating a high number of compound subdivisions.

Dose response analysis

Primary dose response analysis for validation of library screening results was performed by MSU ADDRC using the same compound stocks used for the initial library screening. Dose response analysis for purchased compounds was performed in a 96 well plate. Overnight cultures of the WT and ΔFASII mutant were normalized to an $O.D._{600}$ of 1.0 in PBS. BHI broth supplemented with FAs was used as a positive control to represent unrestricted growth. As a negative control BHI supplemented with FAs and 40 µg/mL chloramphenicol was used to represent complete growth inhibition. Purchased compounds were dissolved in DMSO and diluted in BHI + FAs to a final concentration of 100 µM (with the exception of MSU-40452 which was diluted to a final concentration of 10 µM). Serial two-fold dilutions were made, and the normalized cultures were used to inoculate each well 1:100. 96-well plates were wrapped with parafilm to prevent evaporation. The Plates were incubated at 37 °C for 24 hours, after which the wells were resuspended via pipetting and the $O.D._{600}$ was measured using either an H1 Synergy (biotek) or 800 TS (Biotek) plate reader. Percent inhibition was determined by comparison to the positive and negative control conditions. Dose response curves were calculated using the non-linear regression variable slope (four parameter) function in GraphPad Prism.

Synergy Assay

Overnight cultures of were pelleted and resuspended in PBS. The resuspended cultures were normalized to an $O.D._{600}$ of 1.0 and kept on ice. A 96-well plate was prepared using the checkerboard method described previously (245), with the following modifications. A 150 µL

volume of BHI supplemented with FAs was dispensed into each well except row A. Two solutions of BHI + FA were prepared, to which triclosan was added to a final concentration of 1 μM or 2 μM. A 150 μL volume of the BHI + FA + 1 μM solution was added to wells A1-A11, while 150 μL of the BHI + FA + 2 μM solution was added to A12. Serial two-fold dilutions were made until row G of the 96-well plate. A BHI + FA + 20 μM MSU-40452 solution was prepared, and 150 μL was added to each well in column 12, and serial two-fold dilutions were made until row 2. All wells were inoculated with 1.5 μL of the normalized culture. The plate was sealed with parafilm and incubated at 37°C for 24 hours. Growth in all wells was resuspended and the $O.D._{600}$ was measured using an H1 Synergy (Biotek) plate reader.

Generation of MSU-40452 resistant ΔFASII mutants

A single colony of ΔFASII was used to inoculate 5 mL of BHI + FA and grown overnight. The overnight culture was pelleted, resuspended in PBS and normalized to an $O.D._{600}$ of 1.0. The normalized growth was used to inoculate 5 mL of fresh BHI + FA + 1 μM MSU-40452 (1:100) and incubated at 37 °C with shaking. A control culture of BHI without FA supplementation was also inoculated 1:100 with the normalized ΔFASII to ensure the fatty acid auxotrophic phenotype was maintained. After 21 hours of incubation, the BHI +FA + 1 μM MSU-40452 culture was pelleted, resuspended in PBS and normalized to an $O.D._{600}$ of 1.0. Using the same method as described above, the normalized culture was used to inoculate media supplemented with 8 μM MSU-40452 and incubated at 37 °C with shaking for 21 hours. This process was repeated again at 32 μM MSU-40452, after which, the culture was struck for isolation on TSA + FA. A single colony was obtained and used to make a clonal frozen stock.

Chapter 5: Summary and future directions.

Summary

Chapter 1 explored the specialized pathways *S. aureus* utilizes to adapt its metabolism in response to changes in environmental conditions. These adaptations enable *S. aureus* to maintain energy production despite changes in nutrient abundance, terminal electron acceptor availability, and the inhibitory action of the host immune system. The metabolic versatility of *S. aureus* is driven by a branched aerobic respiratory pathway and nitric oxide resistant fermentative pathways (4, 7, 25). Modulation of these pathways promotes maximal fitness in the host and mutants deficient for either respiration or fermentation display reduced virulence (4, 7–9). This suggests the ability to switch between metabolic states is an important aspect of *S. aureus* pathogenesis. However, once *S. aureus* has established a niche the need for diverse energy producing pathways may be diminished as evidenced by small colony variants (SCVs) (80). The SCV phenotype is associated with persistent and recurrent infections that are often resistant to antibiotic treatment (88, 181). Furthermore, growth in the SCV metabolic state provides advantages to surviving in the host such as increased rates of host cell invasion and resistance to host-produced antimicrobials (96, 108).

Structures present at the *S. aureus* cell surface promote metabolic versatility, which is largely achieved through the maintenance of membrane potential as demonstrated for lipoteichoic acid in Chapter 2. The impermeability of the cell membrane to ions enables the buildup of an ion concentration gradient, while lipoteichoic acid (LTA) likely functions to keep the transported ions close to the cell surface, thus maintaining membrane potential. Wall teichoic acid (WTA) may perform a similar role to LTA given that it has been demonstrated to bind protons, however direct evidence for a role influencing membrane potential has not been reported for this cell surface polymer (70).

Chapter 2 defined the role of LTA in promoting fermentative viability of *S. aureus*. A *ypfP* mutant exhibits alterations in LTA where the polymers are longer and less abundant compared to the WT (58). These alterations in LTA lead to a reduced capacity to maintain membrane potential during fermentative growth, thus reducing viability. One strategy of *S. aureus* to gain resistance to aminoglycoside antibiotics is to enter the SCV metabolic state of growth (88, 181). The *ypfP* mutant was more sensitive to aminoglycoside antibiotics due to its reduced ability to transition into a fermentative state. Suppressor mutants were obtained which acquired amino acid changes in proteins involved in the synthesis of LTA. These suppressor mutations led to the production of LTA that was more similar to that of the WT in length and abundance. Consequently, the ability to maintain membrane potential during fermentative growth was restored; while also increasing the ability to gain resistance to aminoglycosides.

Chapter 3 provided insights into isoprenoid biosynthesis in *S. aureus,* leading to 4 major findings: 1) considerable redundancy exists in the isoprenoid biosynthetic pathway of *S. aureus*, 2) an unknown enzyme is capable of producing farnesyl diphosphate (FPP) during simultaneous inactivation of *ispA* and *hepT*, 3) terminal oxidases exhibit preferences for electron carriers, and 4) isoprenoid biosynthesis supports host colonization. While HepT has long been hypothesized to produce the required isoprenoids for menaquinone (MK) production (114, 118, 194), direct evidence demonstrating this has not been reported. The data presented in chapter 3 show that in the absence of functional HepT, production of MK-7, MK-8 and MK-9 is lost. Further, redundancy in isoprenoid synthesis is largely driven by HepT which was demonstrated to influence the lipid II cycle and prenylated heme production, indicating that this enzyme is involved in more pathways than just its previously hypothesized role in MK synthesis. In keeping with the redundant nature of *S. aureus* isoprenoid synthesis, a mutant simultaneously inactivated for *hepT* and *ispA* was

viable. This mutant background lacks the enzyme known to produce the essential metabolite FPP (IspA) and another enzyme we hypothesize to produce FPP (HepT). Given that FPP is essential for lipid II synthesis, the viability of the *hepT ispA* double mutant suggests another enzyme present in *S. aureus* produces FPP.

Another key finding from chapter 3 is that terminal oxidases exhibit preferences for electron carriers. The absence of prenylated hemes in the *hepT ispA* double mutant means the QoxABCD terminal oxidase is likely inactive, leaving only the CydAB terminal oxidase to carry out aerobic respiration (28). However, supplementation with MK-4 did not restore growth of the *hepT ispA* mutant. This phenotype was recapitulated by the *menB qoxA* double mutant, which is restricted to CydAB for respiration. Conversely, the *menB cydA* double mutant, which is restricted to QoxABCD for respiration, did restore growth when supplemented with MK-4. Lastly, isoprenoid synthesis was shown to influence host colonization in a mouse model of systemic infection. Disruption of isoprenoid biosynthesis via mutation of *hepT* resulted in a colonization defect in the heart and liver, however, this was phenocopied by a *menC* mutant, indicating that this phenotype is driven by loss of MK. On the other hand, an *ispA* mutant displayed a colonization defect in the heart, liver, and kidneys, and supports the notion that isoprenoid synthesis is an important pathway in supporting host colonization.

Chapter 4 described a high throughput chemical screen to identify inhibitors of the fatty acid kinase (FAK) system. *S. aureus* possesses two pathways for generation and acquisition of the fatty acids needed for phospholipid synthesis: the fatty acid synthesis type II (FASII) pathway for endogenous production of fatty acids and the FAK system for importing and incorporating exogenous fatty acids (208, 227). Mutants deficient for the FASII pathway are dependent upon fatty acid supplementation for growth. By performing a chemical screen to identify compounds

that inhibit growth of the ΔFASII mutant but not the WT, putative inhibitors of the FAK system were revealed. Initial screening of the Maybridge library identified two groups of compounds, N-phenylureas and N-phenylthioureas, which may have an inhibitory effect on the FAK system. However, follow up analysis determined that selected N-phenylureas and N-phenylthioureas had either no specific activity against the ΔFASII mutant, or only slightly greater activity against the ΔFASII mutant compared to the WT. Screening of the non-Maybridge libraries revealed a promising compound, MSU-40452, which displayed significantly greater activity against the ΔFASII mutant than the WT. Follow-up analysis determined that MSU-40452 has a synergistic effect with the known FASII inhibitor triclosan, demonstrating the viability of a dual therapy treatment in which endogenous fatty acid synthesis and the FAK system are targeted simultaneously.

Future Directions

Elucidating the mechanism behind LTA mediated maintenance of membrane potential.

Chapter 2 established the role of LTA in supporting *S. aureus* fermentative viability via maintenance of membrane potential. However, LTA was shown to only function in maintaining membrane potential during fermentative growth, whereas the membrane potential of the WT and the LTA disrupted *ypfP* mutant were similar during respiratory growth. The mechanism behind how LTA supports maintenance of membrane potential exclusively during fermentation is unclear. However, a possible explanation for this phenotype is that LTA undergoes modifications during fermentative growth that support maintenance of membrane potential, and mutation of *ypfP* disrupts this process. LTA can be modified by the addition of D-alanines, which alters the overall charge of the polymer (10). However, the effect of D-alanylation on the ion binding capacity of LTA is not known and it remains uncertain if such modifications would influence the ability to

maintain membrane potential. Therefore, to begin elucidating the mechanism by which LTA influences membrane potential the D-alanylation status of LTA from cells grown in a fermentative state and a respiratory state should be measured. This will establish whether or not the metabolic state of the cell effects LTA modifications. Additionally, investigating the impact of *ypfP* mutation on D-alanylation of LTA will determine if alteration of LTA abundance and length influences modification of this polymer.

Furthermore, another teichoic acid, wall teichoic acid (WTA), is also present at the cell surface and shares similar characteristics to LTA (10, 11, 64). Biswas et al. demonstrated that WTA is able to bind and retain protons, therefore it is possible that WTA also plays a similar role to LTA in maintaining membrane potential (70). However, the same study found that a mutant lacking WTA maintained membrane potential similar to that of the WT, though these measurements were carried out on respiring cells (70). It is possible that if WTA plays a role in maintaining membrane potential it may be limited to fermentative growth similar to LTA. Accordingly, the membrane potential of a WTA deficient mutant should be measured under respiration arrested conditions. These proposed experiments will deepen our understanding of how teichoic acids function to maintain membrane potential while offering valuable insights into a pathway that supports metabolic versatility in *S. aureus*.

In vitro characterization of S. aureus PDSs for substrate specificity and product formation.

The study of *S. aureus* isoprenoid biosynthesis in Chapter 3 provided new insights into isoprenoid production and how this pathway supports metabolic versatility. However, questions remain, that if answered, would provide fundamental knowledge about the redundant nature of *S. aureus* isoprenoid synthesis and the downstream physiological consequences of its disruption. First, to more firmly establish that HepT plays a multifunctional role in isoprenoid dependent

pathways, biochemical characterization of this enzyme will be necessary. We hypothesize that in the absence of functional IspA, HepT is capable of condensing IPP and DMAPP to initiate isoprenoid synthesis and provide FPP for downstream pathways. Similar to the analysis carried out by Takahashi et al. for the *E. coli* HepT homolog IspB, purified *S. aureus* HepT can be characterized *in vitro* for its ability to utilize IPP and DMAPP as substrates (176). Further analysis of the products formed from this reaction will determine the specificity for chain length of the isoprenoid product and establish whether HepT can synthesize FPP. Additionally, the viability of the Δ*hepT ispA*::Tn double mutant implies a third PDS is present which is capable of synthesizing FPP for use by UppS. Two hypotheses may explain the identity of the third PDS: 1) UppS can independently condense IPP and DMAPP to produce its own FPP, or 2) an unidentified PDS is present which synthesizes FPP for use by UppS. Biochemical analysis similar to that proposed for HepT will determine the ability of UppS to condense IPP and DMAPP. However, biochemical characterization of UppS homologs in other bacterial species found that this enzyme could not utilize DMAPP as a substrate (161, 196), favoring the second hypothesis. If UppS is found not to condense IPP and DMAPP, the identity of the third PDS can be obtained using the methodology described by Saito et al., in which whole cell lysate was fractionated, and the resulting fractions were evaluated for PDS activity (175). Fractions which displayed PDS activity were further fractionated and re-evaluated until individual proteins in the fraction could be identified and characterized. A similar approach can be used for the Δ*hepT ispA*::Tn double mutant, for which the only fractions with IPP and DMAPP condensing activity should be those containing the third PDS.

Evaluation of CydAB activity in response to isoprenoid tail length of quinone electron carriers.

Chapter 3 also describes preferences of terminal oxidases for isoprenoid chain length of

quinone electron carriers. A MK deficient mutant restricted to CydAB for respiration was unable to utilize MK-4 or menadione (MD) as electron carriers, whereas a MK deficient mutant restricted to QoxABCD could effectively use MK-4 or MD. This is notable, as the native MK species produced by *S. aureus* are MK-7, MK-8 and MK-9 (113, 114). However, the use of these native MK species to complement growth is limited due to their exceptional insolubility, which has been previously described (246). Therefore, further investigation of terminal oxidase preferences for electron carriers requires *in vitro* characterization. Evaluation of terminal oxidases *in vitro* has been described previously and uses the rate of oxygen consumption as a measure of activity (28, 247). Using a similar method, *S. aureus* membrane fragments containing either CydAB or QoxABCD can be isolated and provided MK species of varying isoprenoid tail length. By measuring the rate of oxygen consumption, the activity of either terminal oxidase can be determined. Given that many other bacterial species also utilize branched respiratory chains, similar dynamics may be a common feature of bacterial respiration and warrants similar investigations in other species.

Evaluating the activity of remaining putative ΔFASII inhibitors.

Future investigations stemming from the data presented in Chapter 4 largely center around further verification of compound hits and identifying the target of MSU-40452. The initial screening results of the Maybridge Library identified 100 putative inhibitors of the ΔFASII mutant, however only 33 were included in the dose response follow-up. The activity of the remaining 67 compounds should be verified via dose response to ensure compounds with selective activity toward the ΔFASII mutant are not overlooked. Two other compounds displayed selective activity toward the ΔFASII mutant but were not followed up on: MSU-1799 of the LOPAC library and MSU-9380 of the PKIS library. Dose response analysis of MSU-1799 displayed complete

inhibition of the ΔFASII mutant while the WT was unaffected. Priority was given to other compounds which exhibited activity at lower concentrations, however given the selective nature of MSU-1799, fresh powder should be purchased for validation of activity. MSU-9380 could not be followed up on initially due to the compounds in the PKIS Library being proprietary. However, the initial screen of the PKIS Library indicates that MSU-9380 may be exceptionally selective toward the ΔFASII mutant. Therefore, it is worthwhile to synthesize MSU-9380 to validate its activity, as this may be a potent inhibitor of the FAK system.

Identifying the target of MSU-40452.

Screening of the chemical libraries was designed in such a way that validated hits are likely to be inhibitors of the FAK system. However, for compounds that are selective towards the ΔFASII mutant, such as MSU-40452, direct evidence is necessary to confirm the target. As a first step, generation of mutants resistant to MSU-40452 using the method described in Chapter 4 and subsequent whole genome sequencing may reveal potential targets for this compound. Commonly mutated genes can be cloned and used to complement the ΔFASII mutant to determine if they confer resistance to MSU-40452. This method assumes the primary mechanism of resistance is to mutate the target of MSU-40452 so that it can no longer exert antimicrobial activity. However, it is possible that mutations in non-target proteins, such as transporters, can also confer resistance. In this case, the target of MSU-40452 can be identified by using the drug affinity responsive target stability (DARTS) method for small molecule target identification (248). Briefly, proteins bound to a small molecule exhibit differential susceptibility to proteolysis. Whole cell lysate can be treated with either MSU-40452 or vehicle and subjected to proteolysis. The samples are then separated by gel electrophoresis and stained for visualization. Protein bands which differ from the MSU-40452 treated sample and the vehicle control can be cut from the gel and identified via mass

spectrum analysis. While the DARTS method has been used to identify the targets of several small molecules (249), it makes the assumption that the relevant protein is present at sufficient quantities to be visualized by gel electrophoresis (250). If the protein target is expressed at low levels, other methods are available which do not require separation or visualization of proteins in the cell lysate (250). Identifying the target of small molecules enables structural studies to determine binding motifs, which in turn, allows for informed modifications to be made to the small molecule to increase potency. This is known as structure-based drug design, which has been used in the development of several drugs currently in use (251). A similar approach can be applied to MSU-40452 to increase the binding affinity for its target, thus increasing its effectiveness.

Concluding Remarks

This dissertation identified two pathways that contribute to the metabolic versatility of *S. aureus*: LTA biosynthesis and isoprenoid biosynthesis. The metabolic adaptability of *S. aureus* is a key feature that contributes to the pathogenicity and antibiotic resistance of this pathogen. Therefore, by identifying the mechanisms that facilitate the transition into different metabolic states, we gain a better understanding of how *S. aureus* causes infection and can use this information to develop better treatment strategies. In this pursuit, my research also focused on the development of a combination therapy in which endogenous fatty acid synthesis and exogenous fatty acid acquisition are simultaneously inhibited. A candidate compound was identified that synergistically complements the activity of a known fatty acid synthesis inhibitor, and serves as an initial proof of concept for this treatment strategy. Together, the data presented here highlight the therapeutic potential of targeting the metabolic adaptability of *S. aureus* and lay the foundation for future development of treatment strategies to combat antibiotic resistant bacterial infections.

REFERENCES

1. Tong SYC, Davis JS, Eichenberger E, Holland TL, Fowler VG. 2015. Staphylococcus aureus infections: Epidemiology, pathophysiology, clinical manifestations, and management. Clin Microbiol Rev 28:603–661.

2. Cheung GYC, Bae JS, Otto M. 2021. Pathogenicity and virulence of Staphylococcus aureus. Virulence 12:547–569.

3. Fuchs S, Pané-Farré J, Kohler C, Hecker M, Engelmann S. 2007. Anaerobic gene expression in Staphylococcus aureus. J Bacteriol 189:4275–4289.

4. Hammer ND, Reniere ML, Cassat JE, Zhang Y, Hirsch AO, Hood MI, Skaar EP. 2013. Two heme-dependent terminal oxidases power *Staphylococcus aureus* organ-specific colonization of the vertebrate host. mBio 4:e00241-13.

5. Pires PM, Santos D, Calisto F, Pereira M. 2024. The monotopic quinone reductases from Staphylococcus aureus. Biochim Biophys Acta Bioenerg 1865.

6. Hochgräfe F, Wolf C, Fuchs S, Liebeke M, Lalk M, Engelmann S, Hecker M. 2008. Nitric oxide stress induces different responses but mediates comparable protein thiol protection in Bacillus subtilis and Staphylococcus aureus. J Bacteriol 190:4997–5008.

7. Richardson AR, Libby SJ, Fang FC. 2008. A Nitric Oxide–Inducible Lactate Dehydrogenase Enables *Staphylococcus aureus* to Resist Innate Immunity. Science (1979) 319:1672–1676.

8. Hammer ND, Cassat JE, Noto MJ, Lojek LJ, Chadha AD, Schmitz JE, Creech CB, Skaar EP. 2014. Inter- and intraspecies metabolite exchange promotes virulence of antibiotic-resistant *Staphylococcus aureus*. Cell Host Microbe 16:531–537.

9. Dean MA, Olsen RJ, Wesley Long S, Rosato AE, Musser JM. 2014. Identification of point mutations in clinical *staphylococcus aureus* strains that produce small-colony variants auxotrophic for menadione. Infect Immun 82:1600–1605.

10. Percy MG, Gründling A. 2014. Lipoteichoic acid synthesis and function in gram-positive bacteria. Annu Rev Microbiol 68:81–100.

11. Swoboda JG, Campbell J, Meredith TC, Walker S. 2010. Wall teichoic acid function, biosynthesis, and inhibition. ChemBioChem 11:35–45.

12. Neuhaus F, Baddiley J. 2003. A continuum of Anionic Charge: Structures and Functions of D-Alanyl-Teichoic Acids in Gram-Positive Bacteria. Molecular Biology Reviews 67:686–723.

13. Benarroch JM, Asally M. 2020. The Microbiologist's Guide to Membrane Potential

Dynamics. Trends Microbiol. Elsevier Ltd https://doi.org/10.1016/j.tim.2019.12.008.

14. Mitchel P. 1961. COUPLING OF PHOSPHORYLATION TO ELECTRON AND HYDROGEN TRANSFER BY A CHEMI-OSMOTIC TYPE OF MECHANISM. Nature 191:144–148.

15. Wessner D, Dupont C, Charles T, Neufeld J. 2020. MicrobiologyThird. Wiley.

16. Wolfe AJ. 2015. Glycolysis for Microbiome Generation. Microbiol Spectr 3.

17. Strahl H, Hamoen LW. 2010. Membrane potential is important for bacterial cell division. Proc Natl Acad Sci U S A 107:12281–12286.

18. Kaback HR. 2015. A chemiosmotic mechanism of symport. Proc Natl Acad Sci U S A 112:1259–1264.

19. Poolman B, Konings WN. 1993. Secondary solute transport in bacteria. Biochim Biophys Acta 1183:5–39.

20. Guo H, Suzuki T, Rubinstein J. 2019. Structure of a bacterial ATP synthase. Elife 8:e43128.

21. Schurig-Briccio LA, Yano T, Rubin H, Gennis RB. 2014. Characterization of the type 2 NADH:menaquinone oxidoreductases from Staphylococcus aureus and the bactericidal action of phenothiazines. Biochimica et Biophysica Acta (BBA) - Bioenergetics 1837:954–963.

22. Fuchs S, Pané-Farré J, Kohler C, Hecker M, Engelmann S. 2007. Anaerobic gene expression in *Staphylococcus aureus*. J Bacteriol 189:4275–4289.

23. Schumacher A, Friedrich P, Diehl-Schmid J, Ibach B, Perneczky R, Eisele T, Vukovich R, Foerstl H, Riemenschneider M. 2009. No association of TDP-43 with sporadic frontotemporal dementia. Neurobiol Aging 30:157–159.

24. Carvalho SM, de Jong A, Kloosterman TG, Kuipers OP, Saraiva LM. 2017. The Staphylococcus aureus α-acetolactate synthase ALS confers resistance to nitrosative stress. Front Microbiol 8.

25. Troitzsch A, Van Loi V, Methling K, Zühlke D, Lalk M, Riedel K, Bernhardt J, Elsayed EM, Bange G, Antelmann H, Pané-Farré J. 2021. Carbon source-dependent reprogramming of anaerobic metabolism in staphylococcus aureus. J Bacteriol 203.

26. Hall JW, Ji Y. 2013. Sensing and adapting to anaerobic conditions by staphylococcus aureus, p. 1–25. *In* Advances in Applied Microbiology. Academic Press Inc.

27. Trchounian A, Trchounian K. 2019. Fermentation Revisited: How Do Microorganisms

Survive Under Energy-Limited Conditions? Trends Biochem Sci 44:391–400.

28. Hammer ND, Schurig-Briccio LA, Gerdes SY, Gennis RB, Skaar EP. 2016. CtaM is required for menaquinol oxidase aa3 function in *Staphylococcus aureus*. mBio 7:e00823-16.

29. Borisov VB, Gennis RB, Hemp J, Verkhovsky MI. 2011. The cytochrome bd respiratory oxygen reductases. Biochim Biophys Acta Bioenerg 1807:1398–1413.

30. Mason MG, Shepherd M, Nicholls P, Dobbin PS, Dodsworth KS, Poole RK, Cooper CE. 2009. Cytochrome bd confers nitric oxide resistance to Escherichia coli. Nat Chem Biol 5:94–96.

31. Simmen H-P, Blaser J. 1993. Analysis of pH and p02 in Abscesses, Peritoneal Fluid, and Drainage Fluid in the Presence or Absence of Bacterial Infection During and Mter Abdominal Surgery. The American Journal of Surgery 165:24–27.

32. Filkins LM, O'Toole GA. 2015. Cystic Fibrosis Lung Infections: Polymicrobial, Complex, and Hard to Treat. PLoS Pathog 11.

33. Kobayashi SD, Malachowa N, DeLeo FR. 2015. Pathogenesis of Staphylococcus aureus Abscesses. Am J Pathol 185:1518–1527.

34. Hajdamowicz NH, Hull RC, Foster SJ, Condliffe AM. 2019. The Impact of Hypoxia on the Host-Pathogen Interaction between Neutrophils and Staphylococcus aureus. Int J Mol Sci 20:5561.

35. Dziewanowska K, Patti JM, Deobald CF, Bayles KW, Trumble WR, Bohach GA. 1999. Fibronectin Binding Protein and Host Cell Tyrosine Kinase Are Required for Internalization of Staphylococcus aureus by Epithelial CellsINFECTION AND IMMUNITY.

36. Sinha B, François PP, Nüße O, Foti M, Hartford OM, Vaudaux P, Foster TJ, Lew DP, Herrmann M, Krause KH. 1999. Fibronectin-binding protein acts as Staphylococcus aureus invasin via fibronectin bridging to integrin α5β1. Cell Microbiol 1:101–117.

37. Bayles KW, Wesson CA, Liou LE, Fox LK, Bohach GA, Trumble AWR. 1998. Intracellular Staphylococcus aureus Escapes the Endosome and Induces Apoptosis in Epithelial Cells. Infect Immun 66:336–342.

38. Hess DJ, Henry-Stanley MJ, Erickson EA, Wells CL. 2003. Intracellular survival of Staphylococcus aureus within cultured enterocytes. Journal of Surgical Research 114:42–49.

39. Gresham HD, Lowrance JH, Caver TE, Wilson BS, Cheung AL, Lindberg FP. 2000. Survival of Staphylococcus aureus Inside Neutrophils Contributes to Infection . The

Journal of Immunology 164:3713–3722.

40. Hommes JW, Surewaard BGJ. 2022. Intracellular Habitation of Staphylococcus aureus: Molecular Mechanisms and Prospects for Antimicrobial Therapy. Biomedicines 10.

41. Surmann K, Michalik S, Hildebrandt P, Gierok P, Depke M, Brinkmann L, Bernhardt J, Salazar G. MG, Sun Z, Shteynberg D, Kusebauch U, Moritz L. RL, Wollscheid B, Lalk M, Völker U, Schmidt F. 2014. Comparative proteome analysis reveals conserved and specific adaptation patterns of Staphylococcus aureus after internalization by different types of human non-professional phagocytic host cells. Front Microbiol 5.

42. Burke KA, Lascelles J. 1975. Nitrate Reductase System in *Staphylococcus aureus* Wild Type and Mutants. J Bacteriol 123:308–316.

43. Paunel AN, Dejam A, Thelen S, Kirsch M, Horstjann M, Gharini P, Mürtz M, Kelm M, De Groot H, Kolb-Bachofen V, Suschek C V. 2005. Enzyme-independent nitric oxide formation during UVA challenge of human skin: Characterization, molecular sources, and mechanisms. Free Radic Biol Med 38:606–615.

44. Kadach S, Piknova B, Black MI, Park JW, Wylie LJ, Stoyanov Z, Thomas SM, McMahon NF, Vanhatalo A, Schechter AN, Jones AM. 2022. Time course of human skeletal muscle nitrate and nitrite concentration changes following dietary nitrate ingestion. Nitric Oxide 121:1–10.

45. Li Y, Pan T, Cao R, Li W, He Z, Sun B. 2023. Nitrate Reductase NarGHJI Modulates Virulence via Regulation of agr Expression in Methicillin-Resistant Staphylococcus aureus Strain USA300 LAC . Microbiol Spectr 11.

46. Weber I, Fritz C, Ruttkowski S, Kreft A, Bange FC. 2000. Anaerobic nitrate reductase (narGHJI) activity of Mycobacterium bovis BCG in vitro and its contribution to virulence in immunodeficient mice. Mol Microbiol 35:1017–1025.

47. Bogdan C. 2015. Nitric oxide synthase in innate and adaptive immunity: An update. Trends Immunol 36:161–178.

48. Silhavy TJ, Kahne D, Walker S. 2010. The bacterial cell envelope. Cold Spring Harb Perspect Biol 2.

49. Epand RF, Pollard JE, Wright JO, Savage PB, Epand RM. 2010. Depolarization, bacterial membrane composition, and the antimicrobial action of ceragenins. Antimicrob Agents Chemother 54:3708–3713.

50. Adams J. 2010. Essential of Cell Biology. NPG Education, Cambridge, MA.

51. Kiriukhin MY, Debabov D V., Shinabarger DL, Neuhaus FC. 2001. Biosynthesis of the glycolipid anchor in lipoteichoic acid of Staphylococcus aureus RN4220: Role of YpfP,

the diglucosyldiacylglycerol synthase. J Bacteriol 183:3506–3514.

52. Zhang B, Liu X, Lambert E, Mas G, Hiller S, Veening JW, Perez C. 2020. Structure of a proton-dependent lipid transporter involved in lipoteichoic acids biosynthesis. Nat Struct Mol Biol 27:561–569.

53. Gründling A, Schneewind O. 2007. Genes required for glycolipid synthesis and lipoteichoic acid anchoring in Staphylococcus aureus. J Bacteriol 189:2521–2530.

54. Gründling A, Schneewind O. 2007. Synthesis of glycerol phosphate lipoteichoic acid in Staphylococcus aureus. PNAS 104:8478–8483.

55. LABISCHINSKI H, NAUMANN D, FISCHER W. 1991. Small and medium-angle X-ray analysis of bacterial lipoteichoic acid phase structure. Eur J Biochem 202:1269–1274.

56. Fischer W. 1993. Molecular Analysis of Lipid Macroamphiphiles by Hydrophobic Interaction Chromatography, Exemplified with Lipoteichoic Acids. Anal Chem 208:49–56.

57. Fedtke I, Mader D, Kohler T, Moll H, Nicholson G, Biswas R, Henseler K, Götz F, Zähringer U, Peschel A. 2007. A Staphylococcus aureus ypfP mutant with strongly reduced lipoteichoic acid (LTA) content: LTA governs bacterial surface properties and autolysin activity. Mol Microbiol 65:1078–1091.

58. Burtchett TA, Shook JC, Hesse LE, Delekta PC, Brzozowski RS, Nouri A, Calas AJ, Spanoudis CM, Eswara PJ, Hammer ND. 2023. Crucial Role for Lipoteichoic Acid Assembly in the Metabolic Versatility and Antibiotic Resistance of Staphylococcus aureus. Infect Immun 91.

59. Hesser AR, Matano LM, Vickery CR, McKay Wood B, Santiago AG, Morris HG, Do T, Losick R, Walker S. 2020. The length of lipoteichoic acid polymers controls staphylococcus aureus cell size and envelope integrity. J Bacteriol 202.

60. Lee SH, Wang H, Labroli M, Koseoglu S, Zuck P, Mayhood T, Gill C, Mann P, Sher X, Ha S, Yang S-W, Mandal M, Yang C, Liang L, Tan Z, Tawa P, Hou Y, Kuvelkar R, Devito K, Wen X, Xiao J, Batchlett M, Balibar CJ, Liu J, Xiao J, Murgolo N, Garlisi CG, Sheth PR, Flattery A, Su J, Tan C, Roemer T. 2016. TarO-specific inhibitors of wall teichoic acid biosynthesis restore b-lactam efficacy against methicillin-resistant staphylococci. Sci Transl Med 8:329ra32.

61. D'Elia MA, Henderson JA, Beveridge TJ, Heinrichs DE, Brown ED. 2009. The N-acetylmannosamine transferase catalyzes the first committed step of teichoic acid assembly in Bacillus subtilis and Staphylococcus aureus. J Bacteriol 191:4030–4034.

62. Kojima N, Araki Y, Ito E. 1985. Structure of the Linkage Units Between Ribitol Teichoic Acids and Peptidoglycan. J Bacteriol 161:299–306.

63. Chen L, Hou WT, Fan T, Liu B, Pan T, Li YH, Jiang YL, Wen W, Chen ZP, Sun L, Zhou CZ, Chen Y. 2020. Cryo-electron microscopy structure and transport mechanism of a wall teichoic acid ABC transporter. mBio 11.

64. Brown S, Santa Maria JP, Walker S. 2013. Wall teichoic acids of gram-positive bacteria. Annu Rev Microbiol 67:313–336.

65. Nikaido H. 2003. Molecular Basis of Bacterial Outer Membrane Permeability Revisited. Microbiology and Molecular Biology Reviews 67:593–656.

66. Yamashita S, Buchanan SK. 2010. Solute and Ion Transport: Outer Membrane Pores and Receptors. EcoSal Plus 4.

67. Archibald OAR, Armstrong JJJ, Baddiley FRS, Hay JB. 1961. TEICHOIC ACIDS AND THE STRUCTURE OF BACTERIAL WALLS. Nature 191:570–572.

68. Heptinstall S, Archibald A, Baddiley J. 1970. Teichoic acids and membrane function in bacteria. Nature 225:519–521.

69. Mera MU, Kemper M, Doyle R, Beveridge' TJ. 1992. The Membrane-Induced Proton Motive Force Influences the Metal Binding Ability of Bacillus subtilis Cell Walls. Appl Environ Microbiol 58:3837–3844.

70. Biswas R, Martinez RE, Göhring N, Schlag M, Josten M, Xia G, Hegler F, Gekeler C, Gleske AK, Götz F, Sahl HG, Kappler A, Peschel A. 2012. Proton-binding capacity of staphylococcus aureus wall teichoic acid and its role in controlling autolysin activity. PLoS One 7.

71. Merchante R, Pooley H, Karamata D. 1995. A Periplasm in Bacillus subtilis. J Bacteriol 177:6176–6183.

72. Erickson HP. 2021. How Teichoic Acids Could Support a Periplasm in Gram-Positive Bacteria, and Let Cell Division Cheat Turgor Pressure. Front Microbiol 12.

73. Peschel A, Jack RW, Otto M, Collins LV, Staubitz P, Nicholson G, Kalbacher H, Nieuwenhuizen WF, Jung G, Tarkowski A, Kok ¶, Van Kessel PM, Van Strijp JAG. 2001. Staphylococcus aureus Resistance to Human Defensins and Evasion of Neutrophil Killing via the Novel Virulence Factor MprF Is Based on Modification of Membrane Lipids with L-Lysine. J Exp Med 193:1067–1076.

74. Saar-Dover R, Bitler A, Nezer R, Shmuel-Galia L, Firon A, Shimoni E, Trieu-Cuot P, Shai Y. 2012. D-Alanylation of Lipoteichoic Acids Confers Resistance to Cationic Peptides in Group B Streptococcus by Increasing the Cell Wall Density. PLoS Pathog 8.

75. Weidenmaier C, Peschel A. 2008. Teichoic acids and related cell-wall glycopolymers in

Gram-positive physiology and host interactions. Nat Rev Microbiol 6:276–287.

76. Fischer W, Rösel P. 1980. The alanine ester substitution of lipoteichoic acid (LTA) in Staphylococcus aureus. FEBS Lett 119:224–226.

77. Macarthur AE, Archibald AR. 1984. Effect of Culture pH on the D-Alanine Ester Content of Lipoteichoic Acid in Staphylococcus aureus. J Bacteriol 160:792–793.

78. Hurst A, Hughes A, Duckworth M, Baddiley J. 1975. Loss of D-Alanine during Sublethal Heating of Staphylococcus aureus s6 and Magnesium Binding during Repair. J Gen Microbiol 89:277–284.

79. Peschel A, Otto M, Jack RW, Kalbacher H, Jung G, Götz F. 1999. Inactivation of the dlt Operon in Staphylococcus aureus Confers Sensitivity to Defensins, Protegrins, and Other Antimicrobial Peptides. Journal of Biological Chemistry 274:8405–8410.

80. Proctor R. 2019. Respiration and Small Colony Variants of *Staphylococcus aureus*. Microbiol Spectr 7:1–15.

81. Wolter DJ, Emerson JC, McNamara S, Buccat AM, Qin X, Cochrane E, Houston LS, Rogers GB, Marsh P, Prehar K, Pope CE, Blackledge M, Déziel E, Bruce KD, Ramsey BW, Gibson RL, Burns JL, Hoffman LR. 2013. *Staphylococcus aureus* small-colony variants are independently associated with worse lung disease in children with cystic fibrosis. Clin Infect Dis 57:384–391.

82. Rolauffs B, Bernhardt TM, von Eiff C, Hart ML, Bettin D. 2002. Osteopetrosis, femoral fracture, and chronic osteomyelitis caused by Staphylococcus aureus small colony variants (SCV) treated by girdlestone resection - 6-year follow-up. Arch Orthop Trauma Surg 122:547–550.

83. Von Eiff C, Becker K, Metze D, Lubritz G, Hockmann J, Schwarz T, Peters G. 2001. Intracellular Persistence of Staphylococcus aureus Small-Colony Variants within Keratinocytes: A Cause for Antibiotic Treatment Failure in a Patient with Darier's Disease. Clinical Infectious Diseases 32:1643–1647.

84. Bhattacharyya S, Roy S, Pk M, Rit K, Ganguly U, Ray R. 2012. Small Colony variants of Staphylococcus aureus isolated from a patient with infective endocarditis: a case report and review of the literature. Iran J Microbiol 4:98–99.

85. Kahl BC, Becker K, Löffler B. 2016. Clinical significance and pathogenesis of staphylococcal small colony variants in persistent infections. Clin Microbiol Rev 29:401–427.

86. Chatterjee I, Herrmann M, Proctor RA, Peters G, Kahl BC. 2007. Enhanced post-stationary-phase survival of a clinical thymidine-dependent small-colony variant of Staphylococcus aureus results from lack of a functional tricarboxylic acid cycle. J

Bacteriol 189:2936–2940.

87. Chen F, Zhao Q, Yang Z, Chen R, Pan H, Wang Y, Liu H, Cao Q, Gan J, Liu X, Zhang N, Yang C-G, Liang H, Lan L. 2024. Citrate serves as a signal molecule to modulate carbon metabolism and iron homeostasis in Staphylococcus aureus. PLoS Pathog 20:e1012425.

88. Garcia LG, Lemaire S, Kahl BC, Becker K, Proctor RA, Denis O, Tulkens PM, Van Bambeke F. 2013. Antibiotic activity against small-colony variants of staphylococcus aureus: Review of in vitro, animal and clinical data. Journal of Antimicrobial Chemotherapy 68:1455–1464.

89. Baumert N, Von Eiff C, Schaaff F, Peters G, Proctor RA, Sahl H-G. 2002. Physiology and Antibiotic Susceptibility of Staphylococcus aureus Small Colony Variants. MICROBIAL DRUG RESISTANCE 8.

90. Zheng X, Fang R, Wang C, Tian X, Lin J, Zeng W, Zhou T, Xu C. 2021. Resistance profiles and biological characteristics of rifampicin-resistant Staphylococcus aureus small-colony variants. Infect Drug Resist 14:1527–1536.

91. Lechner S, Lewis K, Bertram R. 2012. Staphylococcus aureus persisters tolerant to bactericidal antibiotics. J Mol Microbiol Biotechnol 22:235–244.

92. Ryan H, Ballard E, Stockwell RE, Duplancic C, Thomson RM, Smith K, Bell SC. 2023. A systematic review of the clinical impact of small colony variants in patients with cystic fibrosis. BMC Pulm Med 23.

93. Guo H, Tong Y, Cheng J, Abbas Z, Li Z, Wang J, Zhou Y, Si D, Zhang R. 2022. Biofilm and Small Colony Variants—An Update on Staphylococcus aureus Strategies toward Drug Resistance. Int J Mol Sci. MDPI https://doi.org/10.3390/ijms23031241.

94. Kolle W, Hetxch H. Die experimentelle Bakteriologie und die Infektionskrankheiten mit besonderer Berücksichtigung der Immunitätslehre. Ein lehrbuch für studierende, ärzte und medizinalbeamte. Urban & Schwarzenberg, Berlin.

95. Nicolaou KC, Rigol S. 2018. A brief history of antibiotics and select advances in their synthesis. Journal of Antibiotics 71:153–184.

96. Vaudaux P, Francois P, Bisognano C, Kelley WL, Lew DP, Schrenzel J, Proctor RA, McNamara PJ, Peters G, Von Eiff C. 2002. Increased expression of clumping factor and fibronectin-binding proteins by hemB mutants of Staphylococcus aureus expressing small colony variant phenotypes. Infect Immun 70:5428–5437.

97. Ou JJJ, Drilling AJ, Cooksley C, Bassiouni A, Kidd SP, Psaltis AJ, Wormald PJ, Vreugde S. 2016. Reduced innate immune response to a Staphylococcus aureus small colony variant compared to its wild-type parent strain. Front Cell Infect Microbiol 6.

98. Wong Fok Lung T, Monk IR, Acker KP, Mu A, Wang N, Riquelme SA, Pires S, Noguera LP, Dach F, Gabryszewski SJ, Howden BP, Prince A. 2020. Staphylococcus aureus small colony variants impair host immunity by activating host cell glycolysis and inducing necroptosis. Nat Microbiol 5:141–153.

99. Ochando J, Mulder WJM, Madsen JC, Netea MG, Duivenvoorden R. 2023. Trained immunity — basic concepts and contributions to immunopathology. Nat Rev Nephrol 19:23–37.

100. Arts RJW, Novakovic B, ter Horst R, Carvalho A, Bekkering S, Lachmandas E, Rodrigues F, Silvestre R, Cheng SC, Wang SY, Habibi E, Gonçalves LG, Mesquita I, Cunha C, van Laarhoven A, van de Veerdonk FL, Williams DL, van der Meer JWM, Logie C, O'Neill LA, Dinarello CA, Riksen NP, van Crevel R, Clish C, Notebaart RA, Joosten LAB, Stunnenberg HG, Xavier RJ, Netea MG. 2016. Glutaminolysis and Fumarate Accumulation Integrate Immunometabolic and Epigenetic Programs in Trained Immunity. Cell Metab 24:807–819.

101. Noore J, Noore A, Li B. 2013. Cationic antimicrobial peptide ll-37 is effective against both extraand intracellular staphylococcus aureus. Antimicrob Agents Chemother 57:1283–1290.

102. Govindarajan DK, Kandaswamy K. 2023. Antimicrobial peptides: A small molecule for sustainable healthcare applications. Medicine in Microecology 18.

103. Popitool K, Wataradee S, Wichai T, Noitang S, Ajariyakhajorn K, Charoenrat T, Boonyaratanakornkit V, Sooksai S. 2023. Potential of Pm11 antimicrobial peptide against bovine mastitis pathogens. Am J Vet Res 84.

104. Zhang D, Chen J, Jing Q, Chen Z, Ullah A, Jiang L, Zheng K, Yuan C, Huang M. 2021. Development of a Potent Antimicrobial Peptide With Photodynamic Activity. Front Microbiol 12.

105. Malanovic N, Lohner K. 2016. Gram-positive bacterial cell envelopes: The impact on the activity of antimicrobial peptides. Biochim Biophys Acta Biomembr 1858:936–946.

106. Kisich KO, Howell MD, Boguniewicz M, Heizer HR, Watson NU, Leung DYM. 2007. The constitutive capacity of human keratinocytes to kill Staphylococcus aureus is dependent on β-defensin 3. Journal of Investigative Dermatology 127:2368–2380.

107. Simanski M, Dressel S, Gläser R, Harder J. 2010. RNase 7 protects healthy skin from staphylococcus aureus colonization. Journal of Investigative Dermatology 130:2836–2838.

108. Gläser R, Becker K, Von Eiff C, Meyer-Hoffert U, Harder J. 2014. Decreased susceptibility of staphylococcus aureus small-colony variants toward human antimicrobial peptides. Journal of Investigative Dermatology 134:2347–2350.

109. Sadowska B, Bonar A, Von Eiff C, Proctor RA, Chmiela M, Rudnicka W, Rozalska B. 2002. Characteristics of Staphylococcus aureus, isolated from airways of cystic fibrosis patients, and their small colony variants 18:1991–197.

110. Gershenzon J, Dudareva N. 2007. The function of terpene natural products in the natural world. Nat Chem Biol 3:408–414.

111. Pelz A, Wieland KP, Putzbach K, Hentschel P, Albert K, Götz F. 2005. Structure and biosynthesis of staphyloxanthin from *Staphylococcus aureus*. J Biol Chem 280:32493–32498.

112. Kumar S, Mollo A, Kahne D, Ruiz N. 2022. The Bacterial Cell Wall: From Lipid II Flipping to Polymerization. Chem Rev 122:8884–8910.

113. Panthee S, Paudel A, Hamamoto H, Uhlemann AC, Sekimizu K. 2020. The Role of Amino Acid Substitution in HepT Toward Menaquinone Isoprenoid Chain Length Definition and Lysocin E Sensitivity in *Staphylococcus aureus*. Front Microbiol 11:2076.

114. Wakeman CA, Hammer ND, Stauff DL, Attia AS, Anzaldi LL, Dikalov SI, Calcutt MW, Skaar EP. 2012. Menaquinone biosynthesis potentiates haem toxicity in *Staphylococcus aureus*. Mol Microbiol 86:1376–1392.

115. Krute CN, Carroll RK, Rivera FE, Weiss A, Young RM, Shilling A, Botlani M, Varma S, Baker BJ, Shaw LN. 2015. The disruption of prenylation leads to pleiotropic rearrangements in cellular behavior in *Staphylococcus aureus*. Mol Microbiol 95:819–832.

116. Ogura K, Koyama T. 1998. Enzymatic Aspects of Isoprenoid Chain Elongation. Chem Rev 98:1263–1276.

117. Svensson B, Lübben M, Hederstedt L. 1993. *Bacillus subtilis* CtaA and CtaB function in haem A biosynthesis. Mol Microbiol 10:193–201.

118. Zhang Y-W, Koyama T, Ogura K. 1997. Two Cistrons of the *gerC* Operon of *Bacillus subtilis* Encode the Two Subunits of Heptaprenyl Diphosphate Synthase. J Biol Chem 179:1417–1419.

119. Klevens RM, Morrison MA, Nadle J, Petit S, Gershman K, Ray S, Harrison LH, Lynfield R, Dumyati G, Townes JM, Craig AS, Zell ER, Fosheim GE, Mcdougal LK, Carey RB, Fridkin SK. Invasive Methicillin-Resistant Staphylococcus aureus Infections in the United States.

120. Keuhnert M, Kruszon-Moran D, Hill H, McQuillan G, McAllister S, Fosheim G, McDougal L, Chaitram J, Jensen B, Fridkin S, Killgore G, Tenover F. 2006. Prevelence of Staphylococcus aureus Nasal Colonization in the United States, 2001-2002. J Infect Dis

193:172–179.

121. Olson ME, Horswill AR. 2013. Staphylococcus aureus Osteomyelitis: Bad to the bone. Cell Host Microbe 13:629–631.

122. Kahl BC. 2010. Impact of Staphylococcus aureus on the pathogenesis of chronic cystic fibrosis lung disease. International Journal of Medical Microbiology https://doi.org/10.1016/j.ijmm.2010.08.002.

123. Schwerdt M, Neumann C, Schwartbeck B, Kampmeier S, Herzog S, Görlich D, Dübbers A, Große-Onnebrink J, Kessler C, Küster P, Schültingkemper H, Treffon J, Peters G, Kahl BC. 2018. Staphylococcus aureus in the airways of cystic fibrosis patients - A retrospective long-term study. International Journal of Medical Microbiology 308:631–639.

124. Bhagirath AY, Li Y, Somayajula D, Dadashi M, Badr S, Duan K. 2016. Cystic fibrosis lung environment and Pseudomonas aeruginosa infection. BMC Pulm Med 16.

125. Proctor RA, von Eiff C, Kahl BC, Becker K, McNamara P, Herrmann M, Peters G. 2006. Small colony variants: A pathogenic form of bacteria that facilitates persistent and recurrent infections. Nat Rev Microbiol 4:295–305.

126. Von Eiff C, Heilmann C, Proctor RA, Woltz C, Peters G, Go¨tz F, Go¨tz G. 1997. A Site-Directed Staphylococcus aureus hemB Mutant Is a Small-Colony Variant Which Persists IntracellularlyJOURNAL OF BACTERIOLOGY.

127. Miller MH, Edberg SC, Mandel,' LJ, Behar,' And CF, Steigbigel' NH. 1980. Gentamicin Uptake in Wild-Type and Aminoglycoside-Resistant Small-Colony Mutants of Staphylococcus aureusANTIMICROBIAL AGENTS AND CHEMOTHERAPY.

128. Xia G, Kohler T, Peschel A. 2010. The wall teichoic acid and lipoteichoic acid polymers of Staphylococcus aureus. International Journal of Medical Microbiology 300:148–154.

129. Winstel V, Xia G, Peschel A. 2014. Pathways and roles of wall teichoic acid glycosylation in Staphylococcus aureus. International Journal of Medical Microbiology 304:215–221.

130. Duckworth M, Archibald AR, Baddiley J. 1975. Lipoteichoic acid and lipoteichoic acid carrier in Staphylococcus aureus H. FEBS Lett 53:176–179.

131. KOCH HU, HAAS R, FISCHER W. 1984. The role of lipoteichoic acid biosynthesis in membrane lipid metabolism of growing Staphylococcus aureus. Eur J Biochem 138:357–363.

132. Richter SG, Elli D, Kim HK, Hendrickx APA, Sorg JA, Schneewind O, Missiakas D. 2013. Small molecule inhibitor of lipoteichoic acid synthesis is an antibiotic for Gram-positive bacteria. Proc Natl Acad Sci U S A 110:3531–3536.

133. Rice KC, Bayles KW. 2008. Molecular Control of Bacterial Death and Lysis. Microbiology and Molecular Biology Reviews 72:85–109.

134. Schaaff F, Bierbaum G, Baumert N, Bartmann P, Sahl H-G. 2003. Mutations are involved in emergence of aminoglycoside-induced small colony variants of *Staphylococcus aureus*. Int J Med Microbiol 293:427–435.

135. Kahl BC. 2014. Small colony variants (SCVs) of Staphylococcus aureus - A bacterial survival strategy. Infection, Genetics and Evolution 21:515–522.

136. Eswara P, Brzozowski R, Viola M, Graham G, Spanoudis C, Trebino C, Jha J, Aubee J, Thompson K, Camberg J, Ramamurthi K. 2018. An essential Staphylococcus aureus cell division protein directly regulates FtsZ dynamics. Elife https://doi.org/10.7554/eLife.38856.001.

137. Filkins LM, Graber JA, Olson DG, Dolben EL, Lynd LR, Bhuju S, O'Toole GA. 2015. Coculture of Staphylococcus aureus with Pseudomonas aeruginosa drives S. aureus towards fermentative metabolism and reduced viability in a cystic fibrosis model. J Bacteriol 197:2252–2264.

138. Machan ZA, Taylor GW, Pttt TL, Cole PJ, Wilson R. 1992. 2-Heptyl-4-hydroxyqiiirjoliiie iV-oxide, an antistaphylococcal agent produced by Pseudomonas aeruginosa. Journal of Antimicrobial Chemotherapy 30:615–623.

139. Hoffman LR, Dé Ziel E, D'argenio DA, Emerson J, Mcnamara S, Gibson RL, Ramsey BW, Miller SI. 2006. Selection for Staphylococcus aureus small-colony variants due to growth in the presence of Pseudomonas aeruginosa. PNAS 103:19890–19895.

140. Biswas L, Biswas R, Schlag M, Bertram R, Götz F. 2009. Small-colony variant selection as a survival strategy for Staphylococcus aureus in the presence of Pseudomonas aeruginosa. Appl Environ Microbiol 75:6910–6912.

141. Voggu L, Schlag S, Biswas R, Rosenstein R, Rausch C, Götz F. 2006. Microevolution of cytochrome bd oxidase in staphylococci and its implication in resistance to respiratory toxins released by Pseudomonas. J Bacteriol 188:8079–8086.

142. Schneewind O, Model P, Fischetti VA. 1992. Sorting of Protein A to the Staphylococcal Cell Wall. Cell 70:267–261.

143. Maloney PC, Kashket ER, Wilson TH. 1974. A Protonmotive Force Drives ATP Synthesis in Bacteria. PNAS 71:3896–3900.

144. Sims PJ, Waggoner AS, Wang C-H, Hoffman JF. 1974. Studies on the Mechanism by Which Cyanine Dyes Measure Membrane Potential in Red Blood Cells and Phosphatidylcholine Vesicles. Biochemistry 13:3315–3330.

145. Kasianowicz J, Benz R, Mclaughlin S. 1984. The Kinetic Mechanism by which CCCP (Carbonyl Cyanide m-Chlorophenylhydrazone) Transports Protons across Membranes. J Membr Biol 82:179–190.

146. Ahmed S, Booth IR. 1983. The use of valinomycin, nigericin and trichlorocarbanilide in control of the protonmotive force in Escherichia coli cells. Biochem J 212:105–112.

147. Corrigan RM, Abbott JC, Burhenne H, Kaever V, Gründling A. 2011. C-di-amp is a new second messenger in staphylococcus aureus with a role in controlling cell size and envelope stress. PLoS Pathog 7.

148. Oku Y, Kurokawa K, Matsuo M, Yamada S, Lee BL, Sekimizu K. 2009. Pleiotropic roles of polyglycerolphosphate synthase of lipoteichoic acid in growth of Staphylococcus aureus cells. J Bacteriol 91:141–151.

149. Weart RB, Lee AH, Chien AC, Haeusser DP, Hill NS, Levin PA. 2007. A Metabolic Sensor Governing Cell Size in Bacteria. Cell 130:335–347.

150. Reichmann NT, Piçarra Cassona C, Monteiro JM, Bottomley AL, Corrigan RM, Foster SJ, Pinho MG, Gründling A. 2014. Differential localization of LTA synthesis proteins and their interaction with the cell division machinery in Staphylococcus aureus. Mol Microbiol 92:273–286.

151. Revilla-Guarinos A, Gebhard S, Mascher T, Zúñiga M. 2014. Defence against antimicrobial peptides: Different strategies in Firmicutes. Environ Microbiol 16:1225–1237.

152. KUSSER W, ZIMMER K, FIEDLER F. 1985. Characteristics of the binding of aminoglycoside antibiotics to teichoic acids: A potential model system for interaction of aminoglycosides with polyanions. Eur J Biochem 151:601–605.

153. Komatsuzawa H, Suzuki J, Sugai M, Miyake Y, Suginaka H. 1994. The effect of Triton X-100 on the in-vitro susceptibility of methicillin-resistant Staphylococcus aureus to oxacillin. Journal of Antimicrobial Chemotherapy 34:885–897.

154. Duthie ES, Lorenz LL. 1952. Staphylococcal Coagulase: Mode of Action and Antigenicity. J Gen Microbiol 6:95–107.

155. Mazmanian SK, Skaar EP, Gaspar AH, Humayun M, Gornicki P, Jelenska J, Joachmiak A, Missiakas DM, Schneewind O. 2003. Passage of heme-iron across the envelope of Staphylococcus aureus. Science (1979) 299:906–909.

156. Lange BM, Rujan T, Martin W, Croteau R. 2000. Isoprenoid biosynthesis: The evolution of two ancient and distinct pathways across genomes. Proceedings of the National Academy of Sciences 97:13172–13177.

157. Takahashi I, Ogura K. 1981. Farnesyl Pyrophosphate Synthetase from *Bacillus subtilis*. The Journal of Biochemistry 89:1581–1587.

158. Lee PC, Petri R, Mijts BN, Watts KT, Schmidt-Dannert C. 2005. Directed evolution of *Escherichia coli* farnesyl diphosphate synthase (IspA) reveals novel structural determinants of chain length specificity. Metab Eng 7:18–26.

159. Fujii H, Koyama T, Ogura K. 1982. Hexaprenyl pyrophosphate synthetase from *Micrococcus luteus* B-P 26. Separation of two essential components. Journal of Biological Chemistry 257:14610–14612.

160. Zhang Y-W, Koyama T, Marecak DM, Prestwich GD, Maki Y, Ogura K. 1998. Two Subunits of Heptaprenyl Diphosphate Synthase of *Bacillus subtilis* Form a Catalytically Active Complex. Biochemistry 37:48.

161. Fujisaki S, Nishino T, Katsuki H. 1986. Isoprenoid Synthesis in *Escherichia coli*. Separation and Partial Purification of Four Enzymes Involved in the Synthesis. J Biochem 99:1327–1337.

162. Baba T, Allen CM. 1978. Substrate specificity of undecaprenyl pyrophophate synthetase from *Lactobacillus plantarum*. Biochemistry 17:5598–5604.

163. Shimizu N, Koyama T, Ogura K. 1998. Molecular Cloning, Expression, and Purification of Undecaprenyl Diphosphate Synthase: NO SEQUENCE SIMILARITY BETWEEN E- AND Z-PRENYL DIPHOSPHATE SYNTHASES. J Biol Chem 273:19476–19481.

164. Shineberg B, Young IG. 1976. Biosynthesis of bacterial menaquinones: the membrane-associated 1,4-dihydroxy-2-naphthoate octaprenyltransferase of *Escherichia coli*. Biochemistry 15:2754–2758.

165. Kellogg BA, Poulter CD. 1997. Chain elongation in the isoprenoid biosynthetic pathway. Curr Opin Chem Biol 1:570–578.

166. Kato J-I, Fujisaki S, Nakajima K-I, Nishimura Y, Sato M, Nakano A. 1999. The *Escherichia coli* Homologue of Yeast Rer2, a Key Enzyme of Dolichol Synthesis, Is Essential for Carrier Lipid Formation in Bacterial Cell Wall Synthesis. J Bacteriol 181:2733–2738.

167. Müller A, Klöckner A, Schneider T. 2017. Targeting a cell wall biosynthesis hot spot. Nat Prod Rep 34:909–932.

168. Malin JJ, De Leeuw E. 2019. Therapeutic compounds targeting Lipid II for antibacterial purposes. Infect Drug Resist 12:2613–2625.

169. Liu GY, Essex A, Buchanan JT, Datta V, Hoffman HM, Bastian JF, Fierer J, Nizet V.

2005. *Staphylococcus aureus* golden pigment impairs neutrophil killing and promotes virulence through its antioxidant activity. J Exp Med 202:209–215.

170. Fey PD, Endres JL, Yajjala VK, Widhelm TJ, Boissy RJ, Bose JL, Bayles KW. 2013. A genetic resource for rapid and comprehensive phenotype screening of nonessential Staphylococcus aureus genes. mBio 4:e00537-12.

171. Rausch M, Deisinger JP, Ulm H, Müller A, Li W, Hardt P, Wang X, Li X, Sylvester M, Engeser M, Vollmer W, Müller CE, Sahl HG, Lee JC, Schneider T. 2019. Coordination of capsule assembly and cell wall biosynthesis in *Staphylococcus aureus*. Nat Commun 10:1404.

172. Wanner S, Schade J, Keinhörster D, Weller N, George SE, Kull L, Bauer J, Grau T, Winstel V, Stoy H, Kretschmer D, Kolata J, Wolz C, Bröker BM, Weidenmaier C. 2017. Wall teichoic acids mediate increased virulence in *Staphylococcus aureus*. Nat Microbiol 2:16257.

173. Thakker M, Park J-S, Carey V, Lee JC. 1998. *Staphylococcus aureus* Serotype 5 Capsular Polysaccharide Is Antiphagocytic and Enhances Bacterial Virulence in a Murine Bacteremia Model. Infect Immun 66:5183–5189.

174. Nanra JS, Buitrago SM, Crawford S, Ng J, Fink PS, Hawkins J, Scully IL, McNeil LK, Aste-Am Éaga J, Cooper D, Jansen KU, Anderson AS. 2013. Capsular polysaccharides are an important immune evasion mechanism for *Staphylococcus aureus*. Hum Vaccin Immunother 9:480–487.

175. Saito K, Fujisaki S, Nishino T. 2007. Short-chain prenyl diphosphate synthase that condenses isopentenyl diphosphate with dimethylallyl diphosphate in *ispA* null *Escherichia coli* strain lacking farnesyl diphosphate synthase. J Biosci Bioeng 103:575–577.

176. Takahashi H, Aihara Y, Ogawa Y, Murata Y, Nakajima K, Iida M, Shirai M, Fujisaki S. 2018. Suppression of phenotype of *Escherichia coli* mutant defective in farnesyl diphosphate synthase by overexpression of gene for octaprenyl diphosphate synthase. Biosci Biotechnol Biochem 82:1003–1010.

177. Pitton M, Oberhaensli S, Appiah F, Pagani JL, Fournier A, Jakob SM, Que YA, Cameron DR. 2022. Mutation to *ispA* Produces Stable Small-Colony Variants of *Pseudomonas aeruginosa* That Have Enhanced Aminoglycoside Resistance. Antimicrob Agents Chemother 66:e0062122.

178. Mercier R, Kawai Y, Errington J. 2014. General principles for the formation and proliferation of a wall-free (L-form) state in bacteria. Elife 3:e04629.

179. Takahashi I, Ogura K, Seto S. 1980. Heptaprenyl Pyrophosphate Synthetase from *Bacillus subtilis*. J Biol Chem 255:4539–4543.

180. Aussel L, Pierrel F, Loiseau L, Lombard M, Fontecave M, Barras F. 2014. Biosynthesis and physiology of coenzyme Q in bacteria. Biochim Biophys Acta Bioenerg 1837:1004–1011.

181. Baumert N, von Eiff C, Schaaff F, Peters G, Proctor RA, Sahl H-G. 2002. Physiology and Antibiotic Susceptibility of *Staphylococcus aureus* Small Colony Variants. Microbial Drug Resistance 8:253–260.

182. Zhou S, Rao Y, Li J, Huang Q, Rao X. 2022. *Staphylococcus aureus* small-colony variants: Formation, infection, and treatment. Microbiol Res 260:127040.

183. Webster CM, Woody AM, Fusseini S, Holmes LG, Robinson GK, Shepherd M. 2022. Proton motive force underpins respiration-mediated potentiation of aminoglycoside lethality in pathogenic *Escherichia coli*. Arch Microbiol 204:120.

184. Lang M, Carvalho A, Baharoglu Z, Mazel D. 2023. Aminoglycoside uptake, stress, and potentiation in Gram-negative bacteria: new therapies with old molecules. Microb Mol Biol Rev 87:e0003622.

185. Vestergaard M, Paulander W, Leng B, Nielsen JB, Westh HT, Ingmer H. 2016. Novel pathways for ameliorating the fitness cost of gentamicin resistant small colony variants. Front Microbiol 7:1866.

186. Okada K, Minehira M, Zhu X, Suzuki K, Nakagawa T, Matsuda H, Kawamukai M. 1997. The *ispB* gene encoding octaprenyl diphosphate synthase is essential for growth of *Escherichia coli*. J Bacteriol 179:3058–3060.

187. Kobayashi K, Ehrlich SD, Albertini A, Amati G, Andersen KK, Arnaud M, Asai K, Ashikaga S, Aymerich S, Bessieres P, Boland F, Brignell SC, Bron S, Bunai K, Chapuis J, Christiansen LC, Danchin A, Dé Barbouillé F M, Dervyn E, Deuerling E, Devine K, Devine SK, Dreesen O, Errington J, Fillinger S, Foster SJ, Fujita Y, Galizzi A, Gardan R, Eschevins C, Fukushima T, Haga K, Harwood CR, Hecker M, Hosoya D, Hullo MF, Kakeshita H, Karamata D, Kasahara Y, Kawamura F, Koga K, Koski P, Kuwana R, Imamura D, Ishimaru M, Ishikawa S, Ishio I, Le Coq D, Masson Aa A, Mauë C, Meima R, Mellado RP, Moir A, Moriya S, Nagakawa E, Nanamiya H, Nakai S, Nygaard P, Ogura M, Ohanan T, O'reilly M, O'rourke M, Pragai Z, Pooley HM, Rapoport G, Rawlins JP, Rivas LA, Rivolta C, Sadaie A, Sadaie Y, Sarvas M, Sato T, Saxild HH, Scanlan E, Schumann W, Seegers Aa JFML, Sekiguchi J, Sekowska A, Sé Ror Aa SJ, Simon M, Stragier P, Studer R, Takamatsu H, Tanaka T, Takeuchi M, Thomaides HB, Vagner V, Van Dijl JM, Watabe K, Wipat A, Yamamoto H, Yamamoto M, Yamamoto Y, Yamane K, Yata K, Yoshida K, Yoshikawa H, Zuber U, Ogasawara N. 2003. Essential *Bacillus subtilis* genes. Proc Natl Acad Sci USA 100:4678–4683.

188. Kawai Y, Mercier R, Wu LJ, Domínguez-Cuevas P, Oshima T, Errington J. 2015. Cell Growth of Wall-Free L-Form Bacteria Is Limited by Oxidative Damage. Curr Biol

25:1613–1618.

189. Clements MO, Watson SP, Poole RK, Foster SJ. 1999. CtaA of *Staphylococcus aureus* Is Required for Starvation Survival, Recovery, and Cytochrome Biosynthesis. J Bacteriol 181:501–507.

190. Noike M, Katagiri T, Nakayama T, Koyama T, Nishino T, Hemmi H. 2008. The product chain length determination mechanism of type II geranylgeranyl diphosphate synthase requires subunit interaction. FEBS J 275:3921–3933.

191. Ohnuma S, Narita K, Nakazawa T, Ishida C, Takeuchi Y, Ohto C, Nishino T. 1996. A role of the amino acid residue located on the fifth position before the first aspartate-rich motif of farnesyl diphosphate synthase on determination of the final product. J Biol Chem 271:30748–30754.

192. Zhou J, Cai Y, Liu Y, An H, Deng K, Ashraf MA, Zou L, Wang J. 2022. Breaking down the cell wall: Still an attractive antibacterial strategy. Front Microbiol 13:952633.

193. Coker MS, Forbes L V., Plowman-Holmes M, Murdoch DR, Winterbourn CC, Kettle AJ. 2018. Interactions of staphyloxanthin and enterobactin with myeloperoxidase and reactive chlorine species. Arch Biochem Biophys 646:80–89.

194. Desai J, Liu YL, Wei H, Liu W, Ko TP, Guo RT, Oldfield E. 2016. Structure, Function, and Inhibition of *Staphylococcus aureus* Heptaprenyl Diphosphate Synthase. ChemMedChem 1915–1923.

195. Huang LY, Wang SC, Cheng TJR, Wong CH. 2017. Undecaprenyl Phosphate Phosphatase Activity of Undecaprenol Kinase Regulates the Lipid Pool in Gram-Positive Bacteria. Biochemistry 56:5417–5427.

196. Allen CM, Keenan M V, Sack J. 1976. *Lactobacillus plantarum* Undecaprenyl Pyrophosphate Synthetase: Purification and Reaction Requirements. Arch Biochem Biophys 175:236–248.

197. Zhu W, Zhang Y, Sinko W, Hensler ME, Olson J, Molohon KJ, Lindert S, Cao R, Li K, Wang K, Wang Y, Liu YL, Sankovsky A, De Oliveira CAF, Mitchell DA, Nizet V, McCammon JA, Oldfield E. 2013. Antibacterial drug leads targeting isoprenoid biosynthesis. Proc Natl Acad Sci U S A 110:123–128.

198. Hassoun A, Linden PK, Friedman B. 2017. Incidence, prevalence, and management of MRSA bacteremia across patient populations-a review of recent developments in MRSA management and treatment. Crit Care 21:211.

199. Engemann JJ, Carmeli Y, Cosgrove SE, Fowler VG, Bronstein MZ, Trivette SL, Briggs JP, Sexton DJ, Kaye KS. 2001. Adverse Clinical and Economic Outcomes Attributable to Methicillin Resistance among Patients with *Staphylococcus aureus* Surgical Site Infection.

Clin Infect Dis 36:592–600.

200. Schneewind O, Missiakas D. 2014. Genetic manipulation of *Staphylococcus aureus*. Curr Protoc Microbiol 32:Unit 9C.3.

201. Bae T, Schneewind O. 2006. Allelic replacement in *Staphylococcus aureus* with inducible counter-selection. Plasmid 55:58–63.

202. Stapels DAC, Ramyar KX, Bischoff M, Von Köckritz-Blickwede M, Milder FJ, Ruyken M, Eisenbeis J, McWhorter WJ, Herrmann M, Van Kessel KPM, Geisbrecht B V., Rooijakkers SHM. 2014. *Staphylococcus aureus* secretes a unique class of neutrophil serine protease inhibitors. Proc Natl Acad Sci U S A 111:13187–13192.

203. Rivett ED, Addis HG, Dietz J V., Carroll-Deaton JA, Gupta S, Foreman KL, Dang MA, Fox JL, Khalimonchuk O, Hegg EL. 2023. Evidence that the catalytic mechanism of heme a synthase involves the formation of a carbocation stabilized by a conserved glutamate. Arch Biochem Biophys 744:109665.

204. O'Neill J. 2014. Antimicrobial Resistance: Tackling a crisis for the health and wealth of nations. The Review on Antimicrobial Resistance.

205. Walker AS, Clardy J. 2024. Primed for Discovery. Biochemistry. American Chemical Society https://doi.org/10.1021/acs.biochem.4c00464.

206. Hutchings M, Truman A, Wilkinson B. 2019. Antibiotics: past, present and future. Curr Opin Microbiol. Elsevier Ltd https://doi.org/10.1016/j.mib.2019.10.008.

207. Grein F, Müller A, Scherer KM, Liu X, Ludwig KC, Klöckner A, Strach M, Sahl HG, Kubitscheck U, Schneider T. 2020. Ca2+-Daptomycin targets cell wall biosynthesis by forming a tripartite complex with undecaprenyl-coupled intermediates and membrane lipids. Nat Commun 11.

208. Yao J, Rock CO. 2013. Phosphatidic acid synthesis in bacteria. Biochim Biophys Acta Mol Cell Biol Lipids 1831:495–502.

209. Wallace J, Bowlin NO, Mills DM, Saenkham P, Kwasny SM, Opperman TJ, Williams JD, Rock CO, Bowlin TL, Moir DT. 2015. Discovery of bacterial fatty acid synthase type II inhibitors using a novel cellular bioluminescent reporter assay. Antimicrob Agents Chemother 59:5775–5787.

210. Smith S, Tsai S-C. 2007. The type I fatty acid and polyketide synthases: a tale of two megasynthases. Nat Prod Rep 24:1041–1072.

211. Payne DJ, Miller WH, Berry V, Brosky J, Burgess WJ, Chen E, DeWolf WE, Fosberry AP, Greenwood R, Head MS, Heerding DA, Janson CA, Jaworski DD, Keller PM, Manley PJ, Moore TD, Newlander KA, Pearson S, Polizzi BJ, Qiu X, Rittenhouse SF,

Slater-Radosti C, Salvers KL, Seefeld MA, Smyth MG, Takata DT, Uzinskas IN, Vaidya K, Wallis NG, Winram SB, Yuan CCK, Huffman WF. 2002. Discovery of a novel and potent class of fabI-directed antibacterial agents. Antimicrob Agents Chemother 46:3118–3124.

212. Yao J, Rock CO. 2017. Exogenous fatty acid metabolism in bacteria. Biochimie 141:30–39.

213. Kodali S, Galgoci A, Young K, Painter R, Silver LL, Herath KB, Singh SB, Cully D, Barrett JF, Schmatz D, Wang J. 2005. Determination of selectivity and efficacy of fatty acid synthesis inhibitors. Journal of Biological Chemistry 280:1669–1677.

214. Tsay JT, Oh W, Larson TJ, Jackowski S, Rock CO. 1992. Isolation and characterization of the β-ketoacyl-acyl carrier protein synthase III gene (fabH) from Escherichia coli K-12. Journal of Biological Chemistry 267:6807–6814.

215. White SW, Zheng J, Zhang YM, Rock CO. 2005. The structural biology of type II fatty acid biosynthesis. Annu Rev Biochem 74:791–831.

216. Hu Z, Ma J, Chen Y, Tong W, Zhu L, Wang H, Cronan JE. 2021. Escherichia coli FabG 3-ketoacyl-ACP reductase proteins lacking the assigned catalytic triad residues are active enzymes. Journal of Biological Chemistry 296.

217. Heath RJ, Rock CO. 1995. Enoyl-Acyl Carrier Protein Reductase (fabI) Plays a Determinant Role in Completing Cycles of Fatty Acid Elongation in Escherichia coli*. J Biol Chem 270:26538–26542.

218. Janßen HJ, Steinbüchel A. 2014. Fatty acid synthesis in Escherichia coli and its applications towards the production of fatty acid based biofuels. Biotechnol Biofuels 7.

219. Frank MW, Whaley SG, Rock CO. 2021. Branched-chain amino acid metabolism controls membrane phospholipid structure in Staphylococcus aureus. Journal of Biological Chemistry 297.

220. Parsons JB, Rock CO. 2013. Bacterial lipids: Metabolism and membrane homeostasis. Prog Lipid Res 52:249–276.

221. Wittke F, Vincent C, Chen J, Heller B, Kabler H, Overcash JS, Leylavergne F, Dieppois G. 2020. Afabicin, a First-in-Class Antistaphylococcal Antibiotic, in the Treatment of Acute Bacterial Skin and Skin Structure Infections: Clinical Noninferiority to Vancomycin/Linezolid. Antimicrob Agents Chemother 64.

222. Slayden RA, Lee RE, Barry CE. 2000. Isoniazid affects multiple components of the type II fatty acid synthase system of Mycobacterium tuberculosis. Mol Microbiol 38:514–525.

223. Butler MS, Blaskovich MA, Cooper MA. 2013. Antibiotics in the clinical pipeline in

2013. Journal of Antibiotics 66:571–591.

224. Brinster S, Lamberet G, Staels B, Trieu-Cuot P, Gruss A, Poyart C. 2009. Type II fatty acid synthesis is not a suitable antibiotic target for Gram-positive pathogens. Nature 458:83–86.

225. Cuypers MG, Subramanian C, Gullett JM, Frank MW, White SW, Rock CO. 2019. Acyl-chain selectivity and physiological roles of Staphylococcus aureus fatty acid– binding proteins. Journal of Biological Chemistry 294:38–49.

226. Subramanian C, Cuypers MG, Radka CD, White SW, Rock CO. 2022. Domain architecture and catalysis of the Staphylococcus aureus fatty acid kinase. Journal of Biological Chemistry 298.

227. Parsons JB, Broussard TC, Bose JL, Rosch JW, Jackson P, Subramanian C, Rock CO. 2014. Identification of a two-component fatty acid kinase responsible for host fatty acid incorporation by Staphylococcus aureus. Proc Natl Acad Sci U S A 111:10532–10537.

228. Lu YJ, Zhang YM, Grimes KD, Qi J, Lee RE, Rock CO. 2006. Acyl-Phosphates Initiate Membrane Phospholipid Synthesis in Gram-Positive Pathogens. Mol Cell 23:765–772.

229. Delekta PC, Shook JC, Lydic TA, Mulks MH, Hammer ND. 2018. Staphylococcus aureus utilizes host-derived lipoprotein particles as sources of fatty acids. J Bacteriol 200.

230. Zhang J, Chung T, Oldenburg K. 1999. A Simple Statistical Parameter for Use in Evaluation an Validation of High Throughput Screening Assays. J Biomol Screen 4:67–73.

231. Djoumbou Feunang Y, Eisner R, Knox C, Chepelev L, Hastings J, Owen G, Fahy E, Steinbeck C, Subramanian S, Bolton E, Greiner R, Wishart DS. 2016. ClassyFire: automated chemical classification with a comprehensive, computable taxonomy. J Cheminform 8:1–20.

232. National Center for Biotechnology Information. 2024. PubChem Compound Summary for CID 676454, Phenylthiourea.

233. Liu J. 2001. Phenylurea Herbicides, p. 1521–1527. *In* Krieger, R, Krieger, W (eds.), Handbook of Pesticide Toxicology (Second Edition)second. Academic Press.

234. Sharma RC, Parashar RK. 1988. Synthesis and Microbicidal Activity of N-(2-Substituted) Phenyl Ureas and Their Metal Complexes. J Inorg Biochem 32:163–169.

235. Liu F, Xia Y, Parker AS, Verma IM. 2012. IKK biology. Immunol Rev 246:239–253.

236. Liu T, Zhang L, Joo D, Sun S-C. 2017. NF-κB signaling in inflammation. Signal Transduct Target Ther 2:17023.

237. Heath RJ, Rubin JR, Holland DR, Zhang E, Snow ME, Rock CO. 1999. Mechanism of Triclosan Inhibition of Bacterial Fatty Acid Synthesis. Journal of Biological Chemistry 274:11110–11114.

238. Gloux K, Guillemet M, Soler C, Morvan C, Halpern D, Pourcel C, Vu Thien H, Lamberet G, Gruss A. 2017. Clinical Relevance of Type II Fatty Acid Synthesis Bypass in Staphylococcus aureus. Antimicrob Agents Chemother 61.

239. Wientjes MG. 2010. Comparison of methods for evaluating drug-drug interaction. Frontiers in Bioscience E2:86.

240. DeMars Z, Singh VK, Bose JL. 2020. Exogenous fatty acids remodel staphylococcus aureus lipid composition through fatty acid kinase. J Bacteriol 202.

241. Ocampo PS, Lázár V, Papp B, Arnoldini M, Abel zur Wiesch P, Busa-Fekete R, Fekete G, Pál C, Ackermann M, Bonhoeffer S. 2014. Antagonism between Bacteriostatic and Bactericidal Antibiotics Is Prevalent. Antimicrob Agents Chemother 58:4573–4582.

242. Levin BR, Rozen DE. 2006. Non-inherited antibiotic resistance. Nat Rev Microbiol 4:556–562.

243. Suller MTE. 2000. Triclosan and antibiotic resistance in Staphylococcus aureus. Journal of Antimicrobial Chemotherapy 46:11–18.

244. Suller MTE, Russell AD. 1999. Antibiotic and biocide resistance in methicillin-resistant staphylococcus aureus and vancomycin-resistant enterococcus. Journal of Hospital Infection 43:281–291.

245. Bellio P, Fagnani L, Nazzicone L, Celenza G. 2021. New and simplified method for drug combination studies by checkerboard assay. MethodsX 8:101543.

246. Fenn K, Strandwitz P, Stewart EJ, Dimise E, Rubin S, Gurubacharya S, Clardy J, Lewis K. 2017. Quinones are growth factors for the human gut microbiota. Microbiome 5:161.

247. Goojani HG, Konings J, Hakvoort H, Hong S, Gennis RB, Sakamoto J, Lill H, Bald D. 2020. The carboxy-terminal insert in the Q-loop is needed for functionality of Escherichia coli cytochrome bd-I. Biochim Biophys Acta Bioenerg 1861.

248. Pai MY, Lomenick B, Hwang H, Schiestl R, McBride W, Loo JA, Huang J. 2015. Drug affinity responsive target stability (DARTS) for small-molecule target identification. Methods in Molecular Biology 1263:287–298.

249. Tabana Y, Babu D, Fahlman R, Siraki AG, Barakat K. 2023. Target identification of small molecules: an overview of the current applications in drug discovery. BMC Biotechnol. BioMed Central Ltd https://doi.org/10.1186/s12896-023-00815-4.

250. Feng F, Zhang W, Chai Y, Guo D, Chen X. 2023. Label-free target protein characterization for small molecule drugs: recent advances in methods and applications. J Pharm Biomed Anal. Elsevier B.V. https://doi.org/10.1016/j.jpba.2022.115107.

251. Batool M, Ahmad B, Choi S. 2019. A Structure-Based Drug Discovery Paradigm. Int J Mol Sci 20:2783.

252. Fuchs S, Mehlan H, Bernhardt J, Hennig A, Michalik S, Surmann K, Pané-Farré J, Giese A, Weiss S, Backert L, Herbig A, Nieselt K, Hecker M, Völker U, Mäder U. 2018. AureoWiki‑The repository of the Staphylococcus aureus research and annotation community. International Journal of Medical Microbiology 308:558–568.

253. Haft DH, Loftus BJ, Richardson DL, Yang F, Eisen JA, Paulsen IT, White O. 2001. TIGRFAMs: a protein family resource for the functional identification of proteinsNucleic Acids Research.

254. Kreiswirth B, Löfdahl S, Betley M, O'Reilly M, Schlievert P, Bergdoll M, Novick R. 1983. The toxic shock syndrome exotoxin structural gene is not detectably transmitted by a prophage. Nature 305:709–712.

255. HOLLOWAY BW. 1955. Genetic recombination in Pseudomonas aeruginosa. J Gen Microbiol 13:572–81.

APPENDIX

Table A-1. Mutational profiles of *ypfP* suppressor mutants

Gene	Name	Product[a]	TIGRFAM role[b]	Mutation type	Protein effect
S1P4					
NWMN_0300	-	Hypothetical protein	Unknown	Missense	G159V
NWMN_0407	*lpl4*	Tandem-type lipoprotein	*Staphylococcus* tandem lipoproteins	Deletion, Insertion	Frame shift, Frame shift
NWMN_0687	*ltaS*	Lipoteichoic acid synthase	Choline-sulfatase, Frataxin	Missense	G39C
NWMN_1774	-	Hypothetical protein	MutS2 family protein	Missense	L14I, T15R
S2P3					
NWMN_0886	*ltaA*	Proton coupled antiporter flippase	Miltidrug resisatance protein, H+ Antiporter protein	Missense	K13N, N14R, F15L, I16V
NWMN_1774	-	Hypothetical protein	MutS2 family protein	Missense	L14I, T15R
S3P3					
NWMN_0309	-	Phage N-acetylglucosamidase	Flagellar rod assembly protein/muramidase FlgJ	Missense	S478A
NWMN_0886	*ltaA*	Proton coupled antiporter flippase	Miltidrug resisatance protein, H+ Antiporter protein	Missense	K13N, N14R, F15L, I16V
NWMN_1622	*tyrS*	Tyrosine tRNA ligase	tRNA aminoacylation	Missense	L9F
NWMN_1774	-	Hypothetical protein	MutS2 family protein	Missense	L14I, T15R
NWMN_2337	-	Amino acid permease	GABA permease, Amino acid permease	Missense	M161L
S4P3					
NWMN_0486	*mcsB*	ATP:guanido phosphotransferase	Unknown	Missense	I84L
NWMN_0886	*ltaA*	Proton coupled antiporter flippase	Miltidrug resisatance protein, H+ Antiporter protein	Missense	K13N, N14R, F15L, I16A, L17E
NWMN_1774	-	Hypothetical protein	MutS2 family protein	Missense	L14I, T15R

[a]Products for each gene were obtained from AureoWiki (252).
[b]The role of the protein product of each gene was predicted by the TIGRFAM database (253). In the case of multiple roles being predicted, the top two highest scoring roles were shown. Protein products without a predicted role were listed as unknown.

Table A-2. Bacterial strains used in chapter 2

Name	Relevant genotype and phenotype	Source
Staphylococcus aureus		
RN4220	Restriction deficient, methylation proficient	(254)
Newman (NWMN)	WT	(154)
ypfP	*ypfP::erm*	this study
ltaA	*ltaA::erm*	this study
Δ*gtrR*	in-frame deletion, heme synthesis deficient small colony variant	this study
Δ*gtrR ypfP*	heme synthesis deficient small colony variant *ypfP::erm*	this study
S1P4	*ypfP::errm* anaerobic suppressor (Table A-1)	this study
S2P3	*ypfP::erm* anaerobic suppressor (Table A-1)	this study
S3P3	*ypfP::erm* anaerobic suppressor (Table A-1)	this study
S4P3	*ypfP::erm* anaerobic suppressor (Table A-1)	this study
Pseudomonas aeruginosa		
PAO1	WT	(255)

Table A-3. Primers used in chapter 2

Primer name	Sequence	Source
NE Buster[a]	GCTTTTTCTAAATGTTTTTTAAGTAAATCAAGTAAC	(170)
NE Martn-ermR[a]	AAACTGAATTTTAGTAAACAGTTGACGATATTC	(170)
ltaA Tn seq.[a]	GCGCTCGAGATGGAAAGGTTCCTTTATATGC	this study
ypfP Tn seq.[a]	GCGTCATTGAGCACGATTTATT	this study
ltaA-F Gibson[a]	ACAATTGAGGTGAACATATGGAAAGGTTCCTTTATATG	this study
ltaA-R Gibson[a]	CTACCCCCTTGTTTGGATCCTTACTTAGCTTTTTCTCTATTTAC	this study
pOS seq. F	TTAGCTTTTCAATGTAGATTGG	this study
pOS seq. R	ATTACGCCAAGCTAGCTTGG	this study
ypfP-F pOS[a]	GCGCTCGAGATGGTTACTCAAAATAAAAAGATAT	this study
ypfP-R pOS[a]	GCGGGATCCTTATTTAACGAAGAATCTTGAATA	this study
ltaA-mut[b]	ATGATTAGCGTAATTATTTAACGAAGAATCTTGC	this study
ltaA-S2P3[b]	AACAGGTTGGTTTTAATGCTTATTATCTTATTTTTAATGGAATTTGCGAG	this study
ltaA-S4P3[b]	AACAGGTTGGCTGAAATGCTTATTATCTTATTTTTAATGGAATTTGCGAG	this study
ltaS-F Gibson[a]	ACAATTGAGGTGAACATATGAGTTCACAAAAAAAGAAAATTAGTC	this study
ltaS-R Gibson[a]	ACTACCCCCTTGTTTGGATCTTATTTTTTAGAGTTTGCTTTAGG	this study
pOS-F Gibson[c]	GATCCAAACAAGGGGGTAGTGT	this study
pOS-R Gibson[c]	CATATGTTCACCTCAATTGTATTTATCCCTAC	this study

[a]Indicates primers used on genomic DNA to amplify its respective target sequence
[b]Indicates the pOS-*ltaA* complementation plasmid was used as the template sequence
[c]Primers used to amplify/linearize pOS for downstream use in Gibson assembly for cloning of *ltaS*

Table A-4. In-frame mutations in *ispA*::Tn gentamicin resistant colonies

Strain	Locus Tag	Gene	Mutation	Protein Effect
ispA::Tn^{115}				
	SAUSA300_1169	*ftsK*	A -> G	K180R
	SAUSA300_1359	*hepT*	G -> T	A72E
	SAUSA300_1611	*valS*	A -> C	None
	SAUSA300_1753	*splF*	C -> G	G11A
	SAUSA300_1993	*fruC*	(C)4 -> (C)5	Frame Shift
ispA::Tn^{144}				
	SAUSA300_1169	*ftsK*	A -> G	K180R
	SAUSA300_1359	*hepT*	G -> T	A72E
	SAUSA300_1611	*valS*	A -> C	None
	SAUSA300_1753	*splF*	C -> G	G11A
	SAUSA300_1993	*fruC*	(C)4 -> (C)5	Frame Shift
ispA::Tn^{164}				
	SAUSA300_1359	*hepT*	G -> T	A72E
	SAUSA300_1611	*valS*	A -> C	None
	SAUSA300_1753	*splF*	C -> G	G11A
ispA::Tn^{165}				
	SAUSA300_1169	*ftsK*	A -> G	K180R
	SAUSA300_1359	*hepT*	C -> T	A165T
	SAUSA300_1611	*valS*	A -> C	None
	SAUSA300_1753	*splF*	C -> G	G11A
	SAUSA300_1993	*fruC*	(C)4 -> (C)5	Frame Shift

Table A-5. Strains used in chapter 3

Strain	Description	Reference
RN4220	Restriction deficient, methylation proficient cloning intermediate	(254)
JE2	USA300, Wild type (WT)	(170)
ispA::Tn	The *ispA* transposon from NE1447 backcrossed into JE2 WT	This study
hepT::Tn	The *hepT* transposon from NE1920 backcrossed into JE2 WT	This study
Δ*hepT*	In-frame deletion of *hepT* using pKOR1-Δ*hepT*	This study
Δ*hepT ispA*::Tn	The ispA transposon from NE1447 transduced into JE2 Δ*hepT*	This study
menE::Tn	*tn917* inserted into *menE*, marked with erythromycin resistance, backcrossed into strain JE2	(114)
Δ*menB*	In-frame deletion of *menB* using pKOR1-Δ*menB*	This study
menC::Tn	*tn917* inserted into *menC*, marked with erythromycin resistance, backcrossed into strain JE2	(114)
qoxA::Tn	The *qoxA* transposon from NE92 backcrossed into JE2 WT	This study
cydA::Tn	The *cydA* transposon from NE117 backcrossed into JE2 WT	This study
Δ*menB qoxA*::Tn	The *qoxA* transposon from NE92 transduced into JE2 Δ*menB*	This study
Δ*menB cydA*::Tn	The *cydA* transposon from NE117 transduced into JE2 Δ*menB*	This study
crtM::Tn	The *crtM* transposon from NE2499 backcrossed into JE2 WT	This study
Δ*hepT crtM*::Tn	The *crtM* transposon from NE2499 transduced into JE2 Δ*hepT*	This study
Δ*ispA*	In-frame deletion of *ispA* using pKOR1-Δ*ispA*	This study
Δ*ispA qoxA*::Tn	The *qoxA* transposon from NE92 transduced into JE2 Δ*ispA*	This study
Δ*ispA cydA*::Tn	The *cydA* transposon from NE117 transduced into JE2 Δ*ispA*	This study
Δ*hepT qoxA*::Tn	The *qoxA* transposon from NE92 transduced into JE2 Δ*hepT*	This study

Table A-5 (cont'd)

Δ*hepT cydA*::Tn	The *cydA* transposon from NE117 transduced into JE2 Δ*hepT*	This study
ispA::Tn suppressor 115	Pigmented JE2 *ispA*::Tn isolated from a gentamicin plate	This study
ispA::Tn suppressor 144	Pigmented JE2 *ispA*::Tn isolated from a gentamicin plate	This study
ispA::Tn suppressor 164	Pigmented JE2 *ispA*::Tn isolated from a gentamicin plate	This study
ispA::Tn suppressor 165	Non-pigmented JE2 *ispA*::Tn isolate from a gentamicin plate	This study
JE2 pOS1	Empty pOS1 carried by JE2 WT	This study
ispA::Tn pOS1	Empty pOS1 carried by *ispA*::Tn	This study
ispA::Tn pOS1-*ispA*	The *ispA* gene cloned into pOS1 and carried by *ispA*::Tn	This study
Δ*hepT* pOS1	Empty pOS1 carried by Δ*hepT*	This study
Δ*hepT* pOS1-*hepT*	The *hepT* gene cloned into pOS1 and carried by Δ*hepT*	This study
Δ*hepT ispA*::Tn pOS1	Empty pOS1 carried by Δ*hepT ispA*::Tn	This study
Δ*hepT ispA*::Tn pOS1-*hepT*	The *hepT* gene cloned into pOS1 and carried by Δ*hepT ispA*::Tn	This study
Δ*hepT ispA*::Tn pOS1-*ispA*	The *ispA* gene cloned into pOS1 and carried by Δ*hepT ispA*::Tn	This study

Table A-6. Primers used in chapter 3

Primer name	Sequence (5'-3')	Reference
Transposon check primers:		
ispA::Tn_Check	AGAAACGCAAAGTTTTGAAGAAA	This study
hepT::Tn_Check	TGCAATGCACCTTGGCTAT	This study
cydA::Tn_Check	GCGTGATATTTCTCTCTTCAAAATCAA	This study
qoxA::Tn_Check	CATATTTTCTTCACTAGTGAAGTTTGGATC	This study
crtM::Tn_Check	TACTGCAATCTTCATTATTCAACCACC	This study
NE_Buster	GCTTTTTCTAAATGTTTTTTAAGTAAATCAAGTACC	(170)
NE_Martn	AAACTGATTTTTAGTAAACAGTTGACGATATTC	(170)
Deletion check primers:		
*hepT*_Del_Check_F	GGTATCTCATACACACTCGCTCCTTTC	This study
*hepT*_Del_Check_R	GTGATAATATCGTGAGGTGTAGACATGGA	This study
*ispA*_Del_Check_F	CAACAAAGACTGCGTTTCATGTTGG	This study
*ispA*_Del_Check_R	CGTTATAAGTGCCATGATGTTCAAAGGTAG	This study
*menB*_Del_Check_F	AAAAATCAATTTGTATACGTCATG	This study
*menB*_Del_Check_F	GGTCACATCCCTATATCTAATTTG	This study
Gibson assembly primers:		
pKOR1_*hepT*_up_F	TTCATAAATAGTTTAACTTTGCCACGTTAATC	This study
pKOR1_*hepT*_up_R	CGGAACCGGTACCAATGGATATTGAAATCTTCATTACATCATC	This study
pKOR1_*hepT*_d_F	GCTGCTAGCTAGCTAGAGATAAAGTTAATCAGTCCGTTTAAAAAAATTATG	This study
pKOR1_*hepT*_d_R	CAAAGTTAAACTATTTATGAAAAGTATTGAAAGCG	This study
pKOR1_*ispA*_up_F	GCTGCTAGCTAGCTAGAGATTTATTCATCGGTAGATTCG	This study
pKOR1_*ispA*_up_R	CGGGTTCAGGTATGCAGATAGTTTAGGTGTAG	This study

Table A-6 (cont'd)

pKOR1_*ispA*_d_F	TATCTGCATACCTGAACCCGTTTCACCAC	This study
pKOR1_*ispA*_d_R	CGGAACCGGTACCAATGGATAAGCAAATATATCGATTAGCAACAATTG	This study
pOS1_*hepT*_F	TGAACATATGCTCGAGGATCATGAACAATGAAATTAAGAAAGTGGAACA	This study
pOS1_*hepT*_R	AGCTTGGCTGCAGGTCGACGCTACGTGTTTCTTGAACCCAT	This study
RE[a]-cloning primers:		
pOS1_*ispA*_F	GCGCATATGACGAATCTACCGATGAATAAATT	This study
pOS1_*ispA*_R	GCGGGATCCTTAGTGATCCCTGCTATAAAATA	This study

[a]Restriction enzyme (RE)

Table A-7. Unique ΔFASII inhibitors from the Maybridge library

Sample I.D.	Subclass[a]	WT Activity (%)[b]	ΔFASII Activity (%)[b]
MSU-34372	1-benzopyrans	1.78	99.45
MSU-29489	Anilides	2.57	59.46
MSU-32757	Anilides	-8.71	71.47
MSU-18020	Aryl thioethers	18.18	101.48
MSU-33170	Aryl thioethers	-1.3	101.81
MSU-33694	Aryl thioethers	4.23	101.07
MSU-33835	Aryl thioethers	-7.84	100.11
MSU-11793	Benzenesulfonamides	6.47	100.07
MSU-21240	Benzo-1,3-dioxanes	1.06	51.84
MSU-30338	Benzoic acids and derivatives	8.27	98.85
MSU-21337	Biphenyls and derivatives	-5.81	99.74
MSU-27344	Carbonyl compounds	0.08	57.64
MSU-27419	Diphenylethers	6.75	62.14
MSU-14091	Ethers	17.17	40.7
MSU-19861	Ethers	11.43	64.4
MSU-20568	Ethers	9.68	73.13
MSU-22172	Ethers	13.04	99.37
MSU-12298	Halobenzenes	13.24	101.71
MSU-26130	Halobenzenes	7.55	98.96
MSU-33764	Halobenzenes	7.29	101.4
MSU-21155	Hydroquinolines	11.2	55.65
MSU-27210	Indoles	8.99	100.69
MSU-17058	N-arylamides	13.82	101.66
MSU-14999	N-phenylthioureas	16.25	99.19
MSU-15783	N-phenylthioureas	13.34	98.93
MSU-20326	N-phenylthioureas	13.45	99.9
MSU-20701	N-phenylthioureas	9.1	100.04
MSU-20928	N-phenylthioureas	1	76.14
MSU-23362	N-phenylthioureas	15.93	98.91
MSU-26221	N-phenylthioureas	9.14	99.82
MSU-32241	N-phenylthioureas	13.07	50.97
MSU-11788	N-phenylureas	1.76	73.02
MSU-15601	N-phenylureas	8.65	64.36
MSU-15890	N-phenylureas	7.9	100.01
MSU-16346	N-phenylureas	15.81	85.96
MSU-16719	N-phenylureas	-1.81	78.89
MSU-17814	N-phenylureas	11.33	72.09
MSU-18605	N-phenylureas	9.05	101.48
MSU-20681	N-phenylureas	-2.28	60.82

Table A-7 (cont'd)

MSU-22374	N-phenylureas	-4.91	69.55
MSU-22522	N-phenylureas	19.95	96.61
MSU-23988	N-phenylureas	9.4	101.85
MSU-24281	N-phenylureas	14.8	68.26
MSU-24901	N-phenylureas	5.25	66.61
MSU-28105	N-phenylureas	1.94	76.97
MSU-28106	N-phenylureas	5.19	50.47
MSU-28428	N-phenylureas	5.68	97.18
MSU-28696	N-phenylureas	-0.59	99.13
MSU-28698	N-phenylureas	-2.33	99.27
MSU-28713	N-phenylureas	13.14	98.3
MSU-30863	N-phenylureas	2.51	86.83
MSU-32278	N-phenylureas	12.27	99.25
MSU-27562	Phenylcarbamic acid esters	8.62	101.56
MSU-31283	Phenylcarbamic acid esters	15.44	47.69
MSU-27861	Piperazines	-6.5	100.69
MSU-29925	Piperazines	5.28	99.27
MSU-20914	Pyrazoles	-16.22	99.72
MSU-23382	Pyrazoles	18.87	101.24
MSU-28435	Pyrazoles	6.18	97.18
MSU-28711	Pyrazoles	8.77	99.13
MSU-28868	Pyrazoles	0.04	98.99
MSU-32348	Pyrazoles	3.78	99.86
MSU-32349	Pyrazoles	-1	96.1
MSU-15747	Pyrimidines and pyrimidine derivatives	11	100.8
MSU-27614	Pyrimidines and pyrimidine derivatives	-5.78	101.06
MSU-32380	Quinoline carboxamides	16.23	99.77
MSU-12778	Substituted pyrroles	3.44	50.07
MSU-25153	Sulfanilides	14.46	51.75
MSU-28220	Sulfanilides	16.29	44.5
MSU-20454	Thiophene carboxylic acids and derivatives	14.91	49.2
MSU-33042	Triazoles	3.99	79.54
MSU-11542	Trifluoromethylbenzenes	3.98	101.71
MSU-27398	Trifluoromethylbenzenes	13.64	101.6
MSU-28075	Trifluoromethylbenzenes	9.24	98.91
MSU-30716	Trifluoromethylbenzenes	8.66	50.22
MSU-33779	Trifluoromethylbenzenes	-7.27	101.8
MSU-11185	Uncategorized	16.05	101.79
MSU-11381	Uncategorized	6.29	61.89
MSU-11813	Uncategorized	4.93	92.99

Table A-7 (cont'd)

MSU-14478	Uncategorized	12.49	101.42
MSU-19277	Uncategorized	7.35	99.52
MSU-21723	Uncategorized	-1.21	89.25
MSU-23454	Uncategorized	13.04	99.24
MSU-24363	Uncategorized	16.24	99.77
MSU-24419	Uncategorized	-1.53	101.48
MSU-25195	Uncategorized	6.18	99.73
MSU-25891	Uncategorized	4.19	101.56
MSU-26736	Uncategorized	15.8	98.65
MSU-27769	Uncategorized	11.32	98.69
MSU-27994	Uncategorized	3.94	69.5
MSU-30591	Uncategorized	11.19	62.49
MSU-30714	Uncategorized	0.34	102.8
MSU-30913	Uncategorized	17.55	99.18
MSU-31049	Uncategorized	11.72	101.88
MSU-31311	Uncategorized	18.18	83.97
MSU-33535	Uncategorized	-4.08	101.96
MSU-33563	Uncategorized	1.95	61.88
MSU-33566	Uncategorized	3.7	42.69
MSU-33568	Uncategorized	10.8	73.17
MSU-33995	Uncategorized	-5.14	102.16

[a]Compounds for which the sub-class level of classification could not be determined by Classyfire are labeled as "Uncategorized".

[b]The percent activity as determined by the initial screening of the Maybridge library

Table A-8. Selected ΔFASII inhibitors from the LOPAC, NCI, NCATS_MIPE and Prestwick libraries

Sample I.D.	ANNOTATIONS[a]	Percent Activity
MSU-3845	RegorafenibBAY 73-4506A-1112	98.26
MSU-1755	Potent, cell permeable, subtype selective retinoic acid receptor (RARalpha) agonist.	98.14
MSU-40248	IKK-2 Inhibitor	98.1
MSU-2332	PKC and CaM kinase III inhibitor	97.98
MSU-1743	Donitriptan is a potent, selective 5-HT1B/1D agonist.	97.89
MSU-1893	Nicotinic acetylcholine receptor antagonist	97.77
MSU-1689	is a muscarinic antagonist and antispasmodic	97.77
MSU-864	Methylhydantoin-5-(D)	97.69
MSU-293	Glafenine hydrochloride	97.68
MSU-1654	Potent group II metabotropic glutamate receptor agonist	97.27
MSU-39979	Pregnane X Receptor (PXR) Agonist	97.11
MSU-41294	Heat Shock Protein 90 (hsp90) Inhibitor	96.99
MSU-40167	Matrix Metalloproteinase Inhibitors	96.85
MSU-40452	IKK Inhibitor	96.6
MSU-1799	Bexarotene, selective retinoid X receptor (RXR) agonist	96.15
MSU-1184	Olmesartan	96.13
MSU-1035	Molindone hydrochloride	77.96
MSU-41126	DNA Methyltransferase (DNMT) Inhibitor	64.4
MSU-370	Benzbromarone	52.22
MSU-2215	Highly selective, ATP/GTP-competitive inhibitor of casein kinase 2 (CK2).	47.49
MSU-2449	Spleen tyrosine kinase (Syk) inhibitor; anti-inflammatory	45.59

[a]Annotations for each compound were obtained from the MScreen data repository